THESIS FOR THE DEGREE OF DOCTOR OF PHILOSOPHY

Quantifying building damage induced by underground construction at city scale

PIERRE WIKBY

Department of Architecture and Civil Engineering

Division of Geology and Geotechnics

CHALMERS UNIVERSITY OF TECHNOLOGY

Gothenburg, Sweden 2025

Quantifying building damage induced by underground construction at city scale
PIERRE WIKBY
ISBN 978-91-8103-352-6

Doktorsavhandlingar vid Chalmers tekniska högskola
Ny serie nr. 5809
ISSN 0346-718X
https://doi.org/10.63959/chalmers.dt/5809

Department of Architecture and Civil Engineering
Division of Geology and Geotechnics
Chalmers University of Technology
SE-412 96 Gothenburg
Sweden
Telephone: +46 (0)31-772 1000

Cover:
Simplified illustration of the leakage-subsidence-damage chain seen on p. 4. Illustration by the author.

Chalmers Digitaltryck
Gothenburg, Sweden 2025

Quantifying building damage induced by underground construction at city scale
Thesis for the degree of Doctor of Philosophy
PIERRE WIKBY
Department of Architecture and Civil Engineering
Division of Geology and Geotechnics
Chalmers University of Technology

ABSTRACT

Leakage of groundwater into underground construction may lead to time-dependent reduction of pore pressures. The resulting subsidence can increase the risk of flooding and damage to structures, causing significant costs to society and individuals. This is especially common in areas with deformation-sensitive clays, typical to Scandinavia. The pore pressure reduction caused by leakage to tunnels built in fractured rock, called underdrainage, is common in Scandinavia and may affect a large area of influence, requiring expensive mitigation measures. Planning for such mitigation measures to prevent significant damage involves a trade-off between costs and benefits of their implementation. We need an understanding of the processes involved in the large-scale subsidence due to underdrainage, and the potential damage. The problem is highly complex, uncertain, and coupled. Thus, a rigorous modelling framework was developed as part of this thesis.

A 2D hydro-mechanically coupled finite element (HMFE) model with an advanced rate-dependent constitutive model was used to assess the influence of key parameters affecting the time-dependent (greenfield) settlements caused by underdrainage. The time-dependent results from the HMFE model were then used along with hydro-stratigraphy as training and validation data for a metamodel, which produced settlements on a 3D hydro-stratigraphic domain. The results of the metamodel were used as input for a large-scale building damage model developed to calculate damage parameters based on various damage criteria. In urban settings, greenfield predictions potentially result in over-prediction of damage, as most buildings on soft deposits are built on piled foundations. Thus, the influence of floating piles was considered via axisymmetric finite element simulations, providing modification factors that can be applied to greenfield settlements for older piled buildings.

The developed models were applied to the case of the construction of an underground railway station in Gothenburg, Sweden, expected to affect a confined aquifer in an area with ongoing background creep settlements. Hypothetical scenarios of uniform pore pressure reduction under the soft clay deposit, and the subsequent consolidation and creep in the soft clay, were simulated to determine the magnitude of settlements at different time intervals. The results showed dependency on time and stratigraphy, where the transitional areas between the soil and rock are most prone to settlements in short term, influenced by the overconsolidation ratio (OCR). The predicted settlements, as well as the modified settlements due to the existence of floating piles were shown to be highly time-dependent, due to the slow consolidation associated with underdrainage in deep clay layers. Furthermore, the results also show that the estimated damage is highly dependent on the chosen damage criteria. Based on the results, only damage parameters derived from differential settlements should be used in early damage assessments.

Keywords: subsidence, groundwater lowering, underdrainage, building damage, consolidation, creep

ACKNOWLEDGEMENTS

The financial support from Trafikverket (Swedish Transport Administration, grant 2020/54637) and Digital Twin Cities Centre from Vinnova (grants 2019-00041 and 2024-03904) is gratefully acknowledged. Furthermore, I would like to thank Trafikverket for providing me with the necessary data.

I would like to thank and greatly acknowledge my main supervisor, Professor Minna Karstunen, for her continuous guidance, patience, encouragement, support and academic supervision throughout this project. Also greatly involved, my project team consisting of Dr Jonas Sundell at Swedish Geotechnical Institute (SGI), Dr Ayman Abed, Dr Ezra Haaf, Professor Lars Rosén, Dr Mats Karlsson and Johanna Merisalu at Chalmers. I could sincerely not have asked for a better and more encouraging team. I am also grateful to Professor Jelke Dijkstra for taking on the role as my examiner and for his guidance and insurmountable support in my final study. Both Minna and Jelke have let me excel tremendously in scientific thinking and communication.

I would also like to acknowledge the reference group of the project, Dr Johan Spross (KTH), Dr Jenny Langford (Norconsult), Dr Tara Wood (Ramboll), Kristy Heng (Swedish Transport Administration) and Ola Forssberg (Swedish Transport Administration). Your comments were invaluable to the success of this project.

At Chalmers I had the wonderful experience of getting to know amazing colleagues, many of whom are now my friends. I am deeply grateful to my line manager, Jenny Norrman, for her excellence in navigating administrative matters and her tremendous support during the challenging times of this PhD project. I want to thank all the PhD students, post-docs and researchers for the interesting discussions at the office, but most importantly for their friendship, technical and emotional support. The people working in the Geotechnics Research Area are like a family to me and I hope we will have continued contact and collaboration in the future.

Finally, I would like to thank all my other friends as well as my mom and dad who have given me tremendous love and support during this journey. Without you, I would not have completed this PhD.

Pierre Wikby
Göteborg, 2025

LIST OF PUBLICATIONS

This thesis consists of an extended summary and the following appended papers:

Paper A Wikby, P., Abed, A., Karlsson, M., Sundell, J., & Karstunen, M. (2023). *The influence of parameter variability on subsidence* (L. Zdravkovic, S. Kontoe, D. Taborda, & A. Tsiampousi, Eds.). International Society for Soil Mechanics; Geotechnical Engineering. https://doi.org/10.53243/NUMGE2023-325

Paper B Haaf, E., Wikby, P., Abed, A., Sundell, J., McGivney, E., Rosén, L., & Karstunen, M. (2024). A metamodel for estimating time-dependent groundwater-induced subsidence at large scales. *Engineering Geology*, *341*(August). https://doi.org/10.1016/j.enggeo.2024.107705

Paper C Wikby, P., Haaf, E., Abed, A., Rosén, L., Sundell, J., & Karstunen, M. (2024). A grid-based methodology for the assessment of time-dependent building damage at large scale. *Tunnelling and Underground Space Technology*, *149*, 105788. https://doi.org/10.1016/j.tust.2024.105788

Paper D Wikby, P., Haaf, E., & Karstunen, M. (2025b). Modeling subsidence and building damage in central Gothenburg using machine learning. In Z. Liu, J. Dai, & K. Robinson (Eds.), *Proc. of the 9th International Symposium on Geotechnical Safety and Risk (ISGSR)* (pp. 375–378). Research Publishing. https://doi.org/10.3850/9789819440757

Paper E Wikby, P., Abed, A., Karstunen, M., & Dijkstra, J. (2025a). Incorporating the impact of floating piles in prediction of large-scale subsidence. *Submitted manuscript*

The author has carried the main responsibility for the work presented in the appended papers A and C-E. For those papers, this work included developing the methodology, formal analyses, visualisation and writing the original drafts. For paper B, Haaf carried the main responsibility of writing the original draft, especially regarding the development and analysis with the metamodel which is fully his work. He also contributed to providing the settlement data for papers C and D. For paper B, the author of this thesis performed all finite element analyses for the cross-sections presented, and contributed with writing of certain parts of the manuscript as well as editing.

As for the other authors, Sundell contributed through Trafikverket to access of data (all papers), the stratigraphic and the groundwater modelling and was involved in papers A-C both regarding writing of original draft, editing and supervision. Karstunen contributed to the main supervision, including the conceptualisation, visualisation and editing of all papers A-E. Abed contributed to the supervision and editing of papers A-C and E, especially regarding the finite element modelling, where he performed the initial setup and performed the FE analyses for calibration of OCR to the bellow hose. Rosén contributed to the supervision, conceptualisation, validation and editing of papers B and C. Dijkstra contributed to the supervision, including the conceptualisation, as well as the editing of paper E. Karlsson contributed to the supervision and editing of paper A, especially regarding the interpretation of results, the conceptualisation of the parametric study and the calibration of in-situ OCR to the bellow hose. Finally, McGivney contributed to implementation of the metamodel in paper B.

OTHER RELATED PUBLICATIONS

- Wikby, P. (2024). *Kvantifiering av byggnadsskador på grund av undermarkskonstruktion i stadsskala*. Trafikverket. Göteborg

TABLE OF CONTENTS

NOTATION

Acronyms

AI	Artificial Intelligence
BP	Before Present
CPT	Cone penetration test
CRS	Constant Rate of Strain
CSS	Current Stress Surface
ctc	centre-to-centre distance
EM	Empirical Method
EP	Elastoplastic
EVP	Elastic Viscoplastic
FD	Finite Difference
FE	Finite Element
HB	Hyperbolic
HM	Hydro-Mechanical
ICS	Intrinsic Compression Surface
IL	Incrementally Loaded
InSAR	Interferometric Synthetic Aperture Radar
LBM	Laminate Beam Model
LE	Linear Elastic
LTSM	Limiting Tensile Strain Method
NC	Normally Consolidated
NCS	Normal Compression Surface
NP	Neutral Plane
NSF	Negative Skin Friction
OC	Overconsolidated
OCR	Overconsolidation Ratio
PSF	Positive Skin Friction
PWP	Pore Water Pressure
RC	Reinforced Concrete
RSM	Relative Stiffness Method
SEM	Semi-Empirical Method
SLS	Serviceable Limit State
SOSM	State-of-Strain Method
SSM	Strain Superposition Method
ST	Standard Piston
TPM	Thick Plate Model
ULS	Ultimate Limit State

Greek symbols

α	Adhesion factor
α	Angular strain
α	Anisotropy
α_0	Initial amount of anisotropy
β	Angular distortion
β	Burland factor for shaft resistance
χ	Amount of bonding in the current state
ΔS	Differential settlements
ΔS_{ult}	Relative pile-soil movement at full mobilisation
Δ	Relative deflection
δ	Soil-pile interface friction angle
$\dot{\Lambda}$	Viscoplastic multiplier
$\dot{\varepsilon^c}$	Viscoplastic (creep) incremental strain
$\dot{\varepsilon^e}$	Elastic incremental strain
$\dot{\varepsilon_d}$	Deviatoric incremental strain
$\dot{\varepsilon_v}$	Volumetric incremental strain
η	Current stress ratio
γ_w	Unit weight of water
κ^*	Modified swelling index
λ^*	Modified compression index
λ_i^*	Modified intrinsic compression index
μ_i^*	Modified intrinsic creep index
ν	Poisson's ratio
ω	Absolute effectiveness of rotational hardening
ω	Tilt
ω_d	Relative effectiveness of rotational hardening
ϕ'	Effective friction angle
ρ	Bulk density
σ_c'	Apparent preconsolidation pressure
σ_z'	Vertical effective stress
σ_{v0}'	Initial vertical effective stress
τ	Reference time
τ_s	Unit shaft friction
θ	Rotation, slope
θ_α	Lode angle
$\varepsilon_{b,max}$	Maximum bending strain
$\varepsilon_{d,max}$	Maximum diagonal strain
ε_{vol}	Volumetric strains at reconsolidation
ξ	Absolute rate of destructuration
ξ_d	Relative rate of destructuration

Roman lower case letters

c'	Apparent effective cohesion
c_u	Undrained shear strength
c_v	Coefficient of consolidation

e	Void ratio
k_h	Horizontal hydraulic conductivity
k_v	Vertical hydraulic conductivity
l_Δ	Inflection length
m_v	Coefficient of compressibility
p'	Mean effective stress
p'_{eq}	Equivalent mean effective stress
p'_{mi}	Projection of the intrinsic preconsolidation pressure on the hydrostatic axis
p'_m	Projection of the maximum preconsolidation pressure on the hydrostatic axis
q	Deviatoric effective stress / Toe resistance
r_k	Hydraulic anisotropy ratio
r_{pile}	Pile radius
t	Time after drawdown / Shaft resistance
w	Natural water content
x	Horizontal position
x_1	Time-based limiting value 1 for the trilinear function
x_2	Time-based limiting value 2 for the trilinear function
y	Vertical position
y_1	MF-based limiting value 1 for the trilinear function
y_2	MF-based limiting value 2 for the trilinear function
z	Depth / Relative displacements
z_i	Interaction Level
z_{NP}	Neutral Plane depth

Roman capital letters

A_s	Circumferential area of the pile
A_t	Pile toe area
D	Pile diameter
E	Elastic modulus
G	Elastic shear modulus
H	Height
I	Second moment of area
K	Elastic bulk modulus
K_0	Lateral earth pressure at rest
K_0^{NC}	Lateral earth pressure at rest in normal consolidation
L	Length
M	Stress ratio at critical state
M_c	Stress ratio at critical state in triaxial compression
M_e	Stress ratio at critical state in triaxial extension
MF^S	Modification factor of settlements
N_c	Bearing capacity factor
P	Point load
Q	Pile head load
Q_n	Dragload
Q_{ult}	Ultimate pile head load
R_s	Shaft resistance
R_t	Toe resistance
S	(Total) settlement
S^p	Settlements along pile centre
S^{gf}	Greenfield settlements
S_0^{gf}	Greenfield surface settlements
S_0^p	Pile surface settlements
S_s	Specific storage
S_t	Sensitivity
S_{tot}	Total pile settlements
T_v	Time factor

Part I
Extended summary

1 Introduction

1.1 Background and motivation

Subsidence, i.e. the vertical displacement of the ground surface due to processes in the subsurface, is a worldwide problem that can have severe consequences, including damage to structures, flooding and other societal costs (Bagheri-Gavkosh et al. 2021). Subsidence affects many densely populated areas in North America (Ortega-Guerrero et al. 1999; Burbey 2002; Calderhead et al. 2011; Chaussard et al. 2021), Europe (Teatini et al. 2006; Gambolati and Teatini 2015) and Asia (Phien-wej et al. 2006; Shen and Xu 2011; Kooi and Yudhedha 2018). If not mitigated, subsidence can have negative effects on society, including increased flood risk and damage to the built environment (i.e. infrastructure, buildings and utilities). The direct and indirect effects include costs related to repairs, property devaluation, legal claims and negative public perception.

The main cause of large-scale subsidence globally is the extraction of groundwater in deep aquifers for freshwater, industrial and agricultural uses (Bagheri-Gavkosh et al. 2021), resulting in the so-called underdrainage. Other triggering factors for large-scale subsidence are natural causes, such as creep settlements, or anthropogenic activities, such as oil or gas extraction, subsurface construction, or mining.

Most of the areas vulnerable for subsidence are located on thick deposits of compressible soils, such as soft natural clays, interbedded between water-bearing aquifers. In such systems, anthropogenic activities, such as groundwater extraction, rapidly lower the pore pressures in the affected aquifers. The equalisation of pore water pressures in an aquitard (a clay layer with low permeability) increases the effective stresses over time, triggering consolidation and creep settlements that result in subsidence. Depending on local hydrogeological conditions, this process can occur on a large scale (Burbey 2002; Huang et al. 2012). The consequences of excessive groundwater extraction, or construction activities that result in reduction of pore water pressures in the clay layer, may not be evident until much later, at a time when it may already be too late to stop the process. In order to predict the subsidence and its consequences in aquifer systems with compressible soils, time-dependent analyses at large-scale are required.

The leakage of groundwater into tunnels can have effects similar to groundwater extraction. In Scandinavia, tunnels are commonly built in hard fractured crystalline rock. Such fractures are often water-bearing and can be drained as a result of tunnelling. If those fractures are also hydraulically connected to the permeable soil layers above the bedrock, widespread pore pressure reduction can occur.

In Scandinavia, the stratification is mainly shaped by complex geological processes during and after the last Ice Age. Due to a highly undulating rock surface (see Figure 1.1), the thickness of the compressible clay layers is highly variable. The layer just above the rock consists typically of coarse-grained materials, either glacial till or glacio-fluvial materials, with high hydraulic conductivity. In low-lying areas, fine-grained materials sedimented in either lacustrine or marine conditions are found, forming thick layers of compressible clays, characterised by large void ratios and high creep rates. As a result of the retreat of the continental ice-sheet, followed by isostatic uplift and changes in groundwater levels, there is a weathered dry crust on top. This crust, together with any fill materials (dredged or quarried materials used to form the landscape in the

urban setting), constitutes an unconfined aquifer, known as the upper aquifer. The coarse-grained materials below the saturated clay layers constitute a confined aquifer, called the lower aquifer (Bergström et al. 2022). Thus, the aquifer system typically comprises an "upper" (unconfined) aquifer, an aquitard and a "lower" (confined) aquifer.

An example of large-scale, time-dependent, subsidence in compressible soils caused by water ingress into tunnels was investigated in a series of studies by Sundell (2018). The problem can be conceptualised by a cause-effect chain (Figure 1.1):

1. The construction of rock tunnels causes potentially leakage of groundwater through the fractures in the rock into the tunnel.
2. The leakage in the tunnel causes a drop in pore pressures in the lower aquifer, called underdrainage.
3. The pore pressure reduction in the lower aquifer results in a time-dependent reduction in the pore pressures in the soft clay layer above, and increases in the effective stresses.
4. In compressible soils, increases in effective stresses often lead to large consolidation and creep settlements.
5. The resulting subsidence may cause damage to buildings and other structures.
6. The effects of subsidence are, however, reduced by the existing foundations, but subsidence also exerts additional loads on piles.
7. The damage to buildings may lead to economic losses, such as costs of repair, reduction in property value, lawsuits, and negative public opinion.

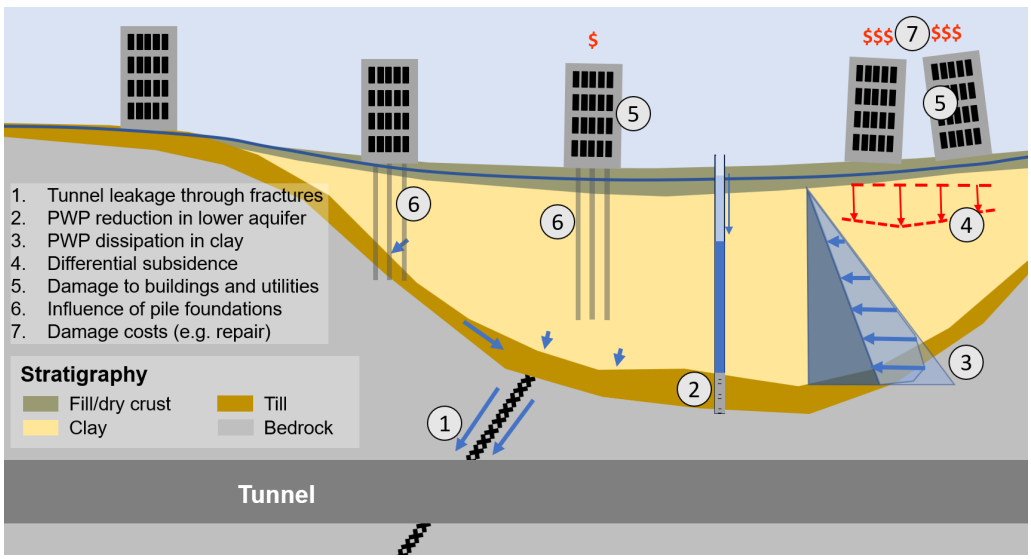

Figure 1.1: *Cause-effect chain of the studied problem (Modified from Sundell 2018).*

Subsidence-induced damage to buildings is often classified according to the severity, ranging from aesthetic damage to loss of function, and ultimately structural damage leading to failure, with much higher economic costs associated with the latter (Burland and Wroth 1974; Eskesen et al. 2004; Sundell et al. 2019b). As such, the predicted (differential or total) settlements need to be translated to actual risk of damage on buildings and utilities. Several damage parameters, which consider the settlement profile and the actual crack-inducing deformations in the building, have been proposed by Burland and Wroth (1974). Moreover, the buildings themselves and their foundations influence the settlement profile by their stiffness and weight, and therefore, the effects of soil-structure interaction should be taken into account when predicting subsidence damage (Potts and Addenbrooke 1997). Such parameters and considerations are commonly used in settlement problems induced by volume loss in tunnelling and localised settlement due to deep excavations, where simplified settlement profiles have been proposed, e.g. Peck (1969) and Hsieh and Ou (1998), often assuming Gaussian shape. However, for large-scale subsidence problems caused by underdrainage in the stratigraphic conditions in Scandinavia, the Gaussian shape is not necessarily valid. Furthermore, the system evolves with time during consolidation and creep processes in the soft clay layers, making the system response dependant on both time and location (4D).

Precautionary and mitigation measures are implemented in several parts of the cause-effect chain, to reduce the damage. In Sweden, groundwater withdrawal by construction is regulated as a water activity under the Environmental Code (*Miljöbalken*), and a permission is granted based on an assessment of potential impacts to groundwater levels and ground deformations. The problem, defined by the cause-effect chain, is both complex and interconnected. Thus, assessments of the potential impacts require advanced models that take into account multiple processes at the system level, especially when it comes to the relationship between groundwater flow and soil deformation (hydro-mechanical coupling), as well as the effect of soil deformation on the buildings and their foundations (soil-structure interaction). In addition, the transient nature of the processes in the soil needs to be accounted for in the analysis of building damage.

In previous projects at Chalmers (Sundell 2018; Merisalu et al. 2021), such holistic modelling frameworks have been proposed. The proposed model chain includes, among others, a stratigraphy model, groundwater model, subsidence and damage model. However, until now, the subsidence and damage models were overly simplified. The subsidence model only considered one-dimensional total settlements based on uncoupled consolidation theory, neglected the effects of creep and soil-structure interaction. In reality, damage is more related to differential than uniform settlement. A highly heterogeneous environment with variable stiffness, stratigraphy, and hydraulic gradients motivates 2D or even 3D hydro-mechanically coupled analysis (Ochoa-González et al. 2018; Sundell 2018; Peduto et al. 2021). Several authors have shown that it is possible to predict subsidence using a hydro-mechanically (HM) coupled 3D model (Yoo 2005; Teatini et al. 2006; Ye et al. 2016; Ochoa-González et al. 2018). The causes for an observed settlement can be many; on-going background settlements caused by previous loading, as a result of the lowering of pore water pressures, or caused by other construction activities nearby. Models that account for creep, or rate-dependency in general, such as Creep-SCLAY1S (Gras et al. 2017; Gras et al. 2018) can be used to model both the ongoing (background) settlements and the additional settlements triggered by consolidation and creep. Together with remote sensing data on displacement rates at the ground surface, background creep simulations can be used for model calibration, but also to identify anomalies that are caused by other loading events (Tornborg et al. 2023; Wikby et al.

2025b). As opposed to the commonly used 1D models, Creep-SCLAY1S accounts for the effects of loading in various directions, benchmarked against both embankments (Amavasai et al. 2018; Amavasai et al. 2022) and deep excavations (Tornborg et al. 2021; Bozkurt et al. 2023; Tornborg et al. 2023). The model captures other important features of natural soft clays, such as anisotropy and destructuration, as necessary for sensitive clays. Moreover, in soft clay deposits with low overconsolidation ratio (OCR), only rate-dependent (creep) models can accurately account for long-term deformations.

Accounting for all aspects of soft clay behaviour at a boundary value level requires computationally demanding large-scale 3D HM coupled models with high spatial and temporal resolution, making them impractical to setup and computationally expensive to run. Therefore, the model chain needs to be parametrised and optimised or simplified. Surrogate models, also called metamodels trained on numerical data from advanced models, are increasingly used to emulate numerical results in a computationally efficient manner (Furtney et al. 2022). In the current work, metamodels have been trained on the non-linear results from 2D Finite Element analyses of representative cross sections to produce the ground settlements at large scale.

Uncertainties related to spatial variability and measurement errors of the hydro-mechanical properties can be significant and should be accounted for (Tahershamsi and Dijkstra 2021). For instance, the determination of the apparent preconsolidation pressure, governed by stress history and complex geo-chemical processes, is uncertain for many cases (Tornborg et al. 2023). In urban settings, the effects of loading and unloading due to construction, excavation and backfill have affected the state of the soil (represented by state variables such as the preconsolidation pressure) to a greater extent than in a greenfield environment. Another uncertain parameter is the hydraulic conductivity of natural clays in different directions.

When it comes to quantifying the damage caused by subsidence, Sundell et al. (2019b) for example considered simplified damage criteria and neglected the soil-structure interaction. Basing the damage estimates on total settlements, as opposed to differential settlements, may overpredict the damage to buildings, depending on the uniformity of the settlement profile (Grant et al. 1974; Prosperi et al. 2023). Neglecting soil-structure interaction, i.e. assuming greenfield conditions, can also (mostly) overpredict the propagation of damage, depending on the relative stiffness of the superstructure and the foundation, the building service load (Franzius et al. 2006). Soil-structure interaction can be considered on an individual building scale by systematic sensitivity analyses where key geometric and stiffness parameters are varied, e.g. the relative stiffness method (Potts and Addenbrooke 1997; Franzius et al. 2006; Korff and Mair 2013), and relating them to the modification factor (relating building and greenfield movements) of specific damage parameters in easy-to-use design charts. Although building responses to drawdown-induced subsidence have been systematically studied (Peduto et al. 2021), such design charts have yet to be provided. Moreover, while the response of piled buildings to subsidence induced by underdrainage has been studied (Rodríguez-Rebolledo et al. 2015), systematic studies of settlement modification factors due to the presence of floating pile foundations have not yet been explored.

1.2 Aims and objectives

The aim of the PhD thesis is to develop a modelling framework to calculate the time-dependent settlements due to underdrainage, and the resulting building damage on a district-to-city scale. The modelling framework should capture relevant time-dependent responses underpinning the cause-effect chain: (1) Background creep settlements, (2) Consolidation and creep in soft natural clay resulting from leakage-induced pore pressure reduction, (3) Impact of piles foundations, and (4) Settlement-induced damage of buildings.

The study investigates the geotechnical and building damage aspects of the cause-effect chain and focuses on, but is not limited to, the conditions found in Gothenburg.

The main objectives for this PhD project are:

1. Development of hydro-mechanically coupled finite element models for simulations of different drawdown scenarios and their effect on spatially distributed time-dependent settlements. To reduce simulation time, the settlements are calculated on 2D cross-sections.
2. Utilisation of the predicted surface settlements from each cross section at a given time to train and validate a metamodel, which calculates the settlements as a function of the hydro-stratigraphy spatially in the whole study area.
3. Validation of the predicted background creep settlements using available data from depth-integrated and surface measurements of settlements (i.e. bellow-hose and InSAR).
4. Estimation of parameter uncertainties important to the consolidation process, e.g. the hydraulic conductivity in different directions and the overconsolidation ratio, as well as their influence on time-dependent settlements, using systematic sensitivity analyses.
5. Development of axisymmetric finite element models to study the influence of pre-existing floating piles on subsidence. The latter model is used to calculate the evolution of time-, clay thickness- and load-dependent neutral planes. This enables to study the modification factors and the interaction levels, used for mapping the modified settlements.
6. Development of an automated building damage model that directly uses the settlement results of the metamodel. The model assesses typically used 2D damage parameters on profiles with longitudinal and latitudinal directions along the area of buildings in the study area.

1.3 Limitations

- The modelled settlements and building damage are assumed to be initiated by a uniform sustained pore pressure drop in the lower (confined) aquifer in the entire model domain, causing consolidation by underdrainage in the clay layer.
- Any settlements caused by past events are only considered in the form of background creep, included in the rate-dependent model.
- The geological and hydromechanical settings relate to the Gothenburg region. However, similar methodology can also be used for other subsiding cities in the world, with different

initial and boundary conditions.

- Early-stage assessment is considered here. For more detailed assessment, e.g. damage assessment of individual buildings, a more detailed numerical framework is required with more information on the initial state of the building damage.
- Uncertainties of the chosen parameters are crudely accounted for in the 2D hydromechanical model based on the distribution of only a few selected parameters. Uncertainties in other stiffness parameters were not considered.
- When building damage is considered, each building is assumed to be initially intact.
- Subsidence also has other consequences, such as damage to utilities and infrastructure, and increased risk of flooding, which are not considered.
- Only soil-structure interaction effects of pre-existing floating piles are considered, while the effects of slab and superstructure are ignored.
- Damage and mitigation costs are not considered.

1.4 Outline of the thesis

The outline of the thesis is presented below:

- In Chapter 2, a review of the cause-effect chain of the problem is discussed to identify the gaps in the chain. The hydromechanical behaviour of clay that is important for subsidence problems is discussed. A review of large-scale hydromechanical models, their advantages and disadvantages, is also included. A section on building damage, how damage is defined and calculated, as well as the current methods for estimating building damage are reviewed. Finally, the response of piles to subsidence is discussed, with a focus on floating piles analysed with the neutral plane method.
- Chapter 3 introduces the site, the local geology, and the construction project, as well as the previous site investigations and models used for the data collection for the studies. It covers briefly the previous work on stratigraphy and groundwater modelling, and introduces the buildings and their foundations and how they were assessed before being accounted for in the building damage and pile model.
- Chapter 4 introduces the methodological development of the research.
- Chapter 5 summarises the overall research (Papers A-E) including the aim of each study, comments on author contribution, and key findings.
- Finally, Chapter 6 discusses the main conclusions and future work.

2 Theoretical background

2.1 Leakage-Subsidence-Damage chain

Underground construction often affects nearby pore pressures, causing possible damage to nearby structures and utilities. The implementation of mitigation measures involves trade-offs between the benefits of the reduced risks and the implementation costs. Erroneous decision-making of such implementation, due to a lack of system understanding of the complexities and uncertainties involved, results in unnecessary costs for society. To facilitate decision support, the system can be understood by a cause-and-effect chain of events (see e.g. Bedford and Cooke 2001), in this case from leakage to the cost of damage (Sundell 2018). This chain for a leaking tunnel in an urban setting is illustrated in Figure 2.1. The time-dependent reduction of pore water pressures is caused by underdrainage at the bottom of a confined aquifer.

The bottom part of Figure 2.1 shows the possible event-specific mitigation measures, as well as an event-tree analysis that describes the triggering factors for the consequent event to occur. The effects of sealing the construction and the infiltration wells are briefly discussed in Section 2.2, whereas stabilisation is not covered in this thesis. The event-tree analysis is simplified to a binary process (Y and N) to improve understanding. This binary process is a simplification, as events can be triggered with magnitudes that vary across space and time, and the subsequent events may respond differently depending on the specific spatio-temporal characteristics of the initial trigger. Additionally, the system is not closed, as other triggering events may occur simultaneously. As an example, the magnitude and extent of the groundwater drawdown due to leakage is a function of several factors including the magnitude of the leakage, the boundary conditions of the hydrogeological system, the water balance and the transmissivity of the aquifers. The triggering factors of the consequent events may not be solely due to the leaking tunnel in question, but also other external sources, such as adjacent subsurface projects or natural (background) creep.

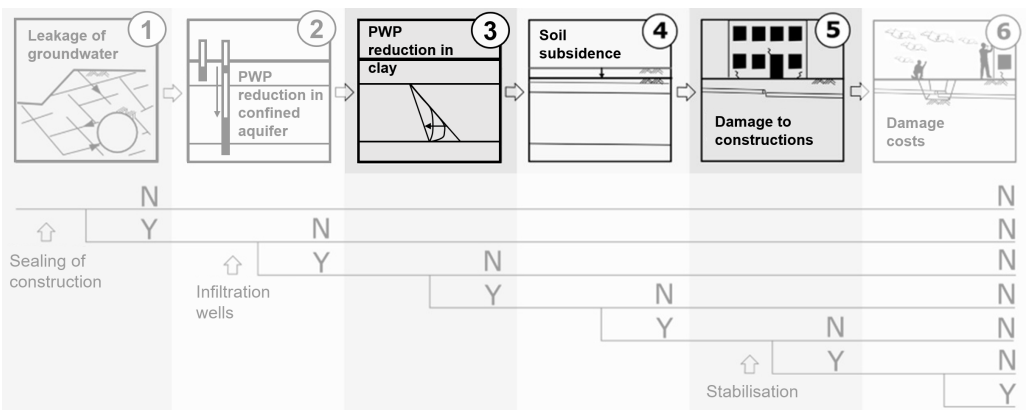

Figure 2.1: *Cause-effect chain (top) with event tree analysis (bottom) including typical mitigation measures (modified from Sundell 2018). PWP = pore water pressure, Y = Yes, N = No. Only parts 3-5 are modelled in this thesis.*

The event tree analysis was used as a basis for the development of a model chain, including a stratigraphy model, groundwater model and a simplified subsidence and damage model that could be probabilistically tied with an economic model. This comprehensive risk framework (Sundell et al. 2019b) was further developed into a probabilistic cost-benefit analysis (Merisalu et al. 2023) in which different design alternatives were evaluated to support decision-making, thus managing the risks of a project. The models proposed in this thesis are intended to replace the simplified subsidence and damage models in the model chain (parts 3-5 in Figure 2.1). Replacement of the models could potentially decrease the risk of erroneous decisions in terms of detecting critical zones with the potential for large or rapid settlements, the interaction between the foundation and the surrounding soil, and more accurate damage assessment based on time-dependent differential, rather than total, settlements.

2.2 Impact of tunnel leakage on pore water pressures

The aquifer system, representing hydrogeological units (i.e. aquifers and aquitards), stacked on top of each other in the typical geological environment in Scandinavia consists of an upper unconfined aquifer, followed by an aquitard (saturated clay) and a lower confined aquifer, see Figure 2.2. These layers and their formation were discussed in more detail in Section 3.1.

The possible extent and magnitude of the reduction in the pore pressures in an aquifer system depends on the water balance (inflow, storage, and outflow to the aquifers). Storage is the amount of water stored in the aquifer that can be released by the change in pore pressure. Because of gravity, the groundwater flows from the higher points in the aquifer system to lower points following Darcy's law. Therefore, if the water balance is changed, such as if a leakage occurs with a certain flow rate, new steady-state (water balance in equilibrium) piezometric levels will eventually be formed.

Figure 2.2(b) shows how the inflow occurs through the fracture zones into the tunnel, causing the pore pressure to drop in the lower aquifer. The leakage into a rock tunnel built in crystalline rock depends on the storage and the hydraulic conductivity of the adjacent fracture zones, and whether the tunnel and the coarse-grained layer above are hydraulically connected; see, e.g. Thörn (2015). To reduce leakage, tunnels are often pre-sealed using grouting techniques, minimizing the hydraulic conductivity in the excavation damage zone. The lowering of the piezometric head in an aquifer in the sub-soil from an extraction/leakage point is, in its simplest form, described as a cone. The extent of the cone of depression is affected by the hydraulic conductivity of the aquifer. Typically, the radial extent of the effects by a leakage of a tunnel or groundwater extraction can be several hundreds of metres (Karlsrud and Sander 1978; Burbey 2002; Huang et al. 2012). The pore pressures in an aquifer can also increase as a result of injection/infiltration in a similar way. As such, infiltration wells are used to counteract the pore pressure reduction in the aquifer. Nevertheless, in this thesis, for the sake of simplicity, a uniform, instant and sustained pore pressure reduction in the lower aquifer is assumed, as the focus is on the time-dependent consolidation of the aquitard (i.e. the soft clay) as a coupled hydro-mechanical process.

The pore pressures in aquifers are typically hydrostatic, due to the high hydraulic conductivity. In saturated clay (aquitard), the initial pore pressure profiles are typically described by a linear interpolation between the pore pressures at the upper and lower boundaries of the aquitard. If the

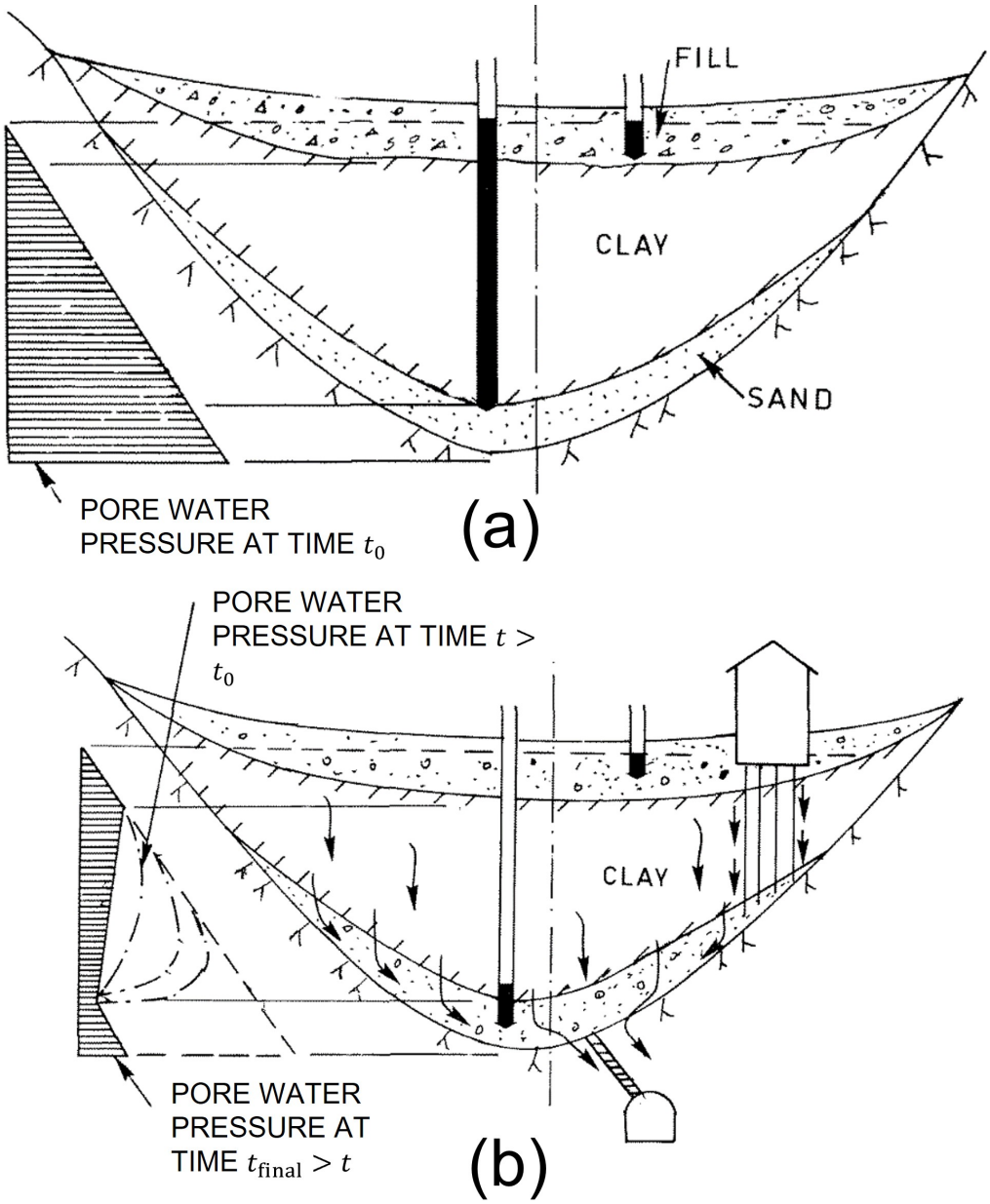

Figure 2.2: *Example of (a) initial conditions and (b) change in pore pressure due to underdrainage (modified from Broms et al. 1976).*

groundwater levels in one of the aquifers changes, there will be delayed pore pressure dissipation in the aquitard due to its low hydraulic conductivity. The flow rate of groundwater towards the aquifer governs the evolving shape of the pore pressure profile. Hence, the pore pressures will reduce immediately at the lower boundary of the clay and the effect will gradually transfer toward the upper clay boundary, causing consolidation (and creep) in the clay due to underdrainage. In final equilibrium, the pore pressure profile can again be described as linear (hydrostatic) from one boundary to the other. The groundwater drawdown can be described as over- or underdrainage, sometimes referred to as top- and bottom-drainage, depending on whether the upper or lower aquifer is affected by the construction activities. In the case of a leaking rock tunnel, underdrainage is most dominant. If hydraulically connected, a change in groundwater levels in the lower aquifer may affect the upper aquifer as well. This happens, for instance, if the drawdown occurs in areas with shallow bedrock outcrops or if end-bearing piles have punctured the aquifer (see Figure 2.2b).

2.3 Hydro-mechanical response of soft natural clays

2.3.1 Consolidation and yielding

The hydromechanical response is important in the consolidation process. The equalisation of pore pressures in clay is a time-dependent process, often represented by Terzaghi's 1D theory, where the flow of water from the pores of the soil is governed by Darcy's law (see e.g. Verruijt 1984). In this theory, the vertical coefficient of consolidation (c_v) is calculated as:

$$c_v[\mathrm{m}^2/\mathrm{s}] = \frac{k_v}{\gamma_w m_v} \tag{2.1}$$

where k_v [m/s] is the vertical hydraulic conductivity (discussed in detail in Subsection 2.3.2), γ_w is the unit weight of water [kN/m^3], and m_v is the coefficient of compressibility. m_v [m^2/kN] is the inverse of the constrained modulus M of the soil, which is dependent of the effective stress level relative to the apparent preconsolidation pressure.

In hydrogeology, a similar formulation is used to relate flow to compressibility via the specific storage (see e.g. Persson 2007):

$$S_s[1/\mathrm{m}] = \gamma_w m_v \tag{2.2}$$

For fully saturated soils, effective stress principle holds, in which a decrease in pore water pressures corresponds to an equal increase in effective stresses, if the total stresses remain constant. Clays typically follow a non-linear effective stress-strain relationship where nearly elastic, stiff, response at pre-yield effective stresses is followed by significantly softer plastic behaviour with increased effective stress post-yield. In one-dimensional loading, as commonly assumed for subsidence, the yield point is represented by the apparent vertical preconsolidation pressure. For other loading paths, the effective stresses at yield depend on the initial anisotropy of the clay (Leroueil et al. 1985).

The main processes affecting the overconsolidation and the general effective stress-strain response is exemplified as in Figure 2.3. The apparent overconsolidation ($OCR = \sigma'_{vc}/\sigma'_{v0}$), where σ'_{v0} and σ'_{vc} are the in situ vertical effective stress and preconsolidation pressure, respectively, can

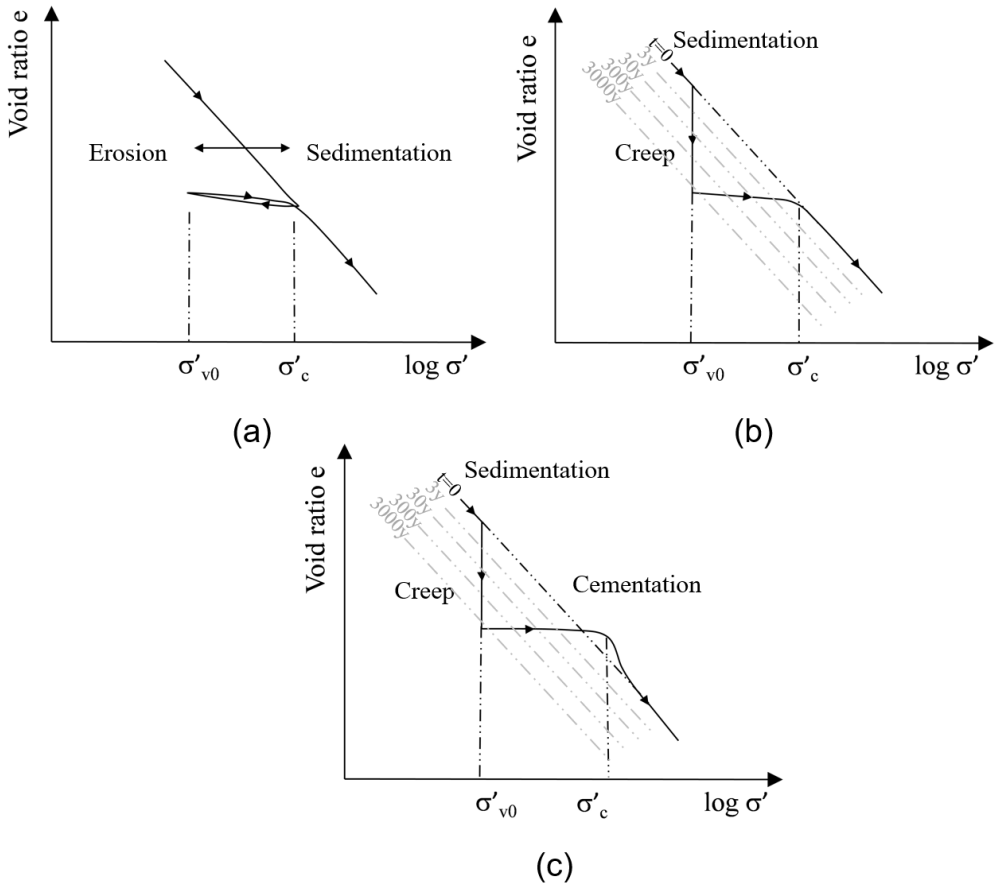

Figure 2.3: *Processes which have affected the apparent overconsolidation. (a) Loading/unloading effects from sedimentation and erosions (or excavation). (b) Decrease in void ratio and increase in the apparent preconsolidation pressure due to creep (with isotach curves). (c) Increase in the apparent preconsolidation due to cementation (modified from Karstunen 2023).*

be attributed to unloading (due to erosion or excavation), creep (ageing) as well as the effects of apparent bonding in sensitive clays (some form of cementation due to mineral or electro-chemical bonding).

The depositional history plays a significant role in the stress-strain response of natural clays. The depositional history started with the sedimentation process in which the effective stresses increased along a virgin compression curve due to the gravitational forces, forming the current preconsolidation pressure (the highest effective stress a soil has experienced) until further sedimentation is discontinued and the deposit has fully consolidated under its own self-weight. Occasional erosion-sedimentation events and groundwater level fluctuations (unloading) may have occurred, depending on the local hydro-geological processes. The memory of the preconsolidation pressure

remains after the erosion process, and the clay becomes over-consolidated as seen in Figure 2.3(a).

Whilst the so-called preconsolidation pressure represents the highest effective stress the clay was ever subjected to (see σ'_c in Figure 2.3a), the apparent, experimentally observed, preconsolidation pressure can be higher due to the effects of creep and ageing.

Figure 2.3(b) illustrates the effect of creep (ageing), defined as time-dependent deformation under constant effective stresses. There has been creep during and after the last ice age for Scandinavian clays. The rate at which creep deformations occur can be explained by the isotach concept (e.g. Bjerrum 1967), shown as grey dashed lines in Figure 2.3(b-c), where each isotach represents a time-dependent isoline parallel to the virgin curve. The creep rate slows down as time passes, often in a semi-logarithmic manner. With continued creep and ageing, the apparent preconsolidation pressure increases with respect of the virgin curve, resulting in overconsolidation. Due to their relatively young depositional history, natural clays in Scadinavia tend to be normally to slightly overconsolidated. If a new load (e.g. a building) is applied on the clay, due to the apparent overconsolidation, the settlement follows the recompression curve before, at the onset of yield, joining the original isotach curve.

Leroueil et al. (1985) showed that during one-dimensional compression of a natural clay there is a unique effective stress-strain-strain rate relationship. From this it follows that the yield stress is dependent on the strain rate, increasing with increasing strain rate. The isotach concept can also be applied to the dependency on strain rate, where each isotach is represented by a unique strain rate (Leroueil et al. 1985).

There are, however, other geochemical processes that affect the apparent preconsolidation pressure. Figure 2.3(c) shows the effect of apparent bonding on the overconsolidation. The apparent bonding results from various geochemical (e.g. cementation) processes occurring over a long time. The apparent bonding develops as long as the clay remains intact, increasing the observed yield stress and providing significant resistance to further deformation. At post-yield loading, this resistance will gradually disappear degrading the stiffness. Consequently, at large deformations, the clay may become completely remoulded (due to gradual destructuration as function of irrecoverable strains), and the actual compression curve converges with the original virgin curve. Complete destructuration occurs usually at very large stress/strain levels, not experienced in most engineering applications (Leroueil and Vaughan 1990).

The stress-strain response of a natural (structured) clay is different from its response in its intrinsic (destructured) state. Typically, the influence of apparent bonding is studied using a comparison of test results from intact and remoulded samples. In Swedish practice, the initial amount of bonding is estimated by sensitivity (S_t), defined as the ratio between the peak undrained shear strength of an intact sample and the undrained shear strength in its remoulded state. This data is often obtained from a fall cone test.

Natural clays are also characterised by anisotropic strength and deformation properties that could be important to consider in problems with various load directions (e.g. extension, shearing and compression). For the problem of regional subsidence, we mainly consider 1D compression for greenfield conditions which yet entails significant shear strains, while additional shearing occurs at the pile-soil interface.

2.3.2 Hydraulic conductivity

Hydraulic conductivity is one of the governing properties for the rate of consolidation and can be highly anisotropic. Fully saturated natural (sensitive) clays have a very low hydraulic conductivity, between 10^{-9} and 10^{-10} m/s. In coarse grained materials, the current void ratio mainly governs the hydraulic conductivity but plays a minor role in fine grained soils (clays). However, a change in the void ratio due to volumetric strains changes the hydraulic conductivity both in coarse- and fine-grained soils.

Hydraulic anisotropy, defined as the ratio between horizontal and vertical hydraulic conductivity, is governed by the microstructure of the soil. In practice, the hydraulic anisotropy is mainly affected by the degree of varving. A varved deposit has alternating thin horizontal layers of clay and silt (or sand), enabling faster consolidation in the horizontal direction. The natural clays in the Gothenburg region were sedimented in cold marine (saline) environment and therefore contain relatively little varving.

The hydraulic conductivity of clays is lower in the vertical direction, which has consolidated due to the self-weight of the material above. For lacustrine clays, the anisotropy can be as high as 14 (DeGroot and Lutenegger 1994), whereas for marine clays it is significantly lower (around 2). The hydraulic anisotropy of marine clays has been studied by many authors, as summarised in Table 2.1.

Regarding the homogeneous marine clays in Sweden, Larsson (1981) could not determine the anisotropy in hydraulic conductivity due to poor quality measurements and therefore assumed it to be equal to 1. The marine clays of Singapore, on the other hand, have a hydraulic anisotropy as large as 2. In addition to varving, on a large scale in the field, the anisotropy is also influenced by the occurrence of sand and silt lenses in the clay layers. If hydraulically connected to a leaking aquifer, such features can significantly speed up consolidation.

2.3.3 Sources of error when measuring properties of clay

There is a large uncertainty in the determination of consolidation properties of sensitive clays. In general, there are three sources of uncertainties in determination of soil properties; inherent soil variability, measurement uncertainty and transformation uncertainty (Phoon and Kulhawy 1999b).

The inherent soil variability is an aleatory uncertainty meaning that it cannot be reduced. The other two, however, are epistemic uncertainties and can be reduced with increased information.

Table 2.1: Hydraulic anisotropy of some marine clays.

Soil	Reference	Hydraulic anisotropy
Marine clays	Olson and Daniel (1981)	1-1.5
Marine clays	Tavenas et al. (1983)	1.1-1.15
Kaolin	Al-Tabbaa and Wood (1987)	1
Bothkennar clay	Leroueil et al. (1992)	1.5
Swedish clay	Larsson (1981)	1
Singapore clay	Win et al. (1998)	2

Increased information by more (high quality) sampling and testing may reduce the uncertainty. Reducing epistemic uncertainties is, however, costly and, as a result, the quality of the data on which parameter determination is based is often compromised.

For example, the determination of the apparent preconsolidation pressure of a natural clay is influenced by many sources of uncertainty, e.g. heterogeneous in-situ conditions, disturbance during sampling, transportation and sample preparation, ageing, disturbance during laboratory testing, temperature, loading sequence, as well as the choice of the evaluation method.

Measurement uncertainty due to sample disturbance has, for example, been studied by Karlsson et al. (2016) for Swedish Utby clay, demonstrating how the sampling technique affects the evaluated values for the apparent preconsolidation pressure. The difference between the standard piston ST-II samples and the much larger mini-block samples could be as much as 30%. This is because the sampling and preparation of the sample can significantly alter the microstructure and saturation of the clay; all of which affect the apparent preconsolidation pressure. The unloading effects after sampling is another source of error.

Errors can also be induced by the type of testing method used to determine the consolidation properties of a clay sample. The most common types of oedometer tests are the incrementally loaded (IL) and the constant-rate-of-strain (CRS) oedometer tests. The preconsolidation pressure from a CRS test is rate-dependent, and so not choosing the right strain rate is a common source of error, studied by Leroueil et al. (1985). As the strain rates increases, the determined value for the apparent preconsolidation consolidation also increases. Leroueil et al. (1985) stressed that the difference in the strain rate between the field and the laboratory could be significant, and thus a sufficiently low strain rate should be used.

Transformation uncertainties are introduced when field or laboratory measurements are transformed into design soil properties using empirical methods or other correlations (Phoon and Kulhawy 1999a). The apparent preconsolidation pressures determined from oedometer tests are subject to some uncertainty, particularly if using semi-log plots, and this is another source of error (Boone 2010).

Various evaluation methods have been proposed to quantify measurement errors, e.g. Larsson et al. (2007) or Lunne et al. (2006). In Larsson et al. (2007) approach, the natural water content is plotted against the volumetric strains at reconsolidation, ε_{vol}. ε_{vol} is retrieved from oedometer tests and is defined as the difference between the intercept (strain at zero effective stress) of the line corresponding to the flattest part of the oedometer curve drawn from the apparent preconsolidation pressure, and the strain at the apparent preconsolidation pressure. In Lunne et al. (2006), the change in the corresponding void ratio is examined instead, with the in situ effective stress as the reference.

2.4 Modelling subsidence

2.4.1 Large-scale hydro-mechanical modelling

Numerous problems induced by large-scale subsidence worldwide (Bagheri-Gavkosh et al. 2021) have led to the development of numerical models. More advanced models have been developed to better understand the processes in the underground that cause subsidence, predict future trends,

and thus contribute to better groundwater management (Guzy and Malinowska 2020).

In simple terms, most numerical models combine (i) a groundwater flow calculation and (ii) a settlement calculation. More precisely, the balance equation for force equilibrium and the storage equation for mass conservation of water and solids need to be solved. For consolidation analysis, a coupling term is introduced in the storage equation, so that excess pore pressures are generated from a change in volume (see e.g. Bear and Verruijt 1987). The Finite Element Method is most commonly used to solve this system of differential equations in space and time. When an uncoupled approach is adopted, the storage equation is simplified to allow the equations to be solved independently from the equilibrium equations, whereas for a coupled approach, the complete system of equations are solved iteratively during each time step. It should be noted that in addition to solving the balance equations in each time (or load) step, the increment in (effective) stress and the incremental stiffness matrix must also be computed if the soil is not considered linear elastic. For further details (see e.g. Carter et al. 1979). The constitutive models used in this research will be discussed in Subsection 2.4.2.

In the hydrogeological modelling community, MODFLOW (Modular finite-difference groundwater flow model, McDonald and Harbaugh 1988) is commonly used. MODFLOW uses a finite-difference scheme to solve the storage equation and is specifically designed to allow simulation of groundwater systems over large spatial domains in 3D or for very large domains (km) by exploiting a depth-averaged 2D approach.

Tailor-made packages for land subsidence have been created and implemented in MODFLOW, e.g. SUB (Hoffmann et al. 2003), SUB-WT (Leake and Galloway 2007), SUB-CR (Kooi and Yudhedha 2018), which in the later versions also incorporate more advanced constitutive relations for the soil (elastoplasticity and viscoelasticity). A limitation of these packages is that they all assume uncoupled 3D flow and 1D deformation. Large-scale settlement analyses have previously been performed by, e.g. Teatini et al. (2006), Calderhead et al. (2011), Shen and Xu (2011), Ochoa-González et al. (2013), Mahmoudpour et al. (2016), Ye et al. (2016), Ochoa-González et al. (2018), Li et al. (2019), Sundell et al. (2019a), and Bootsma et al. (2020).

A summary of modelling techniques for subsidence is shown in Table 2.2. Apart from Mahmoudpour et al. (2016), Sundell et al. (2019a), and Bootsma et al. (2020), most of these applications used the Finite Element Method. Shen and Xu (2011) used both FE and FD, using FE for the spatial analyses and FD for the time-dependent analyses.

A heterogeneous subsurface environment and drawdown that impacts at large distances from the source of leakage motivates 2D or even 3D coupled hydro-mechanical deformation analyses. Although Ye et al. (2016) showed that a 1D deformation model is adequate for cases where horizontal displacements are small in magnitude, Ochoa-González et al. (2018) argued that in cases of non-uniform soil and/or inclined stratigraphy, heterogeneity, fissuring, or where hydraulic gradients are large, the problem can only be represented by a 3D model. Table 2.2 shows that such coupled 3D models already exist. However, the implementation of such modelling strategy on a large scale (km) requires a large number of elements to reach an acceptable precision, as well as relatively small time steps to accurately model the pore pressure changes and deformations with time, making them computationally demanding. Computational efficiency is a must for impact modelling in which uncertainties in the system and loading scenarios need to be accounted for by running a large number of simulations. Therefore, the models have been simplified in the coupling

Table 2.2: List of large scale analyses of drawdown-induced subsidence using a 3D groundwater model with deformation model and their assumptions.

Case	Numerical scheme	HM coupling	Subsidence model	Clay model
Sundell et al. (2019a)	SE	No	1D	EP
Teatini et al. (2006)	FE	Yes	3D	E
Calderhead et al. (2011)	FE	No	1D	EP
Wu et al. (2010)	FE	Yes	1D	EVP
Shen and Xu (2011)	FE/FD	Yes	1D	E
Ochoa-González et al. (2013)	FE	Yes	3D	E
Ye et al. (2016)	FE	Yes	3D	EP
Mahmoudpour et al. (2016)	FD	No	1D	EP
Ochoa-González et al. (2018)	FE	Yes	3D	E
Li et al. (2019)	FE	Yes	3D	HB
Bootsma et al. (2020)	SE	No	1D	EVP
This research	FE	Yes	2D	EVP

HM = Hydromechanical, A = Analytical, FD = Finite Difference, FE = Finite Element, SE = Semi-empirical, E = Elastic, EP = Elastoplastic, EVP = Elastic viscoplastic, HB = Hyperbolic (Non-linear Elastic)

between groundwater flow and subsidence (e.g. Sundell et al. 2019a; Bootsma et al. 2020) or alternatively by introducing a surrogate model as presented in this work (Haaf et al. 2024).

2.4.2 Creep-SCLAY1S model in triaxial space

Creep-SCLAY1S (Gras et al. 2017; Gras et al. 2018) is an extension of SCLAY1 (Wheeler et al. 2003), SCLAY1S (Karstunen et al. 2005) and Creep-SCLAY1 (Sivasithamparam et al. 2015). Creep-SCLAY1S is an advanced elasto-viscoplastic model that incorporates effects of initial and evolving anisotropy, potential destructuration of the initial bonding, as well as rate-dependency. SCLAY1S is the elastoplastic rate-independent version of Creep-SCLAY1S, originally proposed by Karstunen et al. (2005).

The Creep-SCLAY1S model has been shown to accurately replicate the response of natural clays and has been validated against field measurements in several geotechnical problems, such as embankments (Amavasai et al. 2018; Amavasai et al. 2022) and deep excavations (Tornborg et al. 2021; Bozkurt et al. 2023; Isaksson and Dijkstra 2025).

The model assumes the following:

$$\dot{\varepsilon_v} = \dot{\varepsilon_v^e} + \dot{\varepsilon_v^c} \qquad\qquad \dot{\varepsilon_d} = \dot{\varepsilon_d^e} + \dot{\varepsilon_d^c} \tag{2.3}$$

where $\dot{\varepsilon^e}$ is the elastic incremental strain and $\dot{\varepsilon^c}$ is the viscoplastic (creep) incremental strain. The subscripts v and d stand for the volumetric and deviatoric components, respectively. The elastic terms are calculated as:

$$\dot{\varepsilon}_v^e = \frac{\dot{p'}}{K} \qquad\qquad \dot{\varepsilon}_d^e = \frac{\dot{q}}{3G} \tag{2.4}$$

where p' and q are the (time) increments of mean and deviatoric effective stresses, respectively, and K and G are the (effective stress dependent) elastic bulk and shear moduli, respectively.

Creep-SCLAY1S incorporates three reference surfaces; the intrinsic compression surface (ICS), the current stress surface (CSS), and the normal consolidation surface (NCS). These surfaces are inclined at an angle α to represent the initial anisotropy of the fabric, resulting from K_0 loading history of soft natural clays. The surfaces are plotted in the $p' - q$ plane in Figure 2.4.

Normal Compression Surface (NCS) is the rate-dependent bounding surface between small and large creep strains. The imaginary ICS is adopted to include the effect of bonding, and represents the imaginary yield surface for a remoulded sample with same void ratio and fabric. Although ICS and NCS are of the same shape, the size of ICS is smaller than NCS as follows:

$$p_m{}' = p_{mi}{}'(1 + \chi) \tag{2.5}$$

where χ represents the amount of bonding in the current state.

The model assumes that there is no purely elastic region. CSS is used to represent the current state of effective stresses. The relative size of the surfaces can be expressed as:

$$p'_{size} = p' + \frac{(q - \alpha p')^2}{(M(\theta_\alpha)^2 - \alpha^2)\, p'} \tag{2.6}$$

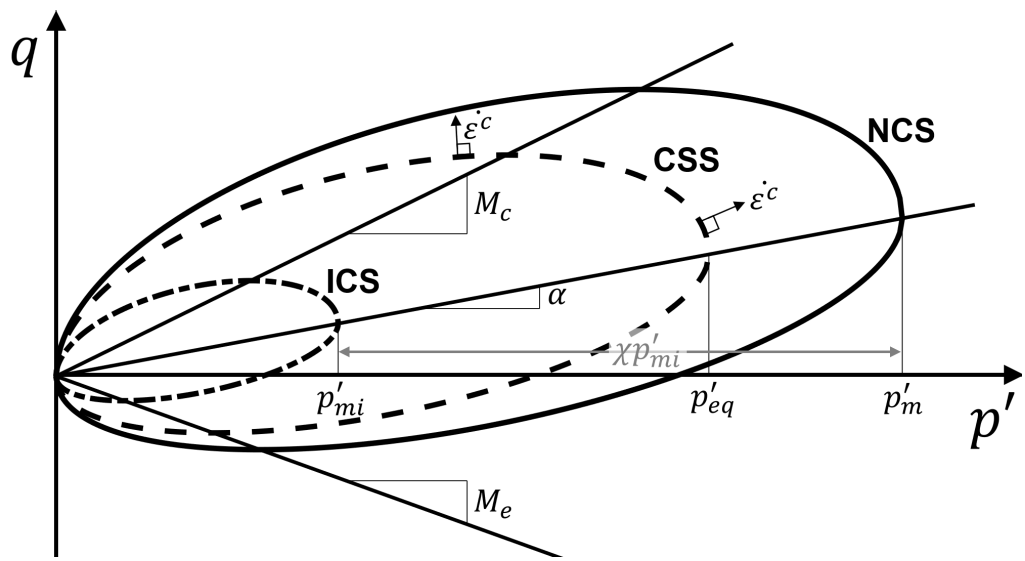

Figure 2.4: *Creep-SCLAY1S reference surfaces in the $p' - q$ plane (modified from Gras et al. 2018).*

where p'_{size} defines the size of the surfaces where $size = mi, eq, m$ for ICS, CSS and NCS respectively. p'_m is the projection of the maximum preconsolidation pressure on the hydrostatic axis, p'_{mi} is the equivalent projection of the intrinsic preconsolidation pressure, and p'_{eq} is representing the current effective stress state. $M(\theta_\alpha)$ is the stress ratio at critical state with Lode angle (θ_α) dependency for the surface to be continuous at any stress state.

The ultimate values M in triaxial compression and extension are noted with M_c and M_e. M_c is the stress ratio at critical state in compression and M_e is the stress ratio at critical state in extension. α_0 is the initial anisotropy that defines the inclination of the three surfaces ICS, CSS, and NCS.

Flow rule

Creep-SCLAY1S assumes associated flow rule which means that the direction of the flow is normal to CSS (see Figure 2.4. The expansion of CSS is due to viscoplastic (creep) strains. The change in the volumetric and deviatoric creep strains are given by:

$$\dot{\varepsilon}^c_v = \dot{\Lambda}\frac{\partial p'_{eq}}{\partial p'} \qquad\qquad \dot{\varepsilon}^c_d = \dot{\Lambda}\frac{\partial p'_{eq}}{\partial q} \tag{2.7}$$

where $\dot{\Lambda}$ is the viscoplastic multiplier which is defined as:

$$\dot{\Lambda} = \frac{\mu^*_i}{\tau}\left(\frac{p'_{eq}}{(1+\chi)p'_{mi}}\right)^{\frac{\lambda^*_i-\kappa^*}{\mu^*_i}}\left(\frac{M_c^2-\alpha^2_{K_0^{NC}}}{M_c^2-\eta^2_{K_0^{NC}}}\right) \tag{2.8}$$

$$\mu^*_i = \frac{\Delta\varepsilon_v}{\Delta \ln t} \tag{2.9}$$

is the modified intrinsic creep index and should either be derived from incrementally loaded (IL) oedometer tests on intact samples at high stress level where any bonding is completely eradicated, or it should be derived from tests conducted on reconstituted samples, see Figure 2.5.

$$\lambda^*_i = \frac{\Delta\varepsilon_v}{\Delta \ln p'} \tag{2.10}$$

is the modified intrinsic compression index derived from IL tests on intact samples at high stress level or on reconstituted samples, and κ^* is the modified swelling index derived from the unloading/reloading curve on $\varepsilon_v - \ln p'$ plot, see Figure 2.5.

Hardening laws

Creep-SCLAY1S consists of three hardening laws; isotropic hardening law, rotational hardening law, and a hardening law related to the degradation of bonding with creep strains. All come with related hardening parameters. Initially, the amount of bonding is represented by $\chi = \chi_0$ and the anisotropy by $\alpha = \alpha_0$ for the in-situ conditions of a lightly overconsolidated clay. Once the size of NCS is defined by the apparent preconsolidation pressure, we can define the size of ICS.

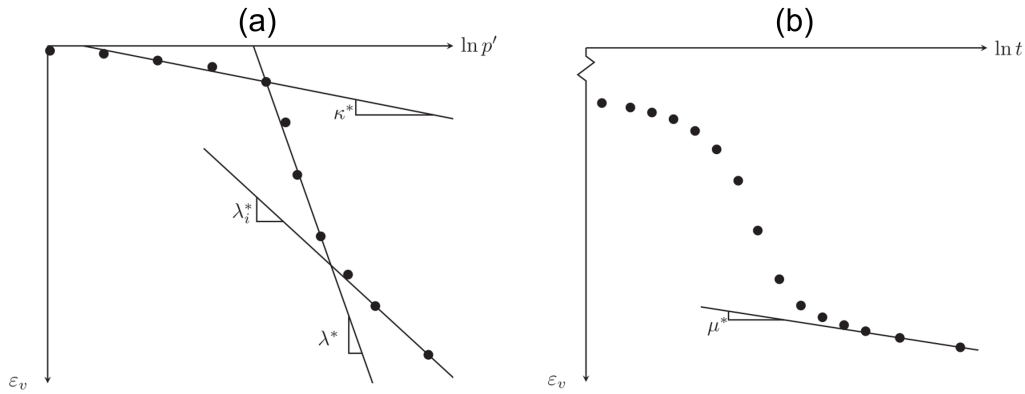

Figure 2.5: *Definition of κ^*, λ_i^* (a) and μ_i^* (b). (From Gras et al. 2017).*

The isotropic hardening law describes the change in size of the ICS, i.e. the change in the intrinsic isotropic preconsolidation pressure as:

$$\dot{p}'_{mi} = \frac{p'_{mi}}{\lambda_i^* - \kappa^*} \dot{\varepsilon}_v^c \tag{2.11}$$

The rotational hardening law stems from the S-CLAY1 model proposed by Wheeler et al. (2003) and relates to the change in anisotropy:

$$\dot{\alpha_d} = \omega \left(\left[\frac{3\eta}{4} - \alpha_d \right] \langle \dot{\varepsilon_v^c} \rangle + \omega_d \left[\frac{\eta}{3} - \alpha_d \right] \left| \dot{\varepsilon_d^c} \right| \right) \tag{2.12}$$

where $\langle\rangle$ is the Macaulay brackets, which ensures that the model predictions remain sensible even when $\dot{\varepsilon_v^c}$ is negative during yielding on the dry side of the critical state line ($\eta > M(\theta_\alpha)$). ω is the absolute effectiveness of rotational hardening, and ω_d is the relative effectiveness of rotational hardening.

Lastly, the hardening law related to the bond degradation is defined by:

$$\dot{\chi} = -\xi \chi \left(\left| \dot{\varepsilon_v^c} \right| + \xi_d \dot{\varepsilon_d^c} \right) \tag{2.13}$$

where ξ is the absolute rate of destructuration, and ξ_d is the relative rate of destructuration.

Some of the drawbacks of the model include neglection of non-linear small-strain stiffness in the "elastic" (OC) region. Such formulation was eventually added to the model, called Creep-SCLAY1Ss, by Tahershamsi et al. (2023). For actual numerical simulations using 2D FE analysis, the generalised version of the model needs to be adopted, and invariants can no longer be used (see Gras et al. 2017; Gras et al. 2018).

2.5 Building damage

2.5.1 Damage definitions and damage categories

Before discussing the different methods for assessing building damage, stakeholders in a geotechnical engineering project must understand and agree on what defines damage. A well-defined system of categorising damage reduces the risk of a project falling subject to claims for excessive damage. In general, there are three broad categories of building damage (Skempton and MacDonald 1956):

- *Aesthetic* or *architectural* damage, only affecting the appearance of the building, such as superficial cracks.
- *Functional* or *serviceable* damage, affecting both appearance and use of the building. Such damage include deeper cracks, jamming of doors and windows.
- *Structural* damage, affecting the stability of the building. These include certain risks of failure of the building elements.

However, there are some general concerns with these broad categories.

Firstly, *serviceable* and *structural* damage are difficult to distinguish. Serviceability depends on the function of the building, the subjective views of the users and owners, as well as economic factors such as devaluation of a building and insurance cover. Even at similar levels of damage, subjective judgment of the severity and causes of damage can vary considerably (Pool 1995).

Secondly, reporting damage is often insufficient to describe the state of serviceability and stability. Statements such as "extensive cracking on interior walls" are often the only description of damage given for a property (Pool 1995).

Burland et al. (1977) hence suggested a consistent and universal system of criteria for damage based on visual damage and ease-of-repair, see Table 2.3. Instead of the three broad categories described above, there are now six categories (ranging from D0 to D5). In general, D0-D2 responds to aesthetic, D3-D4 to functional damage, and D5 to structural damage. The approximate crack width and the number of cracks are included as indicators of the typical severity of the damage. Originally, the table was developed for masonry buildings and not for e.g. concrete buildings. However, since masonry buildings are some of the most sensitive buildings to deformation, with the mortar representing the weakest link, the table is often used for other types of facades as well.

It should be noted that cracks can also develop from other sources than settlements, including internal shrinkage or swelling, structural creep, corrosion or decay, differential thermal movements in dissimilar materials, or poor detail design or workmanship (Burland 1995; Pool 1995). However, moderate (and more severe) damage is usually caused by settlements.

2.5.2 Empirical methods

The evaluation of building damage can be analytically assessed through empirical methods (EM) or semi-empirical methods (SEM). SEMs include a theoretical component (usually beam theory) used for calculation of the damage parameter. Table 2.4 summarises some common methods, discussed in the following.

Table 2.3: Classification of visible damage. Ease-of-repair is highlighted in bold (modified from Burland et al. 1977)

Degree of damage	Description of typical damage*	Approximate crack width [mm]
D0 (Negligible)	Hairline cracks	<0.1†
D1 (Very slight)	**Fine cracks easily treated during normal redecoration.** Perhaps isolated slight fracture in building. Cracks in exterior brickwork visible upon close inspection.	0.1-1†
D2 (Slight)	**Cracks easily filled. Re-decoration probably required.** Several slight fractures inside building. Exterior cracks visible, some repointing may be required for weathertightness. Doors and windows may stick slightly.	1-5†
D3 (Moderate)	**Cracks may require cutting out and patching. Recurrent cracks can be masked by suitable linings. Tuck-pointing and possibly replacement of a small amount of exterior brickwork may be required.** Doors and windows sticking. Utility service may be interrupted. Weathertightness often impaired.	5-15†(or a number of cracks>3)
D4 (Severe)	**Extensive repair involving removal and replacement of sections of walls, especially over doors and windows required.** Windows and door frames distorted, floor slopes noticeably. Walls lean or bulge noticeably, some loss of bearing in beams. Utility service disrupted.	15-25†but depends on a number of cracks.
D5 (Very severe)	**Major repair required involving partial or complete re-construction.** Beams lose bearing, walls lean badly and require shoring. Windows broken by distortion. Danger of instability.	>25†but depends on a number of cracks.

* In assessing the degree of damage account must be taken of its location in the building or structure.
† Crack width is only one aspect of damage and should not be used on its own as a direct measure of it.

Table 2.4: List of methods to quantify settlement-induced building damage. EM = Empirical method, SEM = Semi-empirical method

Method	Type	Reference(s)
Angular distortion	EM	Skempton and MacDonald (1956) and Bjerrum (1963)
Deflection ratio	EM	Polshin and Tokar (1957)
Limiting Tensile Strain Method	SEM	Burland and Wroth (1974)
State-Of-Strain Method	SEM	Boscardin and Cording (1989) and Son and Cording (2005)
Laminate Beam Model	SEM	Finno et al. (2005)
Strain Superposition Method	SEM	Boone (1996)
Thick Plate model	SEM	Namazi and Mohamad (2013)

Empirical methods for building damage are determined by relating the observable movements in the foundation and damage (crack propagation), but do not tie the internal strains through beam theory to the damage. Only calculating settlements is not sufficient, hence a variety of deformation parameters derived from the calculated settlements along the building can be used instead (Burland and Wroth 1974) as visualised in Figure 2.6:

- Total settlement (S) is the downward displacement of the building.
- Differential settlement (ΔS) is the difference in the settlements between two reference points.
- Rotation/slope (θ) is used to describe the change in gradient of the straight line joining two reference points.
- Tilt (ω) describes the rigid body rotation of the entire building or a well-defined part of it.
- Angular distortion/relative rotation (β) describes the rotation of the straight line joining two reference points relative to the tilt.
- Angular strain (α) is the subtraction of two slopes (in the same direction) joining at one arbitrary point. It is positive if it produces sag, and negative if it produces hog. In Figure 2.6 we see an example of sagging mode. If zero, angular strain also indicates that it is an inflection point, i.e. a boundary point between hogging and sagging.
- Relative deflection (Δ) is the maximum displacement relative to the straight line connecting two reference points a distance L apart. Relative sag produces upward concavity, for which Δ is positive. Relative hog produces downward concavity for which Δ is negative.
- Deflection ratio (Δ/L) is a description of the curvature of a segment L.

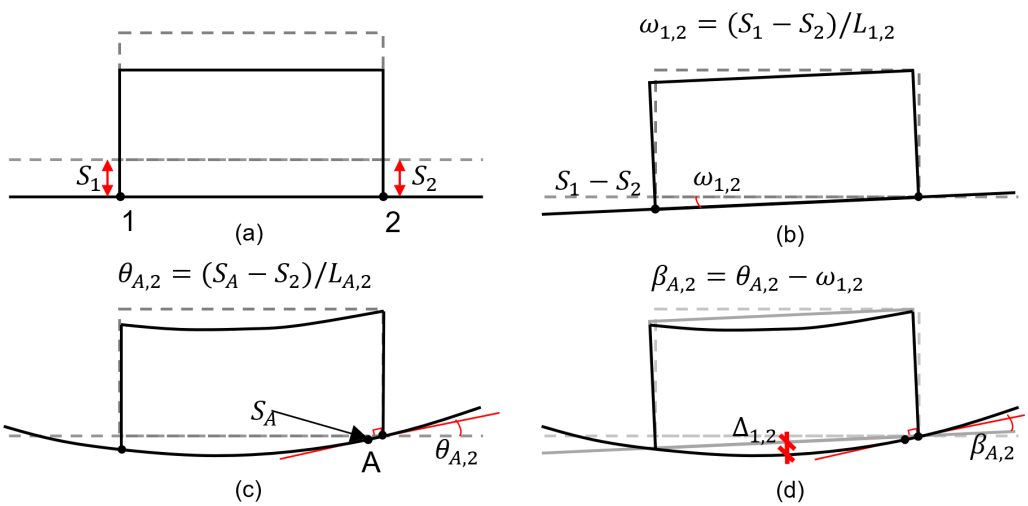

Figure 2.6: *Empirical building deformation parameters; (a) total settlements, (b) rigid body tilt, (c) rotation, (d) angular distortion and relative deflection (modified from Wikby et al. 2024).*

Skempton and MacDonald (1956) and Polshin and Tokar (1957) were among the first to relate the formation of cracks in the building to the distortion of the building, namely β or Δ/L. As an example, Skempton and MacDonald (1956) concluded that for $\beta > 1/300$, visible cracking is likely, and that for $\beta > 1/150$, structural damage is probable. They suggested $\beta = 1/500$ as a design criterion providing some factor of safety against any cracking. For load-bearing brick walls, $\beta > 1/1000$ should be avoided. Since then, several limiting values for β have been proposed, as presented in Table 2.5. Some values have been confirmed by e.g. Bjerrum (1963) and Grant et al. (1974), and are even suggested in Eurocode 7 (EN 1997-1 2005). The limits are generally dependent on the severity of damage and the building type (including structural type and materials used), but not on geometry, loading conditions, previous cracking etc. In general, as for structural types, load-bearing brick walls are more vulnerable than framed walls. Some of these uncertainties can be accounted for by the semi-empirical methods mentioned below.

For first-stage damage assessments, the simpler criterion by Rankin (1988) can be used (Mair et al. 1996), allowing multiple buildings to be screened relatively quickly. The approach uses $\theta = 1/500$ and $S = 10mm$ as limiting values, where buildings that exceed them would be assessed in a second more detailed stage.

The dependency of settlement on damage to buildings (and other structures) can be highly uncertain, due to the large variability in e.g. geometry, material, foundation and structural type, settlement pattern, condition and age (Burland et al. 1977; Wahls 1981; Prosperi 2025). To overcome some of the uncertainties, damage can be considered as a probabilistic function of a damage parameter. Such functions are called empirical fragility curves (Zhang and Ng 2005; Peduto et al. 2017; Peduto et al. 2019; Peduto et al. 2021; Prosperi et al. 2023; Prosperi et al. 2025). Fragility curves rely on significantly large databases of buildings that have been damaged at various degrees and that are properly categorised (e.g. piled/shallow foundations, masonry/framed structures, age etc.).

Table 2.5: Recommended limits using angular distortion as criteria.

Building and damage type	β_{lim}	Reference
Cracking of sensitive brick structures	1/1000	Skempton and MacDonald (1956)
Cracking of other structures	1/500	Skempton and MacDonald (1956)
Structural damage of structures	1/150	Skempton and MacDonald (1956)
Danger to frames with diagonals	1/600	Bjerrum (1963)
Safe limit for no cracking	1/500	Bjerrum (1963)
First cracking in panel walls	1/300	Bjerrum (1963)
Visible tilting of high, rigid walls	1/250	Bjerrum (1963)
Danger of structural damage	1/150	Bjerrum (1963)
Unreinforced load bearing wall (hogging)	1/2000	Meyerhof (1982)
Unreinforced load bearing wall (sagging)	1/1000	Meyerhof (1982)
Cracking of infilled frames	1/500	Meyerhof (1982)
Cracking of open framed structures	1/250	Meyerhof (1982)
Likely limit range	1/2000-1/300	EN 1997-1 (2005)
Limit for most structures	1/500	EN 1997-1 (2005)
Structural damage	1/150	EN 1997-1 (2005)

Zhang and Ng (2005) showed that a log-normal distribution can be attributed to such curves. These databases were originally constructed from field measurements, however, even when aggregating extensive sample sizes within comparable clusters, substantial variability remains, attributed to the inherent lack of control in field sampling conditions. Lately, these fragility curves have been numerically derived, using non-linear crack models, to constrain the sample typology while keeping the possible outcomes variable (Prosperi et al. 2025), thereby reducing their standard deviation. Other advantages include improved sample control and the ability to capture the moment of damage. So far, fragility curves have not been created for Swedish conditions, and were thus not considered in this thesis.

2.5.3 Semi-empirical methods

Semi-empirical methods are also dependent on empirically derived limiting values for analytically derived properties (often tensile strains) from beam models (for 2D calculations). The semi-empirical methods are summarised in Table 2.6, where geometry refers to the deformation geometry for different structural types. The Limiting Tensile Strain (LTSM) and State-Of-Strain (SOSM) methods are explained in the following. In addition, Laminate Beam Model (LBM) (Finno et al. 2005), Strain Superposition Method (SSM) (Boone 1996; Boone et al. 1999) and Thick Plate Model (TPM) (Namazi and Mohamad 2013) have been reported in the literature but were left out due to their overly complicated formulations.

Critical tensile strain concept

The critical tensile strain concept was introduced by Polshin and Tokar (1957). It assumes that the onset of cracking on facade wall is related to a certain amount of tensile strain in the building induced by settlements, known as the critical tensile strain. This concept was further developed by Burland and Wroth (1974) who understood that bending tensile strains on a structural element produce bending cracks in a principal direction perpendicular to the lower wall edge, and that shearing tensile strains yield cracks that run diagonally, see Figure 2.7. Vertical cracking can also occur due to horizontal tensile strains, which should not be neglected in cases involving deep excavations (Boscardin and Cording 1989; Burland 1995). The critical tensile strain concept is widely used in semi-empirical theories.

Table 2.6: List of semi-empirical methods and their considerations. LTSM = Limiting Tensile Strain Method, LBM = Laminate Beam Model, SSM = Strain Superposition Method, TPM = Thick Plate Model.

Can consider/Method	LTSM	LBM	SSM	TPM
Building stiffness	X	X	X	X
Structural type			X	
Influence of several floors		X		
3D deformation				X

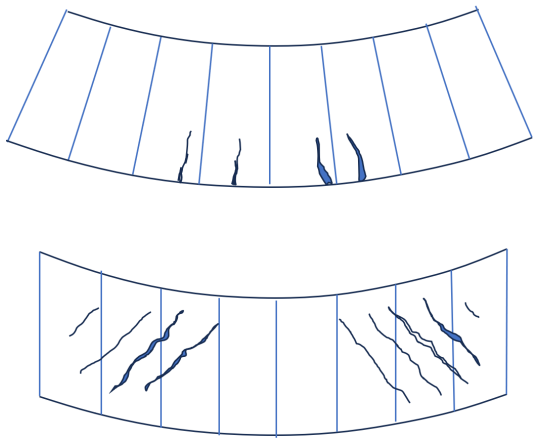

Figure 2.7: *Bending (top) and diagonal (bottom) cracking for sagging mode (modified from Burland and Wroth 1974).*

Limiting Tensile Strain Method (LTSM)

The theory behind the deep beam model or the simple beam model was first introduced by Timoshenko (1957), where a rectangular beam with length L and height H deflects due to a central point load in 2D plane. In this model, the wall of a building is idealised as a rectangular, weightless, isotropic beam with linear elastic (E) and shear (G) moduli, respectively. Depending on its L-to-H ratio, the beam will not only experience stresses from bending, as is assumed in the Euler-Bernoulli equation, but some of the stresses will translate into shear stresses. The deflection ratio Δ/L of a simply supported beam with a central point load P is:

$$\frac{\Delta}{L} = \frac{PL^3}{48EI}(1 + \frac{18I}{L^2H}\frac{E}{G}) \tag{2.14}$$

where L is the length of the deflected section of the beam, and I is the second moment of area [m^4].

Burland and Wroth (1974) combined the critical tensile strain concept and the deep beam analogy into what is now known as Limiting Tensile Strain method (LTSM). They replaced P for tensile strain ε in Equation 2.14, which was developed into two equations, one for pure bending and one for pure shearing, respectively:

$$\frac{\Delta}{L} = (1 + \frac{HL^2}{18I}\frac{G}{E})\varepsilon_{d,max} \tag{2.15}$$

$$\frac{\Delta}{L} = (\frac{L}{12t} + \frac{3I}{2tLH}\frac{E}{G})\varepsilon_{b,max} \tag{2.16}$$

where $\varepsilon_{d,max}$ and $\varepsilon_{b,max}$ are the maximum diagonal and bending strains, respectively. The equations assume a neutral axis (i.e., where $\varepsilon = 0$), where t denotes the neutral axis depth from the edge of the beam in tension. For sagging mode (i.e. concave deflection), the neutral axis is at the middle of the beam ($t = H/2$) and $I = H^3/12$, whereas for hogging mode (i.e. convex deflection), the neutral axis at the bottom of the beam ($t = H$) and $I = H^3/3$. The maximum value of bending and diagonal strain is then compared with the limiting tensile strain.

The relative building stiffness ratio (E/G) is a measure of how flexible the structure is. Burland and Wroth (1974) suggested that for relatively rigid structures, such as masonry load bearing wall with no openings, a Poisson's ratio $\nu = 0.3$ should be used which is the same as $E/G = 2.6$, equivalent to an isotropic beam. On the other hand, relatively flexible structures, such as a reinforced concrete framed structure, can be assumed to have $E/G = 12.5$. Son and Cording (2007) confirmed through numerical sensitivity analyses on the amount of openings (i.e., windows, doors and pre-existing cracks) that an increased number of openings relates to a higher flexibility, and thus a higher global relative building stiffness. More specifically, an increased opening ratio reduces the equivalent shear stiffness (G) of the wall more than the equivalent bending stiffness (E), thus increasing the relative building stiffness.

State-Of-Strain Method (SOSM)

Deep excavations can develop significant horizontal ground displacements over a short amount of time. If a building is situated close to it, these horizontal strains can transfer to its foundation and have quite a significant impact on the development of tensile strains. Therefore, Boscardin and Cording (1989) proposed incorporating horizontal strains in the calculation of maximum bending and diagonal (shear) tensile strains. They also found that cracks may develop at lower shearing with increased horizontal strains. The development of horizontal strains is also prevalent in tunnelling, open excavation and mining subsidence problems, while insignificant in settlements due to self-weight. For subsidence, there is as yet no evidence for significant horizontal building strains developing (Prosperi 2025).

Boscardin and Cording (1989) observed that in almost all cases, diagonal cracking develops with less strain than typical bending cracks. They also observed that β is equivalent to shear strains and suggested that it should be used to calculate tensile strains rather than Δ/L. β ranges between $2\Delta/L$ to $3\Delta/L$ for L/H ranging from zero to infinity, respectively, if a central point load on a simple beam is assumed. Later, Son and Cording (2005) argued that such values are only valid for intact walls and suggested β of up to $4\Delta/L$ for cracked brick walls in hogging mode after rigorous analysis in scaled physical and numerical modelling. On the other hand, Burland et al. (2004) disagreed with using β over Δ/L, since the latter is less ambiguous and should only be used whenever pure shear deformation occurs in the structure. This is in part because the general relationship between Δ/L and ε_{lim} is consistent even for different loading conditions, partly because there is no consistent definition of how or where to measure β. In addition, they show that the relationship between β and Δ/L is sensitive to the loading situation. Netzel (2009) also recommended using β as input for diagonal strains and cracking, even when bending occurs, as it is more conservative for shearing than using Δ/L.

Boscardin and Cording (1989) finally provided a design chart based on the damage classification system by Burland et al. (1977) for critical strains, although with the assumptions of a simple

beam with $L/H = 1$ and $E/G = 2.6$ as well as a neutral axis at the bottom of the beam, which from the discussion earlier represents the hogging mode. These numbers and cases discussed above are general for masonry buildings experiencing the initial stage of settlements from nearby excavation. This in turn developed into the simplified State-Of-Strain Method (SOSM) (Son and Cording 2005) to account for the most common and sensitive cases.

2.5.4 Soil-structure interaction on settlement damage

Most settlement calculation approaches do not take the influence of buildings and foundations into account, i.e. only consider the greenfield conditions. In reality, the displacements are modified by the structure mainly due to the large stiffness differences between the structure and the soil. For instance, a large stiffness difference would yield insignificant movement in the building. Therefore, Potts and Addenbrooke (1997) introduced the relative stiffness method (RSM), in which parametric numerical analyses are performed. The relative axial and bending soil-structure stiffnesses along with additional geometric and settlement conditions are considered against modification factors. The modification factor is defined as the ratio between the predicted actual and greenfield movements. In Potts and Addenbrooke (1997), RSM was developed for undrained tunnelling problems, where building length and relative tunnel position are considered. For modification factors, Potts and Addenbrooke (1997) considered deflection ratios in sagging and hogging and horizontal strain. Later, the effect of building weight, soil-foundation interface, as well as the effect of window openings was considered using the method by Franzius et al. (2006). Since then, variation in geometry, excavation-induced settlements and other bases for modification factors (angular distortion) have been explored numerically (e.g. Son and Cording 2005; Son and Cording 2007; Giardina 2013).

RSM and building damage criteria have been developed for short-term soil response in the construction phase, e.g. settlements due to volume loss from deep excavations or tunnels in stiff soils/soft rock. In these conditions, the settlement profile often can be simplified, e.g. using as a Gaussian curve Peck (1969) and Hsieh and Ou (1998). The simplified RSM equations, however, need to be re-evaluated for lightly overconsolidated clays that may have substantial settlements due to consolidation and creep.

2.5.5 Large-scale damage assessment for non-Gaussian settlements

The pore pressure reduction (due to e.g. pumping of groundwater or leakage to a tunnel) has a significant effect on the subsidence of soft clays. Hence, ordinary approaches to damage assessments discussed so far may underestimate settlements, and subsequently the damage to buildings and other structures (Drougkas et al. 2020). Therefore, in this work the damage assessment will take the soft soil response into consideration.

To assess damage from non-uniform settlement profiles, several frameworks have been proposed, e.g. Peduto et al. (2017), Peduto et al. (2019), Drougkas et al. (2020), Peduto et al. (2021), Piciullo et al. (2021), and Prosperi et al. (2023). They all consider settlement profiles shaped by variation in soil stratigraphy, building types, wall shape and orientation, where the settlement surfaces are either predicted or empirically approximated through measurements (e.g. via InSAR).

2.6 Response of piled buildings to subsidence

2.6.1 Axial pile response

Piles transfer the loads of the structure on the surface to deeper soil layers that have sufficient bearing capacity and stiffness. For axially loaded piles in compression the resistance is mobilised at the shaft and at the pile base (toe). In Sweden precast concrete displacements piles are most commonly used, although historic buildings discussed in this research, are traditionally underpinned by timber piles. End-bearing piles mobilise a large part of the bearing capacity on a stiff stratum below the soft soil layer. In deeper deposits of soft clay, floating piles are used, where the majority of the resistance is mobilised at the pile shaft. Not all shaft friction is mobilised immediately. Piles embedded in soft clay deposits are designed to account for increases in shaft resistance over time due to ongoing background settlements from prior loading (e.g. a fill). The upper part of the pile mobilises negative skin friction (downdrag, short for NSF), as the soil settles more than the pile, whereas the lower part of the pile settles more than the surrounding soil and hence mobilises the resistance. The plane (or zone) of equal settlements between the pile and the soil is denoted the neutral plane and can be easily computed in case the shaft resistance is assumed to be fully mobilised (Fellenius 2006). Note that NSF can also develop for end-bearing piles embedded in a consolidating layer of soft soil. In the latter case, the NP is at or close to the interface between the soft and stiff (bearing) layer. The design of pile foundations requires the dimensioning for geotechnical capacity and structural capacity. In Sweden, the indirect design methods based on the α- or β-method are still most prevalent for the geotechnical ultimate limit state (Eriksson et al. 2004).

The shaft resistance (R_s) over depth (z) is a function of the circumferential area of the pile (A_s) and the local shaft friction (τ_s):

$$R_s = \int A_s \tau_s dz \tag{2.17}$$

The local shaft friction is most commonly calculated through two empirical relationships; α- and β-methods.

The β-method is based on vertical effective stresses (σ'_z), where the unit shaft resistance is related to the dimensionless factor (β) by Burland (1973):

$$\tau_s = \beta \sigma'_z \tag{2.18}$$

The factor is derived from $\beta = K tan(\delta)$, where K is the lateral earth pressure coefficient and δ is the soil-pile interface friction angle. In pile design, the ultimate values (ultimate meaning the highest possible before failure) are chosen. β typically lies between 0.4-0.9 for coarse-grained soils, and 0.25-0.4 for clays (Burland 1973).

The second design method typically used for piles in clay is called the α-method (Tomlinson 1957). This method is based on total stresses, and the shaft frictions (τ_s) are thus assumed to be a function of the undrained shear strength (c_u) multiplied by a dimensionless adhesion factor (α):

$$\tau_s = \alpha c_u \tag{2.19}$$

α has been shown to vary with pile material and geometry, the plasticity and stiffness of the clay, as well as the time after pile installation, as summarised in Karlsrud and Mahan (2010).

The time effects simply relate to the dissipation of excess pore water pressures from pile driving and any subsequent creep in the soil (Karlsson et al. 2019). According to Swedish practice, the recommended value for α under long-term loading conditions, including the mobilisation of NP (see Subsection 2.6.3), is 0.7 (Olsson and Holm 1993).

The equation of toe (or base) resistance R_t is :

$$R_t = A_t N_c c_u \tag{2.20}$$

where A_t is the toe area, and N_c is the bearing capacity factor typically chosen as 9 (see e.g. Olsson and Holm 1993). The ultimate toe resistance (Figure 2.8b) cannot be determined as easily as the shaft resistance from pile load tests. Hence, a limiting (relative) displacement or displacement rate is often chosen as failure criterion.

Whilst the α- & β-methods are perhaps not as accurate as the CPT-based methods that are more commonly used internationally (Lehane et al. 2022), the ultimate bearing capacity of piles in soft clays is rarely governing. Rather, the pile head displacements govern the pile design, especially for floating piles in a (deep) deposit of soft clays.

Predicting the pile displacements under the service loads is less straight-forward. A load – (relative) displacement approach that simplifies the soil surrounding the pile with non-linear springs tied to the shaft and the base of the pile is most commonly used. In the $t - z$ approach, the mobilised load (t) is linked to the relative vertical displacements between the pile and the adjacent soil (z). This is a classic soil-structure-interaction problem where the magnitude of the load depends on the magnitude of relative displacements and vice versa. Examples of $t - z$ response curves, where the response is either plastic, strain-hardening or strain-softening, are shown in Figure 2.8(a) for the shaft. Figure 2.8(b) shows the response for the pile toe (base), sometimes also called the $q - z$-curve.

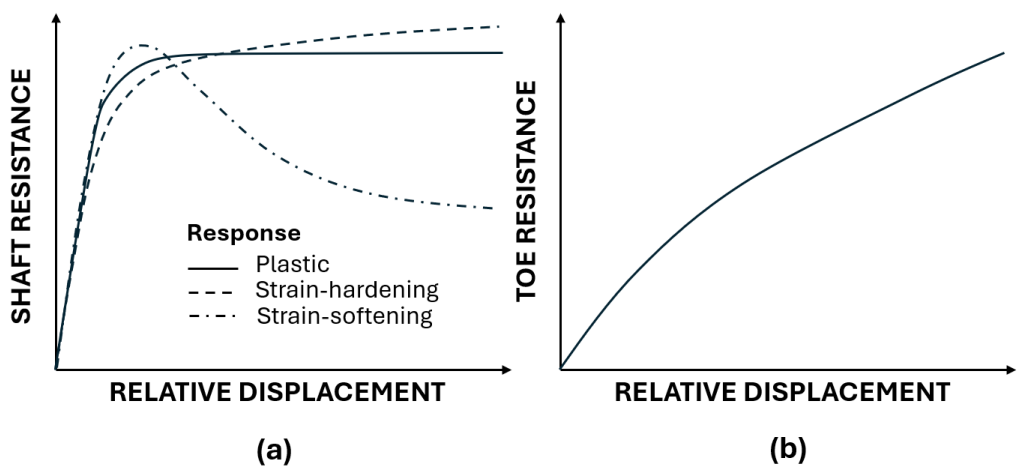

Figure 2.8: *Typical shaft- (a) and toe- (b) resistance curves.*

2.6.2 Externally driven settlements of pile foundations

In this thesis, pile head settlements due to pore pressure reduction in a lower aquifer below the soft clay layer are considered. Auvinet and Hanell (1981) and Lee and Chen (2003) observed changes in downdrag (i.e. settlement-induced pile loads) due to pore pressure changes, where decreased pore pressures increased the downdrag. Analytical frameworks to study drawdown effects on piles in those conditions have been proposed by e.g. Chen and Xiang (2006), Omer (2012), and Rodríguez-Rebolledo et al. (2015). While these studies have focused on the effect of drawdown on pile capacity through induced downdrag, little attention has been paid to the time-dependent development of the modification of greenfield settlements due to the existence of piles.

The modification of settlements has, however, been extensively studied for tunnelling and excavation problems, e.g. Jacobsz et al. (2004), Kaalberg F.J. et al. (2005), Devriendt and Williamson (2011), Korff et al. (2016), Franza et al. (2017), Williamson et al. (2017), Franza and Marshall (2018), and Franza et al. (2021).

The response of piles due to settlements caused by an adjacent deep excavation can be significant, with the largest response occurring closest to the excavation. Deep excavation causes compressive strains along the entire pile, while tunnelling is characterised by zones of both compression and extension strains (Jacobsz et al. 2004). Franza et al. (2017) and Franza and Marshall (2018) found that the gradient of the surface settlement trough was increased by the existence of piles in tunnelling, see Figure 2.9. This was further confirmed by field tests from Selemetas and Standing (2017). Design charts based on the relative stiffness method (see Subsection 2.5.4) were provided by Franza and Marshall (2018) for the modification factors of deflection ratio. For a pile group located right above the tunnel, the modified deflections are much larger than the greenfield ones, thereby increasing the risk of damage. The relationship between greenfield settlements caused by

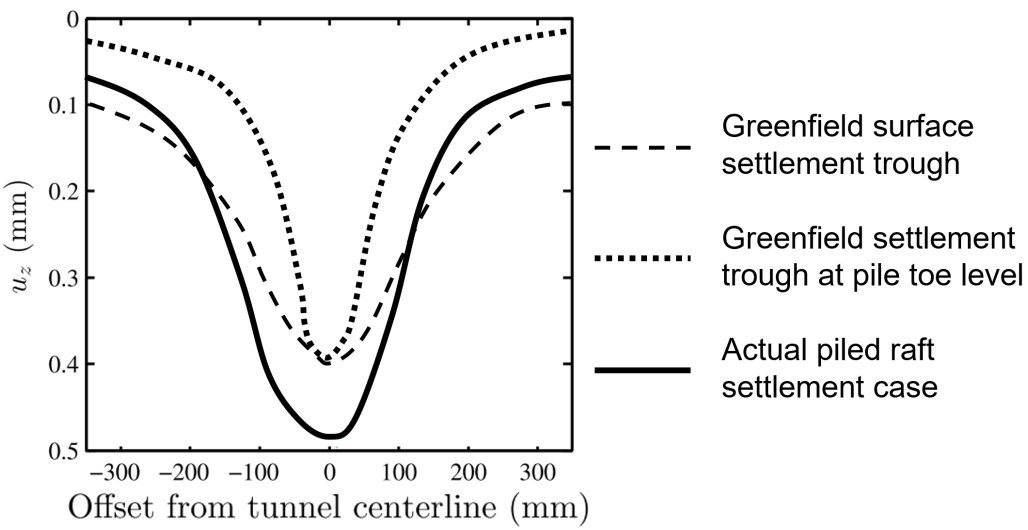

Figure 2.9: *Tunnel-induced settlement trough results from a centrifuge study. Adopted from Franza and Marshall (2018).*

deep excavations and the pile head displacements was characterised by Korff et al. (2016), who presented an analytical model based on dimensionless groups to determine the location of the plane of equal settlements, i.e. the interaction level, discussed in the next subsection.

In simplified analyses for pile foundations subjected to external settlements (such as undrained tunnelling), the predictions are performed in two stages: The greenfield response is calculated first, and then the soil-foundation-superstructure system is modelled, typically either through a Boundary Element Method or via a Winkler Beam Method (Franza 2016). In this way, the soil-single pile or soil-pile group interaction could be included. The most common approach to assess pile settlements in practice is to (1) identify the depth of the plane of equal strain between a single pile and the surrounding soil, and (2) calculate the greenfield settlements at the depth where that plane is located. This depth, commonly called the neutral plane, or interaction level, is discussed in the following.

2.6.3 Neutral plane

A neutral plane (NP), which is the plane of equal settlement between the pile and the surrounding soil, can develop in a soil profile with on-going settlements as a function of depth. The consequences of such settlements also include additional loads in the pile (dragloads) which have been extensively studied by e.g. Endo et al. (1969), Fellenius (1971), and Indraratna et al. (1992). A schematic figure of the mobilisation of a NP is shown in Figure 2.10. Above the NP, the soil settles more than the pile, whereas below this plane, the pile settles more than the soil. Consequently, the relative displacement on the pile shaft above the NP is negative, and positive below. Therefore, negative skin friction (NSF) is generated above the NP which leads to additional normal loads (dragloads) in the pile. In contrast, below the NP, the relative displacement leads to positive shaft friction (PSF) and hence shaft resistance that contributes to the total bearing capacity of the pile.

In clays, a relative displacement between the pile and the soil in the order of millimetres is sufficient to mobilise local shaft friction, either for downdrag loads (NSF) or for shaft resistance (sometimes called positive shaft friction as it contributes to the bearing capacity). Therefore, the maximum structural load in the pile is found at the NP.

The importance of NP is thus two-fold:

1. In pile design for Ultimate Limit State (ULS), there is a risk that the downdrag exceeds the structural capacity of the pile. This problem is prevalent for long slender piles.

2. In pile design for Serviceability Limit State (SLS), NP can be used along with greenfield settlement profiles to determine the settlements of the pile head.

The ideal case for the NP approach assumes rigid-plastic conditions, where the shaft friction is fully mobilised (equal to the ultimate capacity) in which a clear NP is mobilised, see Figure 2.10(a-c). In reality though, soils behave non-linearly, and as such, not all settlements will fully mobilise shaft friction. For partially mobilised shaft friction, a transition zone or zone of equal strain is formed, see Figure 2.10(d-f). The length of this transition zone is governed by the distance for which the relative movement between the pile and the soil is smaller than the limit for full mobilisation (ΔS_{ult}). ΔS_{ult} (Figure 2.10d) can be taken at the relative displacement of the ultimate pile load from pile load tests (Korff et al. 2016). As a result, NSF and PSF are only partially developed, as

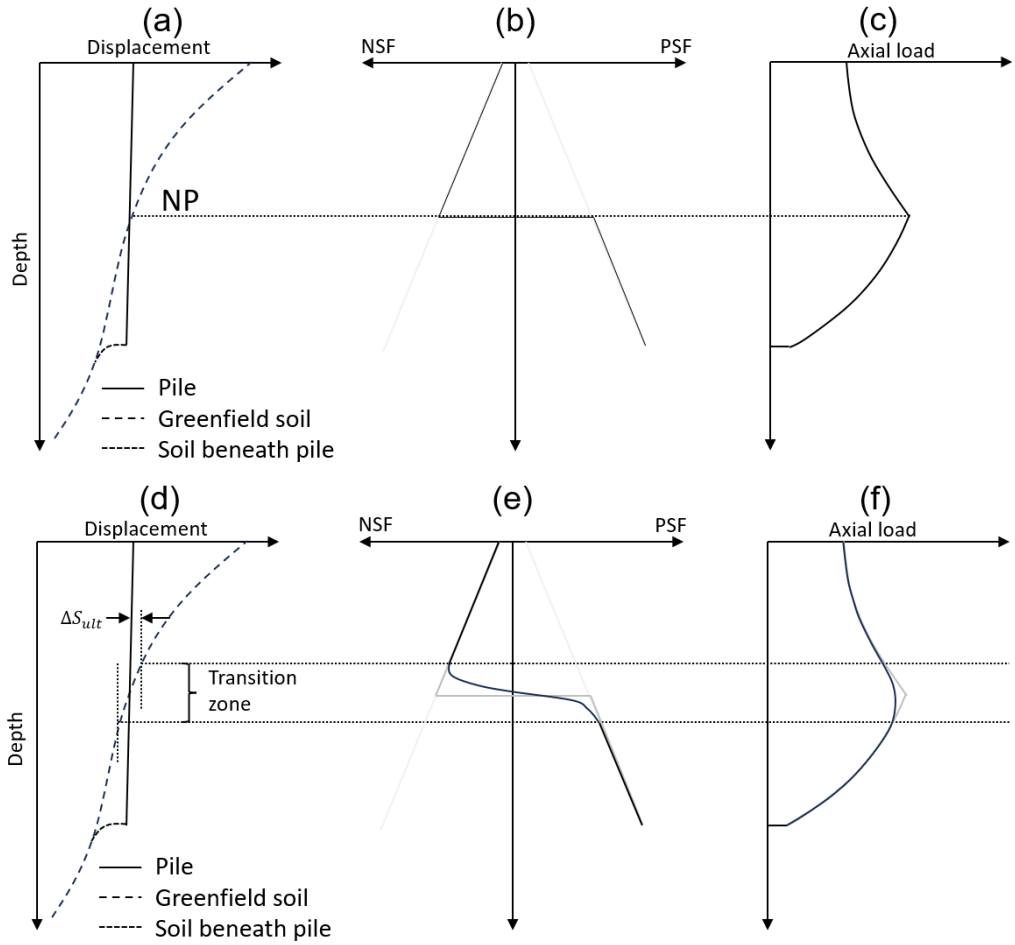

Figure 2.10: *Rigid-plastic (a-c) and elastoplastic (d-f) response curves for downdrag. (a,d) Displacement relationship between pile and soil. (b,e) Negative (NSF) and positive skin friction (PSF). (c,f) The distribution of axial load.*

one can see in Figure 2.10(e) and the tangent of the axial load plot becomes blunted (f).

Furthermore, if rigid-plastic conditions are assumed, both the equilibrium force and the location of the NP depth could be overestimated (Matyas and Santamarina 1994). Despite this, assessing NP in the rigid-plastic sense is still a useful design concept.

The depth of the NP depends on, among other factors, the magnitude of the service load at the pile head and the toe resistance. When the toe resistance is high, NP is at or near the pile base. This case is true for end-bearing piles, where a hard bearing layer prevents the pile toe from penetrating into the layer below and thus large toe resistance develops. However, for lightly loaded, dominantly shaft-bearing "floating" piles in a homogeneous soil with linearly increasing shear resistance, NP typically lies at a depth about equal to the lower third point of the pile embedment length (2/3 pile

depth). In Swedish engineering practice, this level is often used for calculating the settlement of a pile group consisting of floating piles (Eriksson et al. 2004).

Evolution of the position of the neutral plane

The consolidation process in clays affects the development of NSF and thus the position of NP can change with time (Indraratna et al. 1992; Chen et al. 2009; Liu et al. 2012; Wang and Brandenberg 2013; Zhang et al. 2021; Liang et al. 2023) or remain stable (Bozozuk 1972). Indraratna et al. (1992) linked the downward movement to the distribution of settlement along the length of the pile. More specifically, the upper part of the pile saw a faster development of the relative movement between the pile and the soil, which mobilised NSF, compared to the lower part of the pile. However, once the relative displacement is sufficiently large to mobilise the shaft friction along the entire pile, NP stabilises.

Chen et al. (2009) studied the development of NSF numerically under different pile head loads, considering an over-drainage condition (free-draining and impervious boundary at the top and the bottom of the clay layer, respectively). Liu et al. (2012) compared the over-drainage and double-drainage condition numerically and found that they severely affected the developed NP. The over-drainage condition predicted a downward direction of NP, whereas the double-drainage condition created a slight upward direction. Wang and Brandenberg (2013) also studied the effect of drainage condition and reached similar conclusions as Chen et al. (2009) and Liu et al. (2012) regarding the direction of movement of NP. Additionally, Wang and Brandenberg (2013) included also under-drainage in their analyses which resulted in an upward movement of NP. Liang et al. (2023) found that high creep rates lower the final NP position further at a faster rate. The reason for the type of NP movement (down- or upward) is that the mobilised skin friction is largely related to the consolidation (and creep) settlements, which in early stages mostly develop near the free-draining boundary, where the pore pressures rapidly reduce.

Interaction level

Korff et al. (2016) proposed an analytical soil-pile interaction method to study the effects of urban excavations on the response of historic pile foundations. The interaction level was introduced, which is the depth along the pile where additional (e.g. from the deep excavation) greenfield and pile settlements are the same, which appears to be similar to the NP. However, when the shaft friction is not fully mobilised, NP and the interaction level are different. Finally, Korff et al. (2016) and Franza et al. (2021) showed that the interaction level depends on the following dimensionless groups:

- The normalised pile head load.
- The soil settlement profile relative to the ultimate relative displacement of the pile, i.e. the normalised soil settlement gradient.
- The gradient of the ultimate shaft resistance.
- The toe resistance of the pile normalised with the ultimate pile head load.
- The diameter of the pile relative to the ultimate relative displacement of the pile.
- The installation method (displacement vs. non-displacement piles).

2.6.4 Settlements of a pile raft

In stiff soils, such as over-consolidated clays without ongoing settlements, the response of a pile raft depends on the pile-raft-soil system (Reul and Randolph 2003). The soil-structure interaction aspects between the location of the loads of the superstructure, the relative stiffness between base slab, soil and piles need to be considered when studying such pile rafts. If connected to a raft, depending on its flexibility, the piles will conform to it. For a fully rigid raft, the displacements would be equal among the piles, but the compressive loads would be different. In contrast, for a fully flexible raft, the displacements would differ while the exerted load would remain the same on each pile. For the case of hogging settlement mode (see Section 2.5), it would mean larger compressive loads and smaller settlements on the interior piles, depending on the flexibility of the raft.

Depending on the centre-to-centre (ctc) distance between them, often normalised with the pile diameter (D), the piles in larger pile groups respond differently to a single pile. Furthermore, perimeter piles (corner and side piles) and interior piles behave differently. The corner piles usually respond similarly to a single pile as there is the least effect of neighbouring piles. The interior piles have less bearing capacity (mostly at the shaft) than a single pile, as more piles share the same amount of volume. According to Fellenius (2023), the single pile assumption is only valid for a group with a maximum of 4x4 piles.

In Sweden, the recommended $ctc > 5D$ (Olsson and Holm 1993), and consequently the piles are sufficiently far apart that the response is close or equal to a single pile. Furthermore, Lee and Chen (2003) showed that the development of NSF on piles in a pile group approaches that of a single pile of $ctc > 6D$. This finding was also confirmed by (Rodríguez-Rebolledo et al. 2015). In contrast, Rodríguez-Rebolledo et al. (2015) found that the resistance of the piles to these externally triggered settlements is greater for closely spaced piles ($ctc = 3 - 5D$).

In the current work, the settlement analysis of piled buildings is simplified by analysing the response of a single pile, in a unit cell of sufficient size. However, for certain buildings or building complexes, the foundation systems may vary (containing shallow, floating piles, end-bearing piles) due to e.g. different loading situation (light-weight or heavy buildings) and soil heterogeneity (in parameters and stratigraphy), which makes the problem extremely complex to model. In such situations, provided that the foundation systems are well-characterised, detailed analysis with 3D numerical modelling makes sense.

3 Data of studied area

3.1 Geology in Gothenburg

The local geology in Gothenburg region comprises typically of the stratigraphy shown in Figure 3.1. At the bottom, a hard crystalline rock of igneous origin formed about 1500-2000 million years before present (BP) is found. The rock was heavily metamorphosed about 1000 million years BP and has a predominantly gneissic character. The shallower parts have been exposed to fracturing and weathering, and are therefore often water bearing with a hydraulic conductivity in the order of 10^{-7} m/s in the Gothenburg region (Trafikverket 2014). Typically, the fractured zones cause depressions in the landscape due to weathering and erosional processes.

During the glacial period, the weight of the ice sheet caused compression of the Earth's crust, resulting in subsequent rebound and land rise after the retreat of the continental ice sheet (Bergström et al. 2022). As a result, the Gothenburg area was at the end of the glacial period covered by sea water up to about 90-100 meters above the current sea level (Påsse and Daniels 2015).

During the melting process, meltwater tunnels were formed in the ice sheet, creating fast-moving streams that transported materials. The coarse-grained materials were deposited at the mouth of meltwater tunnels in the ice sheet, forming eskers and delta deposits. Fine-grained particles (silts and clays) settled further away from the ice front in deep and calm waters. As the ice retreated further north, the flow velocities of water decreased, and thus clay particles sedimented in valleys and other low-lying areas and formed the thick clay deposits found in Gothenburg today (Bergström et al. 2022).

Due to the postglacial uplift, areas of glacial till and glaciofluvial deposits were exposed to wave erosion and abrasion materials (beach materials) were formed and deposited on top of glacial till, glaciofluvial deposits and the fine-grained materials (clays and silts). The stratigraphy here is mostly formed by a cycle of transgression and regression, depending on the rate of melting, sea level and the land uplift. As the sedimentation/weathering process has been iterative, there may be local sand/silt lenses inside the clay from a time when the water flow was locally higher (Bergström et al. 2022).

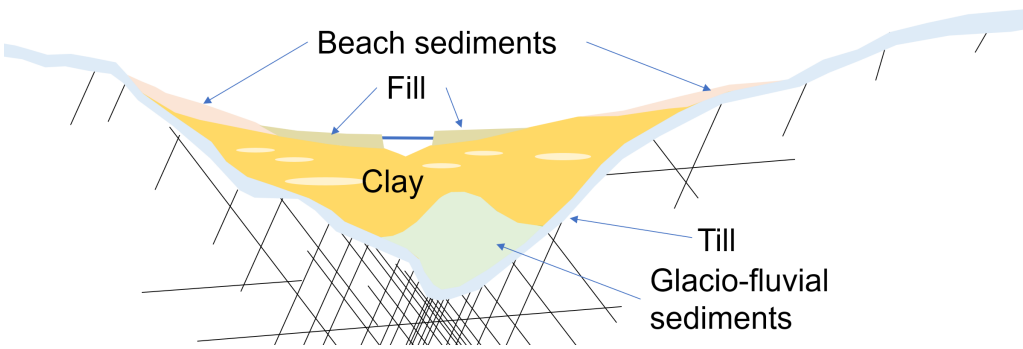

Figure 3.1: *Local geology of a typical cross-section. Black lines represent fractures in the bedrock.*

Finally, in the last 400 years that the city of Gothenburg has existed, the geology has been heavily altered as the construction of the city required modifications to landscape, which may have secondary effects caused by historic and ongoing leakage and groundwater lowering, as explained in the next section.

3.2 Historic development of Gothenburg City

Figure 3.2 illustrates the changes in the land use in central Gothenburg from the foundation of the city in 1621 to present day where reclaimed land is illustrated with blue stripes. It also displays the corridor where the West Link railway tunnel goes underneath the city. In the 1600s and 1700s, the city was surrounded by a caponier, a type of fortress with a moat (which later on formed Rosenlund canal as it is now) and an earth wall which was a few metres high. In the beginning of the 1800's the caponier was demolished in favour of further land reclamation as the city grew. Through dredged materials, probably found in the nearby water, the new land could be constructed. Rosenlund canal was also altered during this time to its current shape.

Since the landscape has changed so much, several loading situations have probably caused site-specific overconsolidation, thus a large variation in the overconsolidation ratio would be expected. The modelling approach in this thesis, however, does not consider this likely spatial variation, given the lack of data from a larger area.

From well archives, information on a pore pressure reduction of 60 kPa in two wells near Rosenlund canal in the spring of 1969 can be found, with unknown origin. However, since then, infiltration

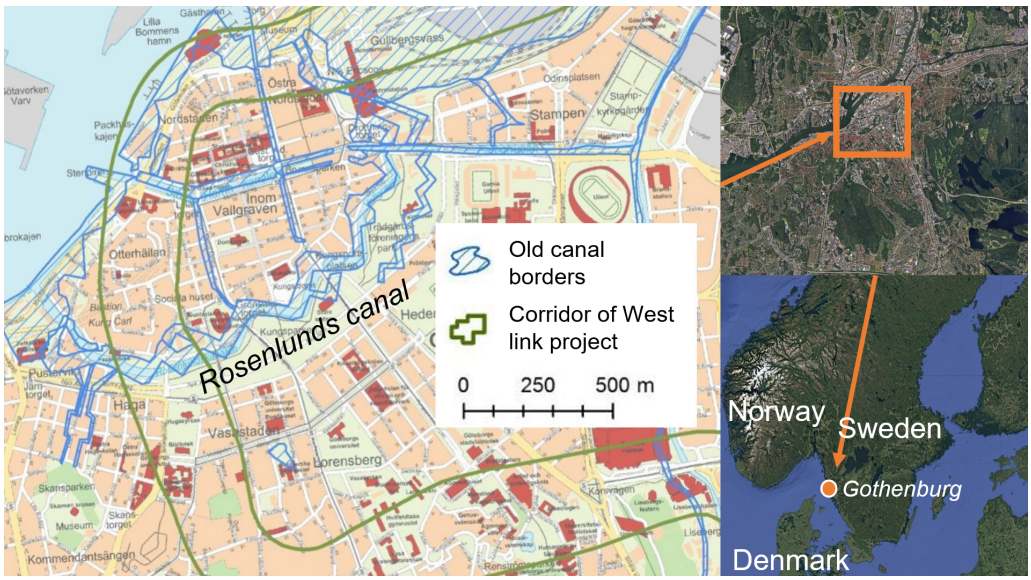

Figure 3.2: *Historic development of central Gothenburg. Historic water zones that have been filled are displayed in blue stripes. From Trafikverket (2014). The right-most maps are retrieved from Google Maps (https://www.google.com/maps).*

programmes were activated in conjunction of three tunnel projects (Göta tunnel, Telia tunnels and Chalmers tunnel), after which the pore pressures have remained relatively stable (Trafikverket 2014).

3.3 West Link project and Haga station

The construction of the West Link project started in 2016, involving 6.6 km underground railway tunnel with three new underground stations: Korsvägen (located south-east of the study area), Centralen (located North-east of the study area) and Haga (located in the study area). The location of the planned tunnel and Haga station is shown in Figure 3.3(a). The station at Haga is constructed partly in clay as an open excavation, with a tunnel subsequently built inside, and in rock under the church of Haga.

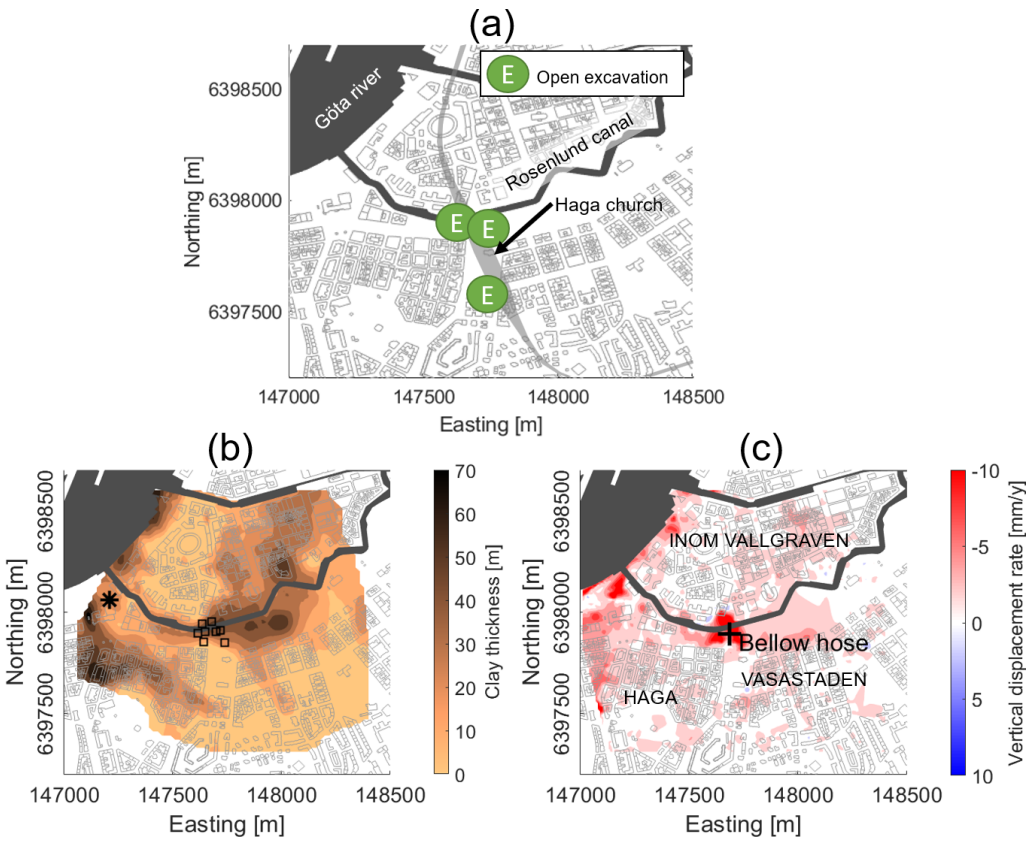

Figure 3.3: *(a) Project location with tunnel shaded in grey. (b) Thickness of calculated clay layer and undisturbed samples retrieved around Haga station (marked with hollow squares) as well as rough borehole location of the nearby Göta tunnel (marked with a star). (c) Measured ground deformation 2023-2024 using InSAR (TreMaps 2024) and location of bellow hose. The reference system is SWEREF99 TM 12 00.*

The open excavation parts of Haga station involves several sections of open excavations with various retaining wall and grouting design. Further north and south, as well as below Haga church, the underground construction continues in bedrock, where the drill-and-blast method with pre-grouting of the rock is adopted. The transition zone between the soil and bedrock is grouted using the curtain method. Thus, the focus on the project is on leakage due to tunnelling (underdrainage) affecting the lower aquifer.

3.4 Boreholes and stratification model

Figure 3.3(b) shows the locations where undisturbed samples have been taken using the ST-II piston sampling technique for performing e.g. CRS tests. Additional data by Tornborg et al. (2021) from the nearby Göta tunnel project, see the top left star in Figure 3.3(b), which has been extremely well characterised, was also used for the calibration of Creep-SCLAY1S model parameters. Soundings of different character were used to create a continuous stratification model in the domain considered. The stratigraphy was modelled using the methodology described in Sundell et al. (2016). This model used different types of soundings: those that reach bedrock (e.g. soil-rock probing) and those that do not (e.g. CPT). The interpolation scheme is based on the kriging method where variograms calculate the uncertainties of the spatial stratigraphy. The model also accounts for the dependency of stratigraphy to eliminate crossings and gaps between two layers. A total of four layers were thus created: A fill layer (upper aquifer), a saturated clay layer (its thickness is seen in Figure 3.3b), a till layer (lower aquifer) and a bedrock layer). The lower aquifer also includes some glacio-fluvial sediments, but from here on we only refer to the till layer.

3.5 Groundwater levels and groundwater model

A steady-state numerical groundwater model, further described in Paper B, is used to create a continuous surface for groundwater piezometric heads in the upper and lower aquifer. The stratification model mentioned previously and the field data of hydraulic properties and observations served as input to the model. Head observations in a total of 129 wells in the lower aquifer, representing average values, served as calibration data.

3.6 Settlement data

The data on measured vertical settlements was retrieved through a bellow hose and InSAR (Interferometric Synthetic Aperture Radar). In a bellow-hose, displacement gauges, installed at different clay depths, were used to measure vertical displacements as a function of depth between 2011-2018. A bellow hose is thus similar to an extensometer. Unfortunately, the first metres are always smeared due to the lack of confinement, but in general the accuracy is claimed to be +/- 1 mm. The measurements of the bellow hose were used to calibrate the constitutive model used in finite element analyses when considering the background creep. The InSAR data provided by TreMaps (2021) interpreted from TerraSAR-X satellite data using the SqueeSAR algorithm to retrieve displacement rates with a resolution of 20x20m. The vertical rates were used to validate creep settlement analyses in paper D.

The location of the bellow hose and the distribution of ground deformations by InSAR are shown

in Figure 3.3(c). The InSAR data, here measured 2023-2024, show relatively low vertical ground displacement rates with maximum settlement rates of 5 mm/year. It should be noted that the reliability of the measurements is highly dependent on a statistically long enough time series (1.5 years in this case), and generally has a low signal-to-noise ratio due to atmospheric noise and other factors. With the shown dataset, the standard deviation is 0.3-0.6 mm/year (higher in the green-field areas). Finally, it should be noted that the isostatic uplift due to the last ice age has not been considered. In Gothenburg region, the uplift is ca 3 mm/year. Figure 3.3(c) also show that most settlements occur in areas close to the water where the previous moats have been filled. The bellow hose data is presented in detail in Subsection 4.2.1 along with the calibration results.

3.7 Buildings in the studied area

In total, 540 buildings are found within the model domain (Figure 3.4a). Out of those, 215 contained detailed records on structural type, foundation type, facade type, age, number of floors (including basement) etc. In damage assessments, it is common to separate buildings into two structural types: buildings with load-bearing walls and framed buildings (mainly reinforced concrete (RC) framed buildings). Typically, the shape and sensitivity of the deformation are different for these two structural types. The database did not initially contain such separation, and thus, it was necessary to manually classify which buildings deformed more like load-bearing wall structures and which ones deformed more like framed structures.

The main criteria for the classification were:

1. If the main structural components of the frame are of the materials steel or reinforced (RC) concrete: Framed structure
2. If the main structural components of the frame is of timber, but the facade material is of masonry or similar: Load-bearing wall
3. If the main structural component of the frame is of timber and the facade material is timber or similar: Framed structure
4. If the main structural component are any type of load-bearing wall including RC and masonry walls: Load-bearing wall

Hence, the number of buildings assumed to be equivalent to load-bearing walls and frames were assessed as 112 and 108, respectively (see Figure 3.4a). Some of the buildings are as old as 160 years (Figure 3.4b), and thus may already have some damage that can affect their overall resistance to continued damage. At this stage, it was assumed that each floor has a height of 3 metres, however, height data may in the future be analysed through e.g. LiDAR data for higher accuracy.

3.8 Foundations in the studied area

The initial classification of the foundation types taken from the database were reduced to three; "Shallow" (including slab or raft on soft ground or unknown/mixed foundations), "Foundations on steady ground" (including slab or raft on stiff ground or end-bearing piles), as well as "Floating piles". Other buildings include ones without any structural information. Their locations are

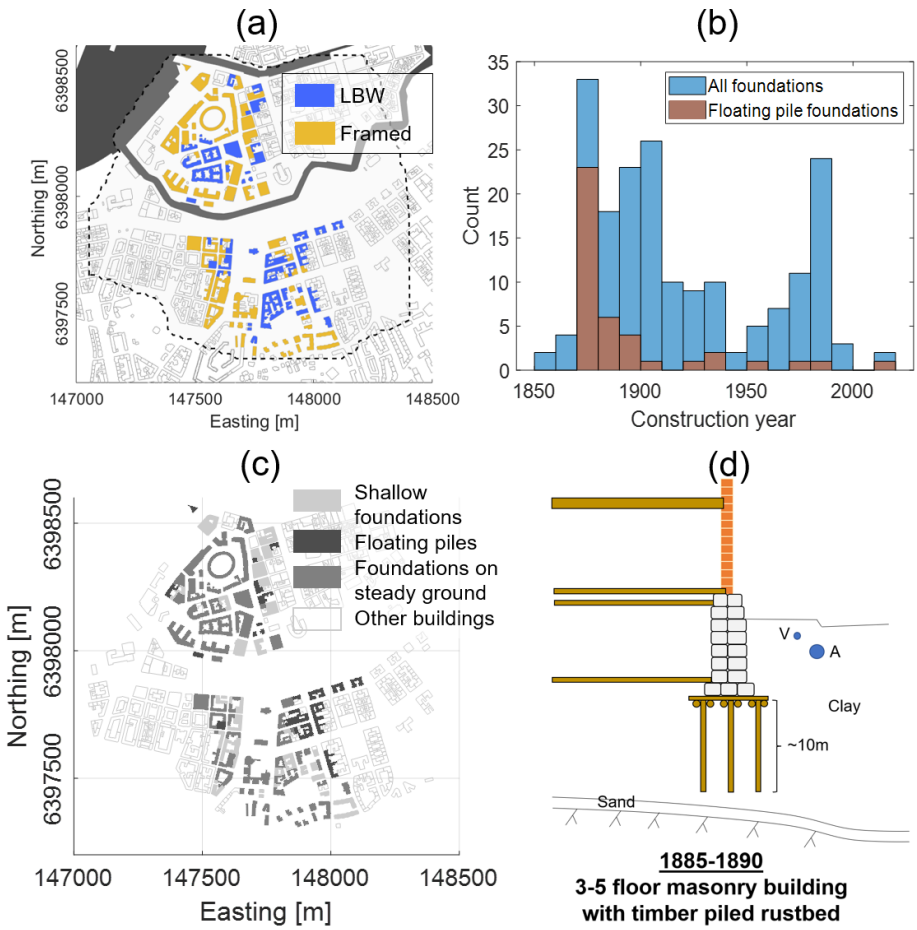

Figure 3.4: *(a) Structural types. LBW is load bearing walls. (b) Building age. (c) Foundation types. (d) Typical cross-section of a wooden pile foundation in Haga.*

displayed in Figure 3.4(c).

A typical cross-section of a wooden pile foundation in Haga is seen in Figure 3.4(d). These wooden pile foundations are very old (ca 100-150 years, see Figure 3.4b) and their effect on settlements were of particular interest to study as they are both sensitive to groundwater lowering, which causes rotting, but also due to their superstructures being of high cultural value. It was commented in the database that the wooden pile foundations were considered end-bearing or floating if the clay depth was below or above ten metres, respectively. However, the actual length of the wooden pile, quality, shape, and their spacing and location is unknown since most drawings are limited to the superstructure. In addition, the piles are tapered, with a larger pile diameter at the pile head and a smaller one at the pile toe. In Gothenburg, the estimated pile head diameters between 15-35 cm are typical for wooden piles (Björdal and Elam 2021). The lengths are typically around 10 metres, with a variations of a metre or two (e.g. Wendel 1900).

4 Methodology

4.1 Overall methodology

In general, this thesis relies on the development of several models in a model chain, as illustrated in Figure 4.1. The purpose of the model chain is to enable risk-based planning of underground infrastructure projects (see e.g. Sundell et al. 2019a and Merisalu et al. 2023) for early planning stages. Figure 4.1 illustrates the connections between the different models. The red text highlights the author's contributions to the model chain, covered in this thesis (Papers A-E). The underlying stratigraphy and groundwater modelling was performed by Jonas Sundell, while the surrogate metamodel was developed and performed by Ezra Haaf. Thus, these models are only briefly described in the thesis. The following sections are dedicated to the methodological development of the 2D subsidence model, building damage model, and the model for floating piles.

4.2 Development of a subsidence model

2D Finite Element analyses were performed to generate the time-dependent 2D subsidence models. The software used for the simulations was PLAXIS 2D v. 21 by Bentley, and the simulations were done using an in-house implementation of Creep-SCLAY1S model, rather than the commercially available version in order to avoid "black box" simulations.

PLAXIS is a Finite Element (FE) software that features a hydro-mechanically coupled (HM) formulation (Galavi 2010), and includes several advanced elastoplastic and elasto-viscoplastic material models. An integrated approach, using coupled 2D finite element analyses, combined with a 3D stratigraphy and groundwater model (explained in Chapter 3), as well as a metamodel, is used to calculate surface settlements for a given pore pressure reduction and time.

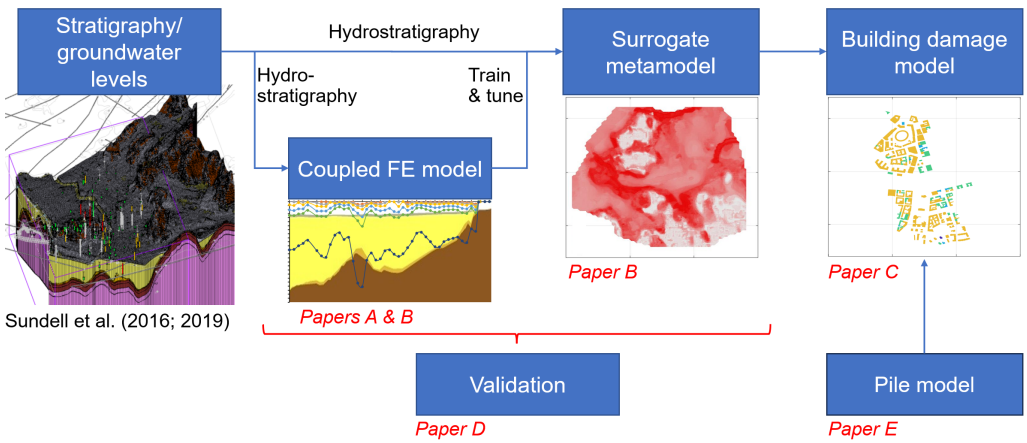

Figure 4.1: *Overview of the methodology.*

4.2.1 Derivation of Creep-SCLAY1S model parameters

The properties of the clay layers were derived based on 48 standard ST-II piston samples from eight boreholes around Haga (see Figure 3.3b). Figure 4.2 shows the key index properties; bulk density (ρ), natural water content (w), sensitivity (S_t), vertical hydraulic conductivity (k_v) and overconsolidation ratio (OCR), derived as a function of depth, plotted as open rectangles. These properties are compared with the properties of the well-characterised Göta tunnel project nearby (Tornborg et al. 2021) using a star symbol, also found in Figure 3.3(b). Figure 4.2 demonstrates that the properties of both sites are very similar. The deviations in the hydraulic conductivity at 20-30m depth is most likely due to the proximity to the frictional layer, attributed to the relatively shallow clay thickness at the site of Göta tunnel. Given most model parameters in Creep-SCLAY1S are intrinsic properties (see Subsection 2.4.2 for extended description on the model), the values of Tornborg et al. (2021) were adopted, combined with site-specific values of OCR.

The layer-specific values of OCR were first estimated based on CRS tests on samples from the Haga station. Due to the rate dependence of Creep-SCLAY1S, OCR is a key model parameter. Thus, depth-integrated background creep measurements from a bellow hose (Figure 4.3) was used for further calibration of OCR. The high strain rates used in CRS tests are namely not fully compatible with the model. Based on calibration of numerical predictions against the measured depth-integrated settlements between 2011-2018 from the bellow hose (Figure 4.3), the OCR-values for the deeper layers were re-evaluated, as the samples used in CRS tests were suspected to

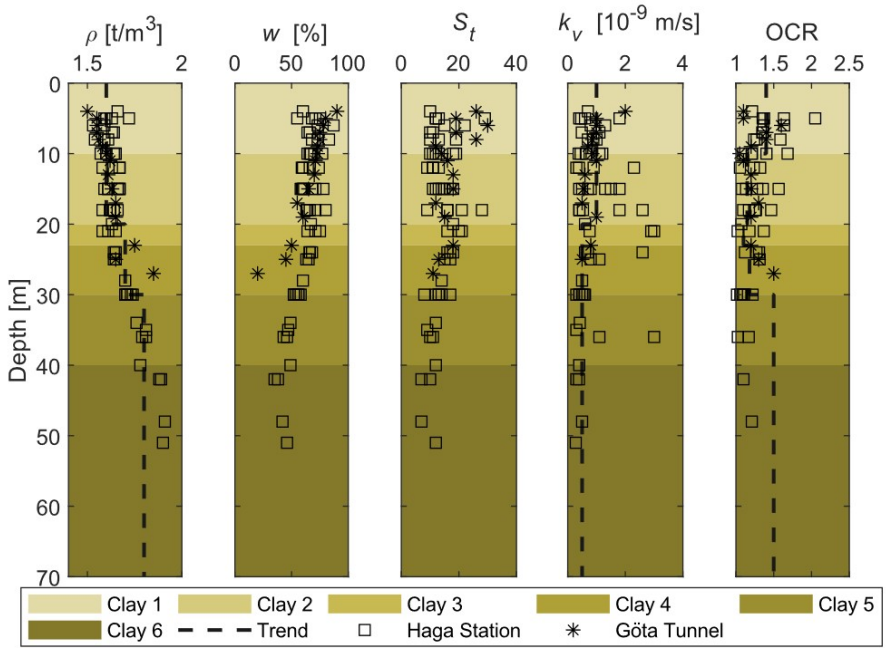

Figure 4.2: *Index properties at Haga and Göta tunnel. The trend lines represent the chosen values for the numerical model.*

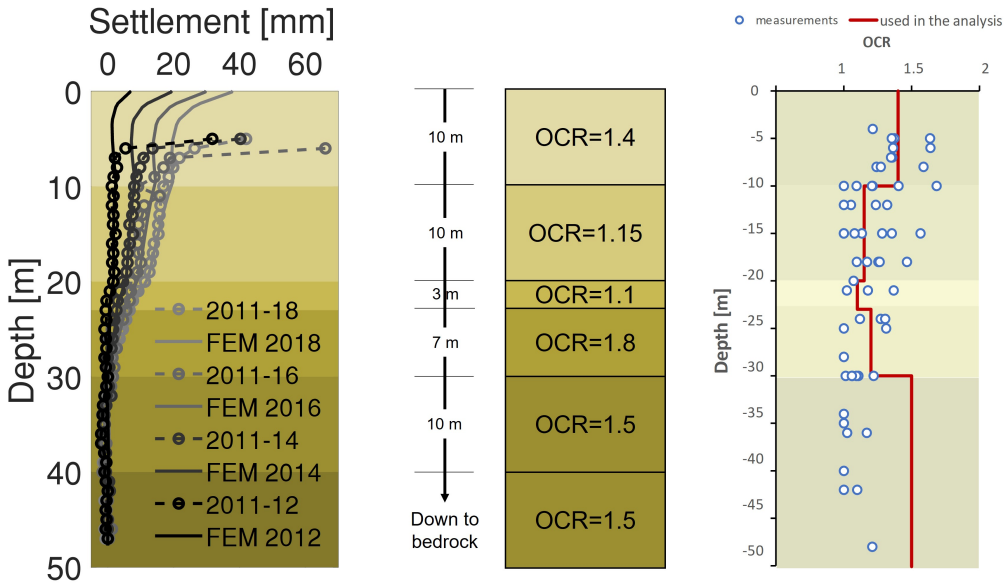

Figure 4.3: *Bellow hose measurements and calibrated values for the numerical model (on the left). Updated OCR distribution based on the bellow hose measurements at >30 m depths (on the right).*

be of poor quality. The sample quality was assessed using the SGI approach (Larsson et al. 2007), see Figure 4.4(a), based on natural water content and volumetric change at reconsolidation (its definition is described in Subsection 2.3.3) from the CRS tests. The results showed that the sample quality decreased with depth (also shown in Figure 4.4b). Figure 4.4(b) further shows that the variation at the top 30 metres cannot be explained by the quality assessment alone. As the bellow hose suggested virtually no settlements at 30-50 m depth, the OCR -values were adjusted upwards to match the measurements.

The discrepancies between the computed settlements and the bellow hose measurements at shallow depths (Figure 4.3) can be explained by a lack of horizontal stresses acting on the bellow hose, thus the values derived from the CRS test were adopted. Six sub-layers in the clay with different OCR values were eventually adopted for further simulation.

The assumed model parameters for the clay can be found in Table 4.1, with the additional state parameters in Table 4.2. The frictional layer (till) was represented with the Mohr-Coulomb model, assuming a Young's modulus of $E' = 30$ MPa, Poisson's ratio of $\nu' = 0.2$, friction angle $\phi' = 35$ degrees, and (for computational reasons) a cohesion intercept $c' = 1$ kPa.

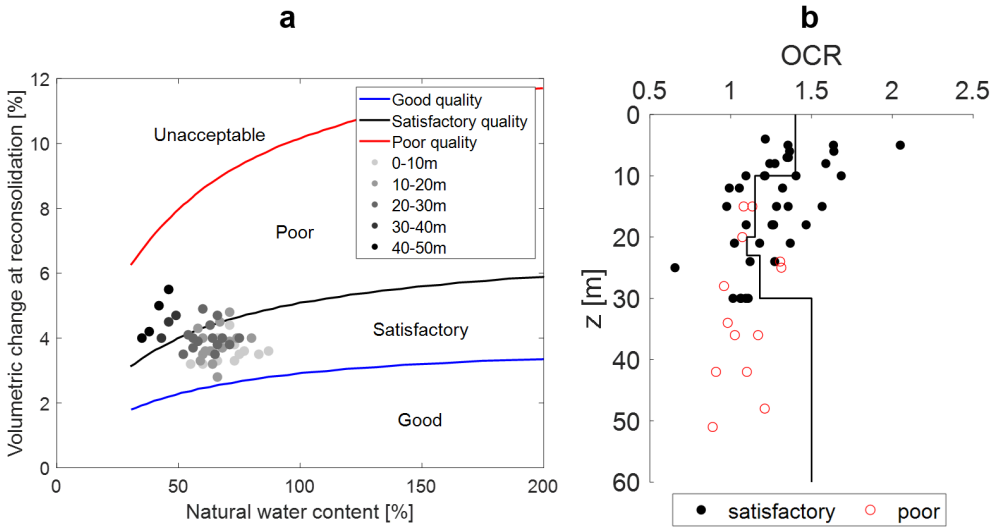

Figure 4.4: *Sample quality from CRS tests: (a) Assessment using the SGI approach (modified from Larsson et al. 2007). (b) Visualisation on OCR vs. depth.*

4.2.2 Cross-sections for analyses with Plaxis 2D

Three cross-sections were selected for performing time-dependent coupled flow-deformation analyses to be subsequently used in training and validating the metamodel, located perpendicular to or along the planned tunnel (Figure 4.5a).

Table 4.1: Creep-SCLAY1S parameters used for all clay layers (modified from Tornborg et al. 2021).

Parameter	Value
Poisson's ratio, ν'	0.2
Modified swelling index, κ^*	0.013
Modified intrinsic compression index, λ_i^*	0.085
Stress ratio at critical state in triaxial comp., M_c	1.45
Stress ratio at critical state in triaxial ext., M_e	1.1
Modified intrinsic creep index, μ_i^*	0.002
Time factor (days), τ	1
Initial anisotropy, α_0	0.57
Rate of rotational hardening, ω	200
Re. rate of rot. hardening due to dev. strain, ω_d	1
Initial amount of bonding, χ_0	15
Rate of destructuration, ξ	8
Rate of destruct. due to deviatoric strain, ξ_d	0.5

Table 4.2: Additional model parameters for all layers (modified from Tornborg et al. 2021).

Layer (depth* [m])	$\gamma[kN/m^3]$	e_0	$k_v[m/s]$	OCR
Fill	16	2.0	1E-9	1.4
Clay 1 (0-10)	16	2.0	1E-9	1.4
Clay 2 (10-20)	16	2.0	1E-9	1.15
Clay 3 (20-23)	17	1.7	5E-10	1.1
Clay 4 (23-30)	17	1.7	5E-10	1.18
Clay 5 (30-40)	18	1.2	5E-10	1.5
Clay 6 (40-70)	18	1.2	5E-10	1.5
Till	18	-	1E-6	-
Rock	20	-	1E-6	-

**Depths are approximate and adjusted to the stratigraphy.*

The FE meshes used for each cross section is shown in Figure 4.6. The mesh fineness was chosen after a careful mesh-sensitivity analysis to ensure mesh-independent results. The meshes for cross-sections BB, DD and FF consist of 21068, 19181 and 21506 6-noded triangular elements, respectively. The depression at $x = 70m$ in profile FF is the bottom of the Rosenlunds canal.

Initial piezometric heads were set for the upper (fill) and lower aquifer (till or frictional material and rock), respectively. These levels were determined using the groundwater model explained in Section 3.5. In between the upper and lower aquifer, the values were interpolated in all clay layers, excepting the fill layer in the upper aquifer, see Figure 4.5(b).

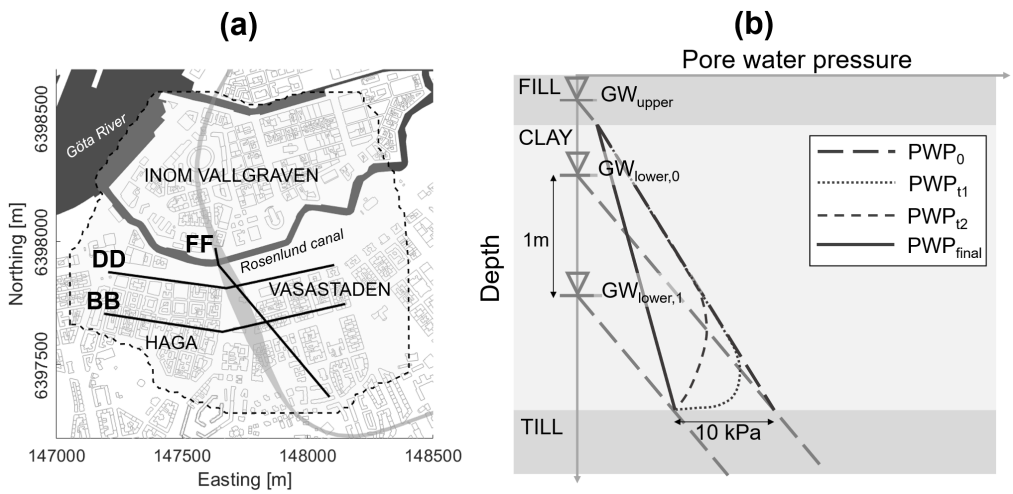

Figure 4.5: *(a) Map of cross-sections used for the 2D numerical analyses and metamodel domain. (b) Example of drawdown due to underdrainage, for a 10 kPa drawdown for times 0, t1, t2 and final. PWP = Pore Water Pressure at various times.*

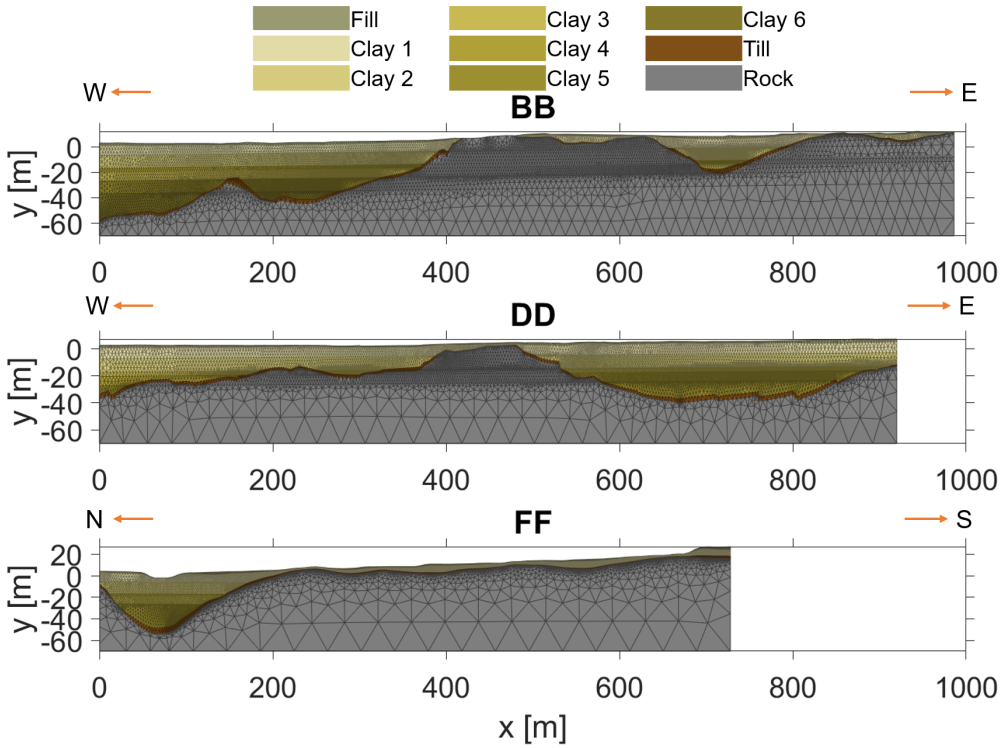

Figure 4.6: *The Finite Element meshes of cross sections BB, DD and FF, and the assumed layering.*

During the initialisation phase of the numerical analysis, all layers were modelled as linear elastic materials to create the initial effective stress state needed to initialise the state parameters of constitutive model, given there were non-horizontal layers. Next, a NIL step was defined, and the material model for the clay layers was changed from the linear elastic model to Creep-SCLAY1S, and the displacements were reset at the end of this step.

The third simulation phase included a uniform drop in pore pressure in the lower aquifer to emulate leakage into the underground construction. One thing to emphasise is that these are purely hypothetical scenarios, as the focus was on on the modelling drawdown-induced subsidence and the consequent building damage, rather than studying the potential leakage to the tunnel. The pressure drops in the lower aquifer consisted of cases with 10 kPa and 40 kPa pore pressure drop, respectively. These values were specifically requested by the Swedish Transport Administration.

First, the background creep rate is emulated by a zero drawdown case (0 kPa), to highlight that there will be continued settlements (with potential damage to the buildings) even if there was no underground construction. This case was used to calibrate the OCR values to match with the bellow hose measurements discussed earlier. The background creep results from the metamodel were also validated with the available InSAR measurements between 2023-2024 (shown in Figure 3.3c).

The remaining phases are consolidation phases, in which the excess pore pressures are allowed to

dissipate from the clay layers due to the underdrainage, see e.g. Figure 4.5(b). The time steps for the consolidation phases were selected as 3 months, 6 months, 1 year, 5 years, 10 years, 30 years and 100 years.

4.2.3 Parametric study

To date, few systematic studies have examined the influence of parameters on the subsidence due to underdrainage. Tahershamsi and Dijkstra (2021) and Tahershamsi and Dijkstra (2022) performed Global Sensitivity Analyses on oedometer tests using Creep-SCLAY1S, and found the apparent preconsolidation pressure to be the most influential model parameter on the predicted vertical strains in the effective stress states around the preconsolidation pressure. Griffiths and Fenton (2009) and Huang et al. (2010) studied the effects of vertical hydraulic conductivity, treating that as a random variable in a random field, on typical consolidation problems and found that this parameter was significant. However, the influence of horizontal hydraulic conductivity on the rate of vertical settlements may also be interesting for a case with largely varying clay thickness. A large influence would motivate further examination of this parameter using oedometer tests with radial drainage, e.g. Rowe cells. Commonly, the horizontal hydraulic conductivity is normalised with the vertical component, referred to as the hydraulic anisotropy ratio ($r_k = k_h/k_v$). Assessing the influence of OCR, k_v [m/s], and r_k on the predicted settlements was the main motivations for conducting the parametric study presented in Paper A.

The setup for systematic analyses included 27 combinations of the three parameters selected. Each of the chosen parameters was varied between three alterations, including the likely minimum, trending and maximum values. The trending values for OCR and k_v were taken directly from the values in Table 4.2. The minimum and maximum values were also taken from the trending values, however, multiplied with a factor each to capture the ranges of OCR and k_v, see Figure 4.7. As mentioned in Subsection 2.3.2, the hydraulic anisotropy is relatively unknown for Swedish soils. However, previous studies elsewhere suggest r_k to be as high as 2 for various marine clays (see Table 2.1). Therefore, the minimum, trending and maximum values were chosen as 1, 1.5 and 2, respectively.

4.3 Development of a building damage model

As discussed in Subsection 2.5.5, it is possible to estimate damage using large-scale settlement profiles. However, a Gaussian profile is often assumed in these methods, while high-resolution settlement results may have several interchanging settlement modes that could worsen the damage. Therefore, an automated method is proposed that directly accounts for the settlement results in Paper C.

Figure 4.8 shows the general strategy (Steps A-E) of the building damage model. In step A, the building-specific data, including 2D geometry, structural type (Load-bearing wall or Framed), and number of floors, were used as input for the building damage model. In step B, the metamodel results (settlements and coordinates), used as input, were assembled on constant x- and y-grids with a resolution of 5 m. In step C, the non-Gaussian settlement profiles from the metamodel grid were reassembled and intersected with building polygons, creating building-specific settlement profiles. In step D, using these building-specific settlement profiles, typical 2D damage parameters were

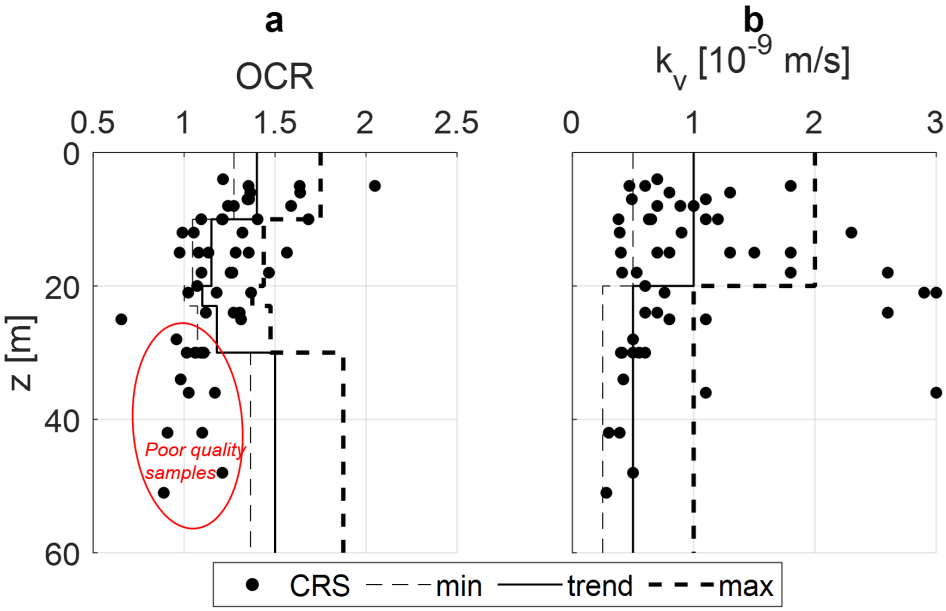

Figure 4.7: *Depth-dependent values for the parametric study; (a) over-consolidation ratio (OCR) and (b) vertical hydraulic conductivity (k_v).*

calculated for each building. The largest parameter-specific values of all building-specific profiles within a building were retrieved. In step E, a damage map was created for each consolidation scenario and damage parameter with designated limiting criteria. The structure of the building damage model was created with MATLAB. The following text is a detailed description of steps C and D.

The settlement data, imported from the metamodel (B), is divided into profiles of constant x- (east-west) and y- (north-south) directions (Step C). If a selected "global" profile (indicated as blue rectangle in Figure 4.8) intersects with a building polygon, intersection points are created, which mark the first and last point of the building-specific profile (marked as solid red circles). As no settlements are calculated previously on the intersection points, they are linearly interpolated between their respective neighbouring points; one inside (filled upward triangle) and the other outside (hollow downward triangle) the building polygon on the "global" settlement profile selected. The points in between the first and last point within the building polygon are then saved in the profile (shown as blue triangles in Figure 4.8). This process is iterated for all building polygons and "global" settlement profiles.

For the calculation of damage parameters (Step D), the well-established parameters by Burland and Wroth (1974) were used (see Subsection 2.5.2), defined in the model as follows: Rotation (θ), tilt (ω) and angular distortion (β) are considered positive in a counter-clockwise direction. Angular strain (α) represents the current deflection mode. When $\alpha > 0$, sagging is the dominant mode while for $\alpha < 0$, hogging is the dominant mode. The model assumes that each inflection point lies in the middle at a shift from positive to negative strain (or vice versa). Locations where $\alpha = 0$ also

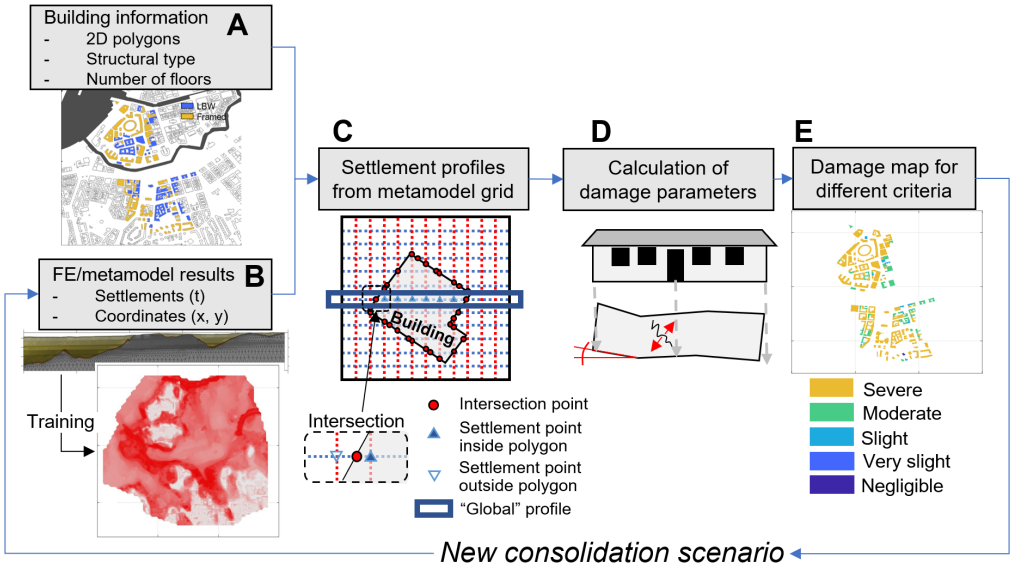

Figure 4.8: *Structure of the building damage model. Data acquisition via (A) building typology and (B) FE/metamodel results. On building-specific settlement profiles (C), the damage parameters are calculated (D) and compared with damage criteria (E). LBW = Load-bearing wall. Maps in A, B and E correspond to the same area.*

represent inflection points. These variables are visualised in an example profile (Figure 4.9).

The inflection points and deflection lengths (l_Δ) with respective deflection mode are then determined based on a series of α, used to calculate the relative deflection (Δ) and the deflection ratio (Δ/l_Δ). First, a vector with the number of inflection points passed along a building-specific settlement profile (pip) is created (including intersection points). This is based on how often α switches sign conventions. Second, the total settlement at each inflection point is calculated by interpolation. Third, a local tilt line, with horizontal distance δl equal to the grid resolution of 5 m, is calculated between two inflection points. Following six types of combination of angular strains (Figure 4.9 top), $l_\Delta/\delta l$ is determined by means of n. Fourth, l_Δ is calculated. Fifth, Δ was calculated for each settlement point as the vertical distance between the main settlement profile and the active local tilt line (referred to as relative deflection base). The active deflection mode is also registered. The lengths are grouped with the deflection to calculate the deflection ratios.

This process is repeated for all buildings in the domain of the metamodel, where the worst-case (largest) parameter values for a building is saved.

Table 4.3 displays the damage criteria used with respective limiting values. The damage criteria chosen are based on one empirical method and two semi-empirical methods, described in detail in Section 2.5 as well as in Paper C (Wikby et al. 2024).

Deflection mode	Combinations of angular strains	$l_\Delta/\delta l$
Hogging (H)	$\alpha^+ \rightarrow n\alpha^- \rightarrow \alpha^+$	n
	$\alpha^0 \rightarrow n\alpha^- \rightarrow \alpha^+$	$n+0.5$
	$\alpha^0 \rightarrow n\alpha^- \rightarrow \alpha^0$	$n+1$
Sagging (S)	$\alpha^0 \rightarrow n\alpha^+ \rightarrow \alpha^0$	$n+1$
	$\alpha^0 \rightarrow n\alpha^+ \rightarrow \alpha^-$	$n+0.5$
	$\alpha^- \rightarrow n\alpha^+ \rightarrow \alpha^-$	n

$\alpha^+: \alpha > 0$
$\alpha^0: \alpha = 0$
$\alpha^-: \alpha < 0$

n = series of α^+ or α^-

δl = profile resolution

α = angular strain

pip = passed inflection points

α	0	-	+	-	+	-	+	-	+	-	+	+	-	+	0
Mode		H	S	H	S	H	S	H	S	H	S	S	H	S	
n		1	1	1	1	1	1	1	1	1	2	2	1	1	
pip	1	1	2	3	4	5	6	7	8	9	10	10	11	12	13

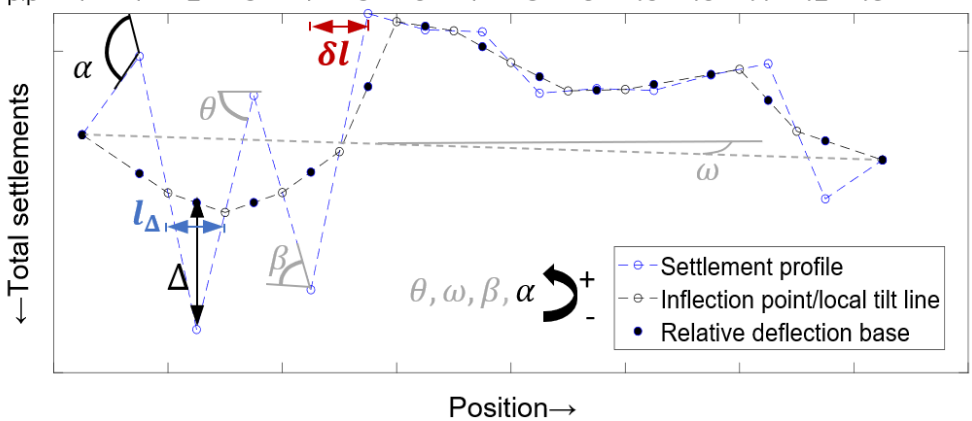

Figure 4.9: *Table showing how the deflection length (l_Δ) was calculated (top). Example of a building settlement profile including table displaying information of α, deflection mode, n and pip for each settlement point (bottom): Further definition of key damage parameters α, l_Δ, relative deflection (Δ), rotation (θ), angular distortion (β), δl and tilt (ω).*

4.4 Numerical model for deriving modification factors for floating piles

So far in this research, subsidence has been modelled in greenfield conditions. In reality, the buildings together with their foundations influence the settlement profile of a building. In this

Table 4.3: Damage classification table with the different criteria.

Method			**SOSM**	**LTSM**
Reference	Rankin (1988)		Son and Cording (2005)	Burland and Wroth (1974)
Category	S [mm]	θ [–]	β [10^{-3}]	$\epsilon_{t,\max}$ [%]
N.	0–10	0–1/500	0–1	0–0.05
V.Sl.	–	–	0–1	0.05–0.075
Sl.	10–50	1/500–1/200	1.5–3.33	0.075–0.15
M.	50–75	1/200–1/50	3.33–6.67	0.15–0.3
S.	>75	>1/50	>6.67	>0.3

section, a numerical framework is proposed to quantify the interaction levels and modification factors for floating piles in soft soils subject to underdrainage conditions. Subsequently, the modification factors will be used to assess the consequent damage due to the existence of floating piles.

4.4.1 Numerical model

A series of axisymmetric 2D models were created in PLAXIS 2D v. 2024.3, to investigate how, when and where the piles would modify the deformations in the clay. An example scenario with a clay thickness $H = 15$ m is shown in Figure 4.10. The radius of the domain is fixed at $100r_{pile}$, where r_{pile} is the radius of the pile, which is in excess of the distance required to obtain single pile behaviour ($12r_{pile}$), which is considered conservative for the pile raft. Simultaneously, from a numerical point of view, the right-hand boundary does not significantly affect the results.

The displacements at the lower boundary of the model are assumed to be fully fixed in the horizontal and vertical direction, due to the existence of bedrock. An unstructured mesh was used with six-noded triangular elements with an average size of ca 3 cm inside the pile that gradually coarsens toward the right-hand and lower boundaries of the model. A total of three clay thicknesses ($H = 15, 20, 30$ m) were chosen with each model geometry containing 6397, 4967 and 5604 elements, respectively.

The layering is similar to the model described in Subsection 4.2.1. The clay was modelled with the SCLAY1S model (Karstunen et al. 2005), due to issues with numerical stability when using the creep version of the model, likely due to the stiffness gradient between the much stiffer pile and the soft clay. The model parameters for SCLAY1S are similar to Creep-SCLAY1S (Table 4.1), but without the parameters for rate dependency (μ_i^* and τ), resulting in higher values for κ^* and λ_i^*, see Table 4.4 for identical 1D stress-strain response. The clayey fill layer at the surface was modelled similar to the clay layer, but with a higher vertical hydraulic conductivity ($k_v = 1E-6$ m/s), emulating the effects of a fissured dry crust. Meanwhile, the till at the bottom of the clay layer was modelled as described in Subsection 4.2.1.

The pile was modelled with volume elements using a linear elastic (LE) model, see Table 4.4. Meanwhile, the pile–clay interface was modelled with the Soft Soil model, using the modified compression index (λ^*), made equal to the intrinsic value. Choosing the Soft Soil model is not unreasonable, as the clay near the pile is considered remoulded after pile installation (Isaksson

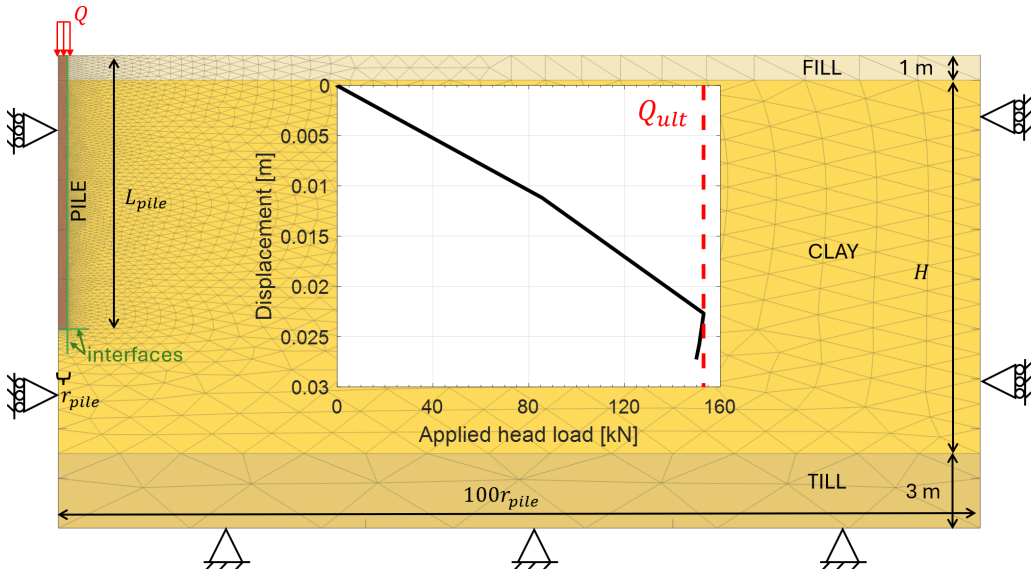

Figure 4.10: *The finite element model (not to scale) with mesh, boundary conditions, layers and materials as well as test results of a pile load test: Example where* $H = 15$ *m,* $L_{pile} = 11$ *m and* $r_{pile} = 0.15$ *m. (Modified from Paper E).*

and Dijkstra 2025) and provides more numerical stability for the interface elements.

The modelling of initialisation, activation and load application of the pile and equalisation, followed by the drawdown phase is visualised in Figure 4.11. As a normalisation parameter, the ultimate

Table 4.4: Parameters used in the pile model for $\gamma = 16$ kN/m^3 and $K_0 = 0.6$. c' is the cohesion intercept and ϕ' is the friction angle. LE = linear elastic. Other parameter descriptions are found in Table 4.1.

Material Model Parameter	Pile LE Value	Clay/fill SCLAY1S Value	Interface Soft Soil Value
E [kPa]	5E6	-	-
$\nu^{(\prime)}$	0.3	0.2	0.2
κ^*	-	0.04	0.04†
λ_i^*		0.215	-
λ^*	-	-	0.215†
M	-	1.45	-
c' [kPa]	-	-	2
ϕ' [°]	-	-	35

† $\kappa^* = 0.013$ and $\lambda^* = 0.085$ was used for cases H30PWP10Q75 and H15PWP40Q75,100y to gain numerically stable results (see Table 4.5).

pile head load (Q_{ult}) was calculated by simulating a pile load test. The results of the test can be found in Figure 4.10 where $Q_{ult} = 153$ kN.

Several modelling phases are needed to model a building on a floating pile foundation in soft clay subjected to underdrainage. The steps are summarised in Figure 4.11. Here, we decided to focus on modelling historic pile foundation comprising wooden piles (ca. 100-150 years old), as they are likely more sensitive for subsidence than end-bearing piles. Yet, compared to shallow foundations, smaller settlements are expected, and hence less building damage.

The initial state of the soil at the site is assumed to have horizontal soil layers and hydrostatic pore pressures, referred to as *initialisation phase*.

Subsequently, the piles were activated (installed as wished in place) and then loaded with the building (service load) in the *pile activation and loading phase*, following a consolidation period of 100-150 years depending on the construction year. This phase was numerically calculated as a plastic phase in drained conditions to eliminate any excess pore pressures from loading prior to the next phase.

In the *drawdown phase*, the pore pressures in the lower aquifer are reduced, representing the effect of a leaking tunnel, triggering consolidation in the soft clay above. The magnitude and extent of

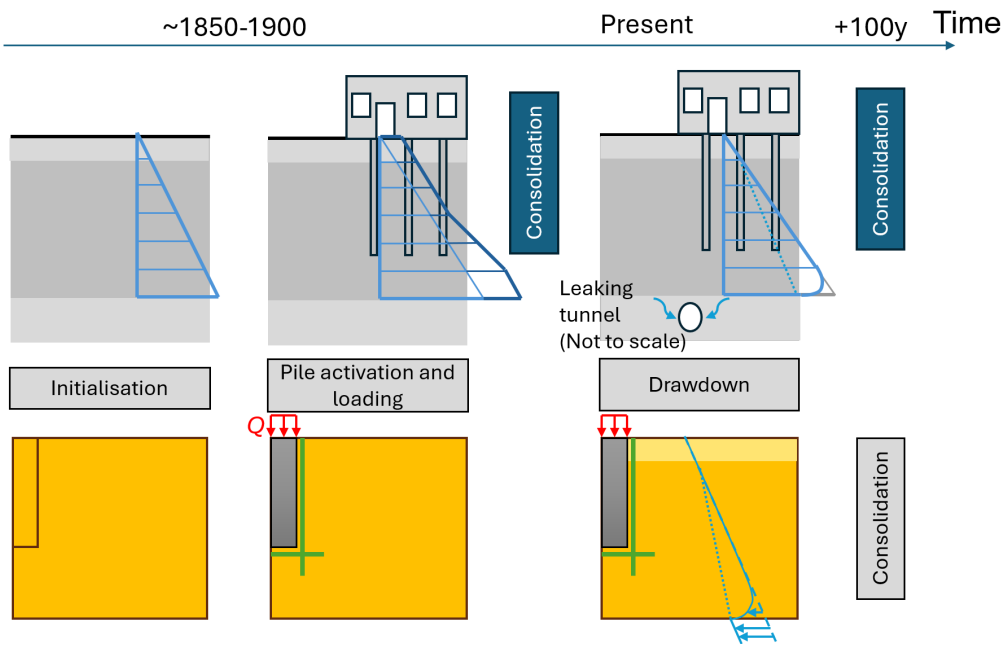

Figure 4.11: *Life cycle of an old piled building subjected to underdrainage drawdown. Upper part show the conceptualisation. Lower part show the numerical considerations. The timeline shows the assumed conditions before 1850 (initialisation), between 1850 and 1900 (pile activation and loading). From 1900 to present times, the excess pore pressures from loading are assumed to fully dissipate. At present time (drawdown following consolidation phases).*

these deformations will be modified by the pile foundation.

4.4.2 Parametric study

A parametric study was conducted to cover the variety of hypothetical scenarios of underdrainage in the study area, see Table 4.5. The initial geometry and boundary conditions to be varied were the pore water pressure reduction (PWP) in the lower aquifer, consolidation time after drawdown (t), clay thickness (H), and pile head load (mobilisation) Q. The PWP reductions chosen were 10 and 40 kPa (same as in Papers A-C). For time-dependent scenarios, short-term (3 months and 1 year), as well as long-term 10 years and 100 years were considered. The short-term scenarios represent the time window at which mitigation measures usually are implemented if severe subsidence is expected. Meanwhile, the most long-term scenario represents the designed life span of the tunnel, assuming that no mitigation measures are taken to minimise the PWP reduction. To represent the large variation in the clay thickness in the study area, three thickness-to-length (H/l) ratios were chosen (denoted H for the considered scenarios). In this case, l denotes the length of the pile beneath the fill layer. Finally, the added pile head load Q was normalised with Q_{ult}, into the degree of mobilisation (Q/Q_{ult}).

4.4.3 Interaction levels

From the analyses for each scenario, the greenfield settlements (S^{gf}) and pile settlements (S^{p}) were extracted at the right and left boundaries of the model. The settlement profiles were then corrected with the settlements prior to the drawdown. The intersection between the corrected S^{gf} and S^{p} profiles is called the interaction level (z_i) proposed by Korff et al. (2016). Note that z_i is related to but not equal to the neutral plane (NP).

Once calculated, z_i was plotted against the time factor (T_v):

$$T_v = (c_v t)/H^2 \tag{4.1}$$

where c_v is the coefficient of consolidation in the vertical direction (assumed here to have a constant value of 10^{-7} m^2/s), t is the consolidation time, and H is the clay thickness.

The numerically derived z_i values were then compared with empirically calculated NPs (using the 2/3- and α-methods) to see whether the prediction of interaction levels could be simplified. The first method (2/3 -method) always considers the NP level at 2/3 of the pile length depth. For an

Table 4.5: Scenarios modelled in the parametric study (time variation is left out).

H/l, PWP	$Q/Q_{ult} = 25\%$	$Q/Q_{ult} = 50\%$	$Q/Q_{ult} = 75\%$
$H/l = 1.5$, PWP = 10 kPa	H15PWP10Q25	H15PWP10Q50	H15PWP10Q75
$H/l = 1.5$, PWP = 40 kPa	H15PWP40Q25	H15PWP40Q50	H15PWP40Q75
$H/l = 2$, PWP = 10 kPa	H20PWP10Q25	H20PWP10Q50	H20PWP10Q75
$H/l = 2$, PWP = 40 kPa	H20PWP40Q25	H20PWP40Q50	H20PWP40Q75
$H/l = 3$, PWP = 10 kPa	H30PWP10Q25	H30PWP10Q50	H30PWP10Q75
$H/l = 3$, PWP = 40 kPa	H30PWP40Q25	H30PWP40Q50	H30PWP40Q75

11-metre pile, this would be roughly 7 metres. For the second method, the α-method (Tomlinson 1957), the shaft friction was assumed to be fully mobilised over the entire pile length. Moreover, base resistance was neglected according to common Swedish practice for long slender floating piles in clay. To calculate the location of NP (z_{NP}), dragload (Q_n) and resistance (R_s) profiles were first calculated for a cylindrical pile with constant radius (r_{pile} [m]):

$$Q_n(z) = \int_0^z 2\pi r_{pile} \tau_s(z) dz \tag{4.2}$$

$$R_s(z) = \int_z^{L_p} 2\pi r_{pile} \tau_s(z) dz \tag{4.3}$$

where τ_s [kPa] is the unit shaft friction:

$$\tau_s(z) = \alpha c_u(z) \tag{4.4}$$

$c_u(z)$ [kPa] is the undrained shear strength, and was retrieved from simulations of triaxial tests at different depths using the PLAXIS soil test with SCLAY1S, assumed to increase linearly with depth z. The typically recommended value of $\alpha = 0.7$ for long-term loads in Sweden was adopted.

Finally, the intersection point (NP) was calculated assuming equilibrium at this point:

$$Q + Q_n(z_{NP}) = R_s(z_{NP}) \tag{4.5}$$

where Q is the pile head load for the different scenarios (Q25, Q50 and Q75). An example for the scenario with Q75 is shown in Figure 4.12(a).

4.4.4 Modification factors and their integration with the building damage model

For the calculation of modification factors for the settlements ($MF^S = S_0^{gf} / S_0^p$), the predicted settlement at the surface for greenfield conditions S^{gf} and at the pile head S^p were taken (denoted subscript 0 here). After plotting scenario-specific MF^S against T_v, tri-linear functions with scenario-dependent limiting values of x_1, x_2, y_1 and y_2 were fitted against these data. An example for the scenario H15PWP40Q75 is shown in Figure 4.12(b).

The trilinear functions were then used to calculate the modification factors MF^S for each building characterised as having floating piles, for a given PWP scenario in the study area. For each piled building, the average clay thickness beneath the building was calculated. In the database, construction age was also utilised. Equation 4.1 was used to calculate building-specific T_v. For buildings older than 100 years, the functions for Q75 was assumed. The reason for this is that these piles were likely not designed with current-day safety factors (SF) in mind. Meanwhile, the younger buildings were assumed to follow the Q50 functions (SF=2), as some form of design consideration was probably made before their construction. From this information, the correct empirical function was chosen and building- and time-specific MF^S could thus be determined. In total, 48 buildings were analysed together with settlement and damage results of time-dependent scenarios 1 year and 30 years from Paper C. These damage results were retrieved via the Rankin (1988) criteria. Both Rankin(S) and Rankin(θ) were therefore analysed using the MF^S, which limiting values can be found in Table 4.3. An example of how predicted building damage is modified with pile foundations is found in Figure 4.13.

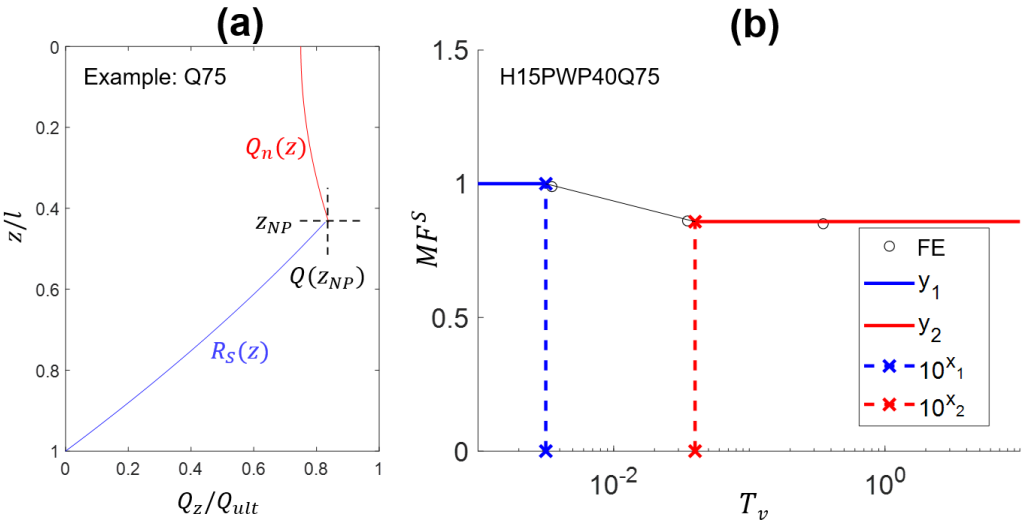

Figure 4.12: *(a) Axial load distribution for a fully mobilised pile with normalised load Q75 according to the empirical solution using the α-method. R_s is the shaft resistance, Q_n is the dragload, and z_{NP} is the depth of the neutral plane. (b) Empirical functions created from the FE-resulted modification factors (MF^S) vs. time factor (T_v). Definition of the trilinear function variables x_1, x_2, y_1 and y_2, example H15PWP40Q75.*

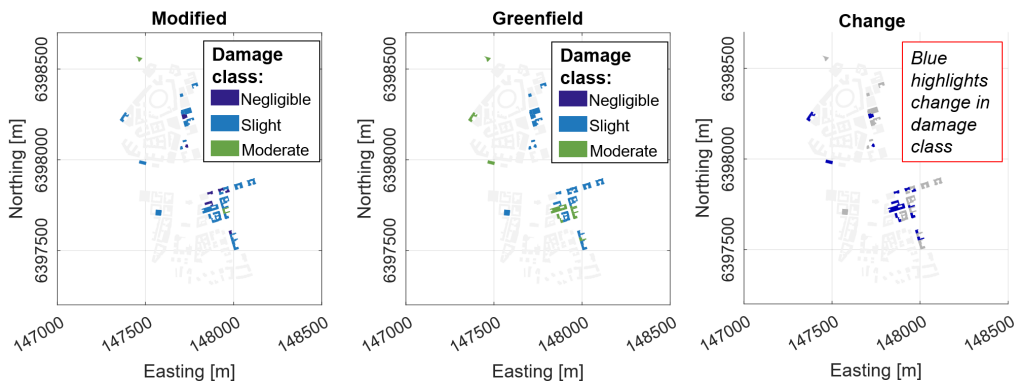

Figure 4.13: *Application of the predicted modification factors to building damage. Example of 10 kPa 30 year case using Rankin(θ) criteria.*

5 Summary of appended papers

Figure 4.1 shows a general overview of the papers and how they are linked with the research in the thesis.

5.1 Paper A: "The influence of parameter variability on subsidence"

The aim of the paper was to (i) develop a hydro-mechanically coupled numerical model of 2D cross-sections, and (ii) study the influence of key soil parameters on time-dependent subsidence. Creep-SCLAY1S, implemented in PLAXIS 2D, was used for modelling the clay response. The creep rate was calibrated using depth-integrated measurements from a nearby bellow hose. The subsidence was simulated as a uniform sustained drawdown of 10 kPa in the lower aquifer over 1 year. Systematic sensitivity analyses were performed with unique parameter combinations of likely minimum, trending, and maximum values of the chosen key parameters. The three parameters studied included over-consolidation ratio (OCR), vertical hydraulic conductivity (k_v), and the hydraulic anisotropy ratio (r_k).

I carried out all research activities, data analyses and drafted the manuscript.

A brief summary of some key results is provided in the following:

- In general, the subsidence was largest at the transitions between clay and rock. It would be advisable to concentrate site investigation to these locations if there are concerns about subsidence due to underdrainage.
- OCR influenced the settlement results the most, followed by vertical hydraulic conductivity. Thus, these parameters need to be derived based on testing of high quality samples.
- The change in hydraulic anisotropy, using typical values for marine clay, had no significant impact on the predicted settlement results despite the clear stratigraphic variation in the 2D cross-section. The result is unlikely to apply to varved clays.

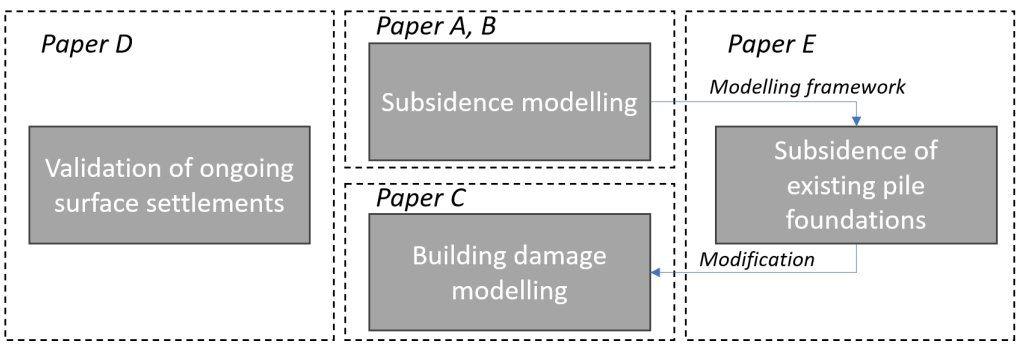

Figure 5.1: *Paper overview*

5.2 Paper B: "A metamodel for estimating time-dependent groundwater-induced subsidence at large scales"

The aim of the paper was to develop a large-scale subsidence model using machine learning to create a simplified surrogate model, referred to as a metamodel. The metamodel emulates time-dependent subsidence results from a hydro-mechanically coupled FE model incorporating Creep-SCLAY1S in PLAXIS 2D (Paper A). The hydro-stratigraphic features, available at high resolution for the entire model domain, were used as input to the metamodel. The algorithm was trained using both the features and the predicted subsidence by coupled FE analyses on two cross-sections as the target variable, while a third cross-section was reserved for validation and not included in the training process. A machine learning-based approach was used due to its relative computational efficiency, which is essential for evaluating multiple drawdown scenarios in large-scale, as relevant to planning of underground infrastructure.

The research activities relating to the methodological development of the metamodel were carried out by my colleague, Ezra Haaf. I was responsible for conducting the finite element analyses. The introduction chapter and sections 3.3, 3.4 and 4.1 were partly drafted by me, while other parts were mainly written by Haaf.

A brief summary of some key results and conclusions is provided in the following:

- The metamodel demonstrated high accuracy in emulating the hydro-mechanically coupled 2D model (developed in Paper A), enabling efficient calculation of subsidence over a large area.
- Shapley values interpreted the influence of individual hydro-stratigraphic features, such as clay thickness and initial aquifer heads, on subsidence, aligning with established understanding of the hydromechanical processes.
- The magnitude of the settlements was found to be strongly influenced by the clay thickness, which is reflected by the assumed depth-dependent values of OCR at the lower boundary of the clay, as well as the drainage length. The largest settlements occur in the transition zones where the clay layer tapers off. The metamodel demonstrates good replicability for such non-linear conditions.

5.3 Paper C: "A grid-based methodology for the assessment of time-dependent building damage at large scales"

The aim of the paper was to develop an automated large-scale building damage model that uses non-Gaussian (irregular) settlement profiles as input. The profiles were extracted from the metamodel for each time-dependent drawdown scenario, calculated within building-specific polygons. Common differential settlement variables were calculated, e.g. rotation, relative rotation (angular distortion) and limiting tensile strain, where the maximum value within a building was extracted for further analysis. The results were compared with damage criteria for each variable following the suggestions by Burland and Wroth (1974). Comparative analyses between each variable, settlement scenario, and resulting damage classes were performed. The effect of grid resolution was also examined. The resulting building-specific damage classes were displayed as maps, which can be used as a decision support in the initial planning of underground infrastructure projects.

I conducted all research activities, performed data analysis, and drafted the manuscript.

A brief summary of some key results is provided in the following:

- Grid-based non-Gaussian subsidence forecasts were used as input into simultaneous multi-building damage predictions at a large scale. This approach works for commonly used 2D damage parameters and time-dependent drawdown scenarios.
- Comparative analyses between the different damage parameters showed that the total settlement parameter had a significantly lower statistical correlation with other parameters. This is likely due to the subtraction of uniform settlements for other damage parameters. Therefore, due to their relatively high correlation and simplicity, rotation and angular distortion are recommended as damage parameters.
- An increased grid resolution yielded more conservative values for differential settlement parameters (e.g. rotation). On the other hand, the total settlement parameter showed no significant difference. As resolution decreases, the predicted damage will be underestimated for parameters describing differential settlement.
- The proposed method considered settlement profiles in two directions only, potentially leading to unconservative results. Further development is recommended to focus on accounting for several orientations.
- The proposed method could be further developed to include effects of soil-structure interaction, previous damage and horizontal strains. The limiting values of selected damage parameters could be based on the local building typologies (material, structural and foundation types, age, condition, geometries etc.).

5.4 Paper D: "Modelling subsidence and building damage in central Gothenburg using machine learning"

The aim of the paper was to study the response of the metamodel to background creep, as well as to validate the results against InSAR measurements. The background creep and its effects on building damage were simulated over a 30-year period.

I conducted the 2D subsidence and building damage modelling, performed data analysis, and prepared the manuscript. Ezra Haaf was in charge of the metamodel.

A brief summary of some key results is provided in the following:

- The metamodel is shown to overestimate the background creep by a maximum of 5mm/year. One likely reason is that the soil-structure interaction is neglected.
- Other discrepancies from the validation with the InSAR data can be attributed to other excavation projects and construction of high-rise buildings.
- The modelling results suggest that there will be severe damage to some buildings due to the differential settlements after 30 years.

5.5 Paper E: "Incorporating the impact of floating piles in prediction of large-scale subsidence"

The aim of this paper was to derive time-dependent modification factors for floating pile foundations subjected to subsidence due to underdrainage, that could be directly applied to greenfield settlement predictions. Furthermore, the newly derived modification factors allow assessing the impact of floating pile foundations on the change to consequent building damage. First, a series of numerical studies were conducted by modelling a single pile in axisymmetric conditions using several plausible scenarios and to identify key variables. Secondly, the interaction levels were studied, resulting in modification factors for greenfield settlements. Finally, these factors were fitted as time-dependent functions and applied to investigate building-specific subsidence and damage.

I conducted all research activities, performed data analysis, and drafted the manuscript.

A brief summary of some key results and conclusions is provided in the following:

- The modification of subsidence due existing floating pile foundations was shown to be time-dependent in the case of underdrainage, and in particular the long-term subsidence was significantly reduced (ca 10-40% depending on the drawdown magnitude and clay thickness) by the pile foundations.
- There is a clear influence of the clay thickness and the magnitude of the drawdown on long-term modification factors, where the degree of mobilisation of the pile is most significant for extreme drawdown cases.
- The long-term numerically derived interaction levels were shown to match well with standard empirical approaches, e.g. the α-method and the method considering 2/3 of the pile depth, for calculation of the neutral planes, indicating that most of the shaft resistance is fully mobilised.
- Building damage modification is not only shown to depend on the modified settlement predictions, but also the criteria used. Some criteria are more coarse and are thus less sensitive to changes in the predicted subsidence. Lower-level damage predictions are more likely to yield significant damage class modification (ca 40% for one such scenario).

6 Concluding remarks and recommendations

6.1 Conclusions

The aim of the thesis was to develop a modelling framework to calculate time-dependent settlements due to underdrainage and to assess the consequent building damage on a district-to-city scale.

The aim was successfully met by (1) developing a Hydro-Mechanical coupled 2D Finite Element (FE) model with the Creep-SCLAY1S constitutive model to compute settlement profiles due to consolidation and creep, (2) studying the influence of parameter uncertainty on the predicted time-dependent settlements, (3) developing an axisymmetric model that studies the influence of pre-existing floating piles on the predicted subsidence, and (4) developing a building damage model based on settlement predictions at large scale.

The following main conclusions can be drawn from this research:

- The resulting subsidence due to underdrainage was not only time-dependent but also strongly influenced by stratigraphy, especially soft clay thickness. Thus, the problem is four-dimensional.
- The stratigraphy dependence is related to the overconsolidation ratio (OCR), which delimits the small and large strains, as well as the distance to the drainage boundary. Consequently, for the short term, the most severe settlements were predicted in the transition zone with low clay thickness and bedrock near the surface.
- Time-dependent modification factors were proposed for total settlements of piled buildings undergoing underdrainage subsidence, readily applicable for large-scale predictions.
- The dependence of time and clay thickness was corroborated for the case with floating pile foundations.
- OCR is particularly sensitive to sample disturbance. The high-quality sampling should be concentrated to the transition zones if subsidence in the short term is of highest concern.
- In soft clay areas, the subsidence model needs to be calibrated for depth-integrated measurements of background creep, as for larger depths, the likelihood for sample disturbance is high.
- An automated large-scale building damage model was developed, incorporating non-Gaussian grid-based settlement profiles.
- The predicted building damage showed a high sensitivity to the damage criterion used. The angular distortion or rotation is recommended to be used over the limiting total settlement and tensile strain due to their high correlation and simplicity.
- Damage assessed based on total settlements showed very low correlations with the other damage parameters and is therefore not recommended.
- Buildings on floating pile foundations are equally sensitive to the damage criterion used in the long-term, specifically for cases with low levels of damage.

6.2 Recommendations for future work

The following directions for future work will be proposed:

- From a practical point of view, it would be good to couple the developed models in other parts of the cause-effect chain, such as (1) a groundwater model that considers leakage- and infiltration-induced groundwater level changes (Sundell et al. 2019b). Furthermore, (2) a societal cost-benefit analysis (CBA) should be performed to assess the overall impact of the design and production of subsurface construction, including mitigation measures, helping decision making (Sundell 2018; Merisalu et al. 2023).
- The developed model chain should be further explored to include parametric and geometric uncertainties in all aspects of the cause-effect chain through system level probabilistic analyses. For example, this could be done effectively using the Design of Experiments (DoE) method (Tahershamsi et al. 2023).
- It would be useful to further automate the computations for the entire cause-effect chain, e.g. by training the metamodel on additional features (for example, the location of the tunnel and the infiltration wells and the magnitudes and variability of key parameters within the system).
- The sampling and monitoring strategy for large-scale subsidence problems for large underground infrastructure projects should consider the findings of this study. To calibrate the subsidence parameters, high-quality samples taken at shallow clay depths (<20 m) that are spatially distributed within the area of interest are needed. Additionally, bellow hoses should ideally be placed in areas with thicker clay deposits around the area of influence and monitored both before and after tunnel construction.
- For buildings predicted to have high levels of damage (moderate or severe) using the proposed modelling framework, detailed 3D numerical analyses on building scale should be developed. Using those results, fragility curves (e.g. Prosperi 2025), that consider the probability of damage, could be developed to determine damage thresholds with improved accuracy while considering variability in local conditions.
- Modification factors for the influence of buildings on shallow foundations or mixed (shallow and deep) foundations in areas with the most severe differential settlement prediction results should be developed. The influence of pre-existing damage on the buildings should also be included in such analyses.
- In addition to building damage, other consequences should be quantified, such as damage to infrastructure and utilities, as well as increased flood risk. Both the direct and indirect economic consequences of these should be explored further (Merisalu et al. 2023).

References

Al-Tabbaa, A., & Wood, D. M. (1987). Some measurements of the permeability of kaolin. *Géotechnique*, *37*(4), 499–514. https://doi.org/10.1680/geot.1987.37.4.499

Amavasai, A., Sivasithamparam, N., Dijkstra, J., & Karstunen, M. (2018). Consistent Class A & C predictions of the Ballina test embankment. *Computers and Geotechnics*, *93*, 75–86. https://doi.org/10.1016/j.compgeo.2017.05.025

Amavasai, A., Gras, J.-P., Sivasithamparam, N., Karstunen, M., & Dijkstra, J. (2022). Towards consistent numerical analyses of embankments on soft soils. *European Journal of Environmental and Civil Engineering*, *26*(7), 2616–2634. https://doi.org/10.1080/19648189.2017.1354784

Auvinet, G., & Hanell, J. (1981). *Negative skin friction on piles in Mexico City clay* (Vol. 2). A. A. Balkema.

Bagheri-Gavkosh, M., Hosseini, S. M., Ataie-Ashtiani, B., Sohani, Y., Ebrahimian, H., Morovat, F., & Ashrafi, S. (2021). Land subsidence: A global challenge. *Science of The Total Environment*, *778*, 146193. https://doi.org/10.1016/j.scitotenv.2021.146193

Bear, J., & Verruijt, A. (1987). *Modeling groundwater flow and pollution*. D. Reidel Publishing Company.

Bedford, T., & Cooke, R. (2001). *Probabilistic risk analysis: foundations and methods*. Cambridge University Press.

Bergström, U., Pile, O., Curtis, P., & Eliasson, T. (2022). *Göteborgsområdets berggrund, jordarter och geologiska utveckling*. Swedish Geological Survey.

Bjerrum, L. (1963). Allowable settlement of structures. *Proceedings of the 3rd European Conference on Soil Mechanics and Foundation Engineering*, *2*, 135–137.

Bjerrum, L. (1967). Engineering Geology of Norwegian Normally-Consolidated Marine Clays as Related to Settlements of Buildings. *Géotechnique*, *17*(2), 83–118. https://doi.org/10.1680/geot.1967.17.2.83

Björdal, C. G., & Elam, J. (2021). Bacterial degradation of nine wooden foundation piles from Gothenburg historic city center and correlation to wood quality, environment, and time in service. *International Biodeterioration and Biodegradation*, *164*. https://doi.org/10.1016/j.ibiod.2021.105288

Bootsma, H., Kooi, H., & Erkens, G. (2020). Atlantis, a tool for producing national predictive land subsidence maps of the Netherlands. *Proceedings of the International Association of Hydrological Sciences*, *382*, 415–420. https://doi.org/10.5194/piahs-382-415-2020

Boone, S. J., Westland, J., & Nusink, R. (1999). Comparative evaluation of building responses to an adjacent braced excavation. *Canadian Geotechnical Journal*, *36*(2), 210–223. https://doi.org/10.1139/t98-100

Boone, S. J. (2010). A critical reappraisal of "preconsolidation pressure" interpretations using the oedometer test. *Canadian Geotechnical Journal*, *47*(3), 281–296. https://doi.org/10.1139/T09-093

Boone, S. J. (1996). Ground-Movement-Related Building Damage. *Journal of Geotechnical Engineering*, *122*(11), 886–896. https://doi.org/10.1061/(ASCE)0733-9410(1996)122:11(886)

Boscardin, M. D., & Cording, E. J. (1989). Building Response to Excavation-Induced Settlement. *Journal of Geotechnical Engineering*, *115*(1), 1–21. https://doi.org/10.1061/(ASCE)0733-9410(1989)115:1(1)

Bozkurt, S., Abed, A., & Karstunen, M. (2023). Finite element analysis for a deep excavation in soft clay supported by lime-cement columns. *Computers and Geotechnics*, *162*(August), 105687. https://doi.org/10.1016/j.compgeo.2023.105687

Bozozuk, M. (1972). Downdrag Measurements on a 160-Ft Floating Pipe Test Pile in Marine Clay. *Canadian Geotechnical Journal*, *9*(2), 127–136. https://doi.org/10.1139/t72-014

Broms, B. B., Fredriksson, A., & Carlsson, L. (1976). Land subsidence in Sweden due to water-leakage into deep-lying tunnels and its effects on piled supported structures. *International Association of Hydrological Sciences Proceedings of the Anaheim Symposium*, (121), 375–388.

Burland, J. B., Mair, R. J., & Standing, J. (2004). Ground performance and building response due to tunnelling. *Advances in Geotechnical Engineering: The Skempton Conference*, 291–342.

Burland, J. B., & Wroth, C. P. (1974). Settlement of Buildings and Associated Damage. In Building Research Establishment (Ed.), *Conf. Settlement of structures* (pp. 611–654).

Burland, J. B., Broms, B. B., & de Mello, V. F. (1977). Behaviour of foundations and structures. *Proceedings of the 9th International Conference on Soil Mechanics and Foundation Engineering*, 495–536.

Burbey, T. J. (2002). The influence of faults in basin-fill deposits on land subsidence, Las Vegas Valley, Nevada, USA. *Hydrogeology Journal*, *10*(5), 525–538. https://doi.org/10.1007/s10040-002-0215-7

Burland, J. (1973). Shaft friction of piles in clay: a simple fundamental approach. *Ground Engineering*, *6*(3), 30–42.

Burland, J. B. (1995). Asssessment of risk of damage to buildings due to tunnelling and excavation. *Earthquake Geotechnical Engineering*, 1189–1201.

Calderhead, A. I., Therrien, R., Rivera, A., Martel, R., & Garfias, J. (2011). Simulating pumping-induced regional land subsidence with the use of InSAR and field data in the Toluca Valley, Mexico. *Advances in Water Resources*, *34*(1), 83–97. https://doi.org/10.1016/j.advwatres.2010.09.017

Carter, J. P., Booker, J. R., & Small, J. C. (1979). The analysis of finite elasto-plastic consolidation. *International Journal for Numerical and Analytical Methods in Geomechanics*, *3*(2), 107–129. https://doi.org/10.1002/nag.1610030202

Chaussard, E., Havazli, E., Fattahi, H., Cabral-Cano, E., & Solano-Rojas, D. (2021). Over a Century of Sinking in Mexico City: No Hope for Significant Elevation and Storage Capacity Recovery. *Journal of Geophysical Research: Solid Earth*, *126*(4), 1–18. https://doi.org/10.1029/2020JB020648

Chen, S., & Xiang, Y. (2006). A procedure for theoretical estimation of dewatering-induced pile settlement. *Computers and Geotechnics*, *33*(4-5), 278–282. https://doi.org/10.1016/j.compgeo.2006.05.002

Chen, R. P., Zhou, W. H., & Chen, Y. M. (2009). Influences of soil consolidation and pile load on the development of negative skin friction of a pile. *Computers and Geotechnics*, *36*(8), 1265–1271. https://doi.org/10.1016/j.compgeo.2009.05.011

DeGroot, D., & Lutenegger, A. (1994). A Comparison Between Field and Laboratory Measurements of Hydraulic Conductivity in a Varved Clay. In D. E. Daniel & S. J. Trautwein (Eds.), *Hydraulic Conductivity and Waste Contaminant Transport in Soil* (pp. 300–317). American Society for Testing; Materials. https://doi.org/10.1520/STP23894S

Devriendt, M., & Williamson, M. (2011). Validation of methods for assessing tunnelling-induced settlements on piles. *Ground Engineering*, 25–30.

Drougkas, A., Verstrynge, E., Van Balen, K., Shimoni, M., Croonenborghs, T., Hayen, R., & Declercq, P.-Y. (2020). Country-scale InSAR monitoring for settlement and uplift damage calculation in architectural heritage structures. *Structural Health Monitoring*, 1–20. https://doi.org/10.1177/1475921720942120

EN 1997-1. (2005). Eurocode 7: Geotechnical design - Part 1: General rules.

Endo, M., Minou, A., Kawasaki, T., & Shibata, T. (1969). Negative skin friction acting on steel pipe pile in clay. *Proceedings of the 7th international conference on soil mechanics and foundation engineering*, 85–92. https://doi.org/10.1016/0266-1144(84)90012-8

Eriksson, P., Jendeby, L., Olsson, T., & Svensson, T. (2004). *Cohesion piles*. Commission on Pile Research (Report 100, In Swedish). Linköping.

Eskesen, S. D., Tengborg, P., Kampmann, J., & Holst Veicherts, T. (2004). Guidelines for tunnelling risk management: International Tunnelling Association, Working Group No. 2. *Tunnelling and Underground Space Technology*, *19*(3), 217–237. https://doi.org/10.1016/j.tust.2004.01.001

Fellenius, B. H. (2006). Results from long-term measurement in piles of drag load and downdrag. *Canadian Geotechnical Journal*, *43*(4), 409–430. https://doi.org/10.1139/t06-009

Fellenius, B. H. (2023). *Basics of Foundation Design* (Electronic).

Fellenius, B. H. (1971). *Negative skin friction on long piles driven in clay*. Swedish Geotechnical Institute (Proceedings No. 25). Stockholm.

Finno, R. J., Voss, F. T., Rossow, E., & Blackburn, J. T. (2005). Evaluating Damage Potential in Buildings Affected by Excavations. *Journal of Geotechnical and Geoenvironmental Engineering*, *131*(10), 1199–1210. https://doi.org/10.1061/(ASCE)1090-0241(2005)131:10(1199)

Franzius, J. N., Potts, D. M., & Burland, J. B. (2006). The response of surface structures to tunnel construction. *Proceedings of the Institution of Civil Engineers - Geotechnical Engineering*, *159*(1), 3–17. https://doi.org/10.1680/geng.2006.159.1.3

Franza, A., Marshall, A. M., Haji, T., Abdelatif, A. O., Carbonari, S., & Morici, M. (2017). A simplified elastic analysis of tunnel-piled structure interaction. *Tunnelling and Underground Space Technology*, *61*, 104–121. https://doi.org/10.1016/j.tust.2016.09.008

Franza, A., & Marshall, A. M. (2018). Centrifuge Modeling Study of the Response of Piled Structures to Tunneling. *Journal of Geotechnical and Geoenvironmental Engineering*, *144*(2), 04017109. https://doi.org/10.1061/(asce)gt.1943-5606.0001751

Franza, A., Marshall, A. M., & Jimenez, R. (2021). Non-linear soil–pile interaction induced by ground settlements: Pile displacements and internal forces. *Geotechnique*, *71*(3), 239–249. https://doi.org/10.1680/jgeot.19.P.078

Franza, A. (2016). *Tunnelling and its effects on piles and piled structures* [Doctoral dissertation, University of Nottingham].

Furtney, J. K., Thielsen, C., Fu, W., & Le Goc, R. (2022). Surrogate Models in Rock and Soil Mechanics: Integrating Numerical Modeling and Machine Learning. *Rock Mechanics and Rock Engineering*, *55*(5), 2845–2859. https://doi.org/10.1007/s00603-021-02720-8

Galavi, V. (2010). *Groundwater flow , fully coupled flow deformation and undrained analyses in PLAXIS 2D and 3D*. Plaxis BV report.

Gambolati, G., & Teatini, P. (2015). Geomechanics of subsurface water withdrawal and injection. *Water Resources Research*, *51*(6), 3922–3955. https://doi.org/10.1002/2014WR016841

Giardina, G. (2013). *Modelling of settlement induced building damage* [Doctoral dissertation, TU Delft].

Gras, J. P., Sivasithamparam, N., Karstunen, M., & Dijkstra, J. (2017). Strategy for consistent model parameter calibration for soft soils using multi-objective optimisation. *Computers and Geotechnics*, *90*, 164–175. https://doi.org/10.1016/j.compgeo.2017.06.006

Gras, J. P., Sivasithamparam, N., Karstunen, M., & Dijkstra, J. (2018). Permissible range of model parameters for natural fine-grained materials. *Acta Geotechnica*, *13*(2), 387–398. https://doi.org/10.1007/s11440-017-0553-1

Grant, R., Christian, J. T., & Vanmarcke, E. H. (1974). Differential Settlement of Buildings. *Journal of the Geotechnical Engineering Division*, *100*(9), 973–991. https://doi.org/10.1061/AJGEB6.0000101

Griffiths, D. V., & Fenton, G. A. (2009). Probabilistic Settlement Analysis by Stochastic and Random Finite-Element Methods. *Journal of Geotechnical and Geoenvironmental Engineering*, *135*(11), 1629–1637. https://doi.org/10.1061/(asce)gt.1943-5606.0000126

Guzy, A., & Malinowska, A. (2020). State of the Art and Recent Advancements in the Modelling of Land Subsidence Induced by Groundwater Withdrawal. *Water*, *12*(7), 2051. https://doi.org/10.3390/w12072051

Haaf, E., Wikby, P., Abed, A., Sundell, J., McGivney, E., Rosén, L., & Karstunen, M. (2024). A metamodel for estimating time-dependent groundwater-induced subsidence at large scales. *Engineering Geology*, *341*(August). https://doi.org/10.1016/j.enggeo.2024.107705

Hoffmann, J., Leake, S., Galloway, D., & Wilson, A. M. (2003). *MODFLOW-2000 ground-water model—User guide to the Subsidence and Aquifer-System Compaction (SUB) Package*. US Geological Survey. Tucson, AZ.

Hsieh, P. G., & Ou, C. Y. (1998). Shape of ground surface settlement profiles caused by excavation. *Canadian Geotechnical Journal*, *35*(6), 1004–1017. https://doi.org/10.1139/t98-056

Huang, J., Griffiths, D. V., & Fenton, G. A. (2010). Probabilistic Analysis of Coupled Soil Consolidation. *Journal of Geotechnical and Geoenvironmental Engineering*, *136*(3), 417–430. https://doi.org/10.1061/(asce)gt.1943-5606.0000238

Huang, B., Shu, L., & Yang, Y. S. (2012). Groundwater Overexploitation Causing Land Subsidence: Hazard Risk Assessment Using Field Observation and Spatial Modelling. *Water Resources Management*, *26*(14), 4225–4239. https://doi.org/10.1007/s11269-012-0141-y

Indraratna, B., Balasubramaniam, A. S., Phamvan, P., & Wong, Y. K. (1992). Development of negative skin friction on driven piles in soft Bangkok clay. *Canadian Geotechnical Journal*, *29*(3), 393–404. https://doi.org/10.1139/t92-044

Isaksson, J., & Dijkstra, J. (2025). Modeling the Pile Cycle of an Axially Loaded Pile in Sensitive Natural Clay. *Journal of Geotechnical and Geoenvironmental Engineering*, *151*(7), 1–15. https://doi.org/10.1061/jggefk.gteng-13179

Jacobsz, S., Standing, J., Mair, R., Hagiwara, T., & Sugiyama, T. (2004). Centrifuge Modelling of Tunnelling Near Driven Piles. *Soils and Foundations*, *44*(1), 49–56. https://doi.org/10.3208/sandf.44.49

Kaalberg F.J., Teunissen E.A.H., van Tol A.F., & Bosch J.W. (2005). Dutch research on the impact of shield tunnelling on pile foundations. In *Proceedings of the 16th International Conference on Soil Mechanics and Geotechnical Engineering* (pp. 1615–1620). IOS Press. https://doi.org/10.3233/978-1-61499-656-9-1615

Karstunen, M., Krenn, H., Wheeler, S. J., Koskinen, M., & Zentar, R. (2005). Effect of Anisotropy and Destructuration on the Behavior of Murro Test Embankment. *International Journal of Geomechanics*, *5*(2), 87–97. https://doi.org/10.1061/(ASCE)1532-3641(2005)5:2(87)

Karlsrud, K., & Mahan, A. (2010). *Evidence of Long Term Ageing Effects on Axial Capacity of Piles in Soft Clay* (M. H. Hussein, J. B. Anderson, & M. W. Camp, Eds.). American Society of Civil Engineers. https://doi.org/10.1061/41093(372)13

Karlsson, M., Emdal, A., & Dijkstra, J. (2016). Consequences of sample disturbance when predicting long-term settlements in soft clay. *Canadian Geotechnical Journal*, *53*(12), 1965–1977. https://doi.org/10.1139/cgj-2016-0129

Karlsson, M., Yannie, J., & Dijkstra, J. (2019). Modeling Aging of Displacement Piles in Natural Soft Clay. *Journal of Geotechnical and Geoenvironmental Engineering*, *145*(10), 1–8. https://doi.org/10.1061/(asce)gt.1943-5606.0002110

Karlsrud, K., & Sander, L. (1978). Subsidence Problems Caused By Rock-Tunnelling in Oslo. *International Conference on Evaluation and Prediction of Subsidence*, 1–10.

Karstunen, M. (2023). From theory to practice - numerical modelling of geostructures on soft natural clays. In L. Zdravkovic, S. Kontoe, D. Taborda, & A. Tsiampousi (Eds.), *Proceedings of the 10th European Conference on Numerical Methods in Geotechnical Engineering* (pp. 1–11). International Society for Soil Mechanics; Geotechnical Engineering. https://doi.org/10.53243/NUMGE2023-434

Kooi, H., & Yudhedha, A. T. (2018). *Updated subsidence scenarios Jakarta: MODFLOW SUB-CR calculations for Sunter, Daan Mogot and Marunda*. Deltares.

Korff, M., & Mair, R. J. (2013). *Response of piled buildings to deep excavations in soft soils* (P. Delage, Ed.; Vol. 3). Presses des Ponts.

Korff, M., Mair, R. J., & Van Tol, F. A. F. (2016). Pile-Soil Interaction and Settlement Effects Induced by Deep Excavations. *Journal of Geotechnical and Geoenvironmental Engineering*, *142*(8), 04016034. https://doi.org/10.1061/(ASCE)GT.1943-5606.0001434

Larsson, R., Sällfors, G., Bengtsson, P.-E., Alén, C., Bergdahl, U., & Eriksson, L. (2007). *Skjuvhållfasthet - utvärdering i kohesionsjord*. Statens Geotekniska Institut (Information 3). Linköping.

Larsson, R. (1981). *Drained behaviour of Swedish Clays*. Swedish Geotechnical Institute (Report No. 12). Linköping.

Leake, S., & Galloway, D. L. (2007). MODFLOW ground-water model: User guide to the subsidence and aquifer-system compaction package (SUB-WT) for water-table aquifers. In *Techniques and Methods* (pp. 1–42). US Geological Survey.

Lee, C. J., & Chen, C. R. (2003). Negative skin friction on piles due to lowering of ground water table. *Geotechnical Engineering*, *34*(1), 13–24.

Lehane, B., Bittar, E., Lacasse, S., Liu, Z., & Nadim, F. (2022). New CPT methods for evaluation of the axial capacity of driven piles. In G. Gottardi & Tonni (Eds.), *Cone Penetration Testing 2022* (pp. 3–15). CRC Press. https://doi.org/10.1201/9781003308829-1

Leroueil, S., Kabbaj, M., Tavenas, F., & Bouchard, R. (1985). Stress–strain–strain rate relation for the compressibility of sensitive natural clays. *Géotechnique*, *35*(2), 159–180. https://doi.org/10.1680/geot.1985.35.2.159

Leroueil, S., & Vaughan, P. R. (1990). The general and congruent effects of structure in natural soils and weak rocks. *Géotechnique*, *40*(3), 467–488. https://doi.org/10.1680/geot.1990.40.3.467

Leroueil, S., Leart, P., Hight, D. W., & Powell, J. J. M. (1992). Hydraulic conductivity of a recent estuarine silty clay at Bothkennar. *Géotechnique*, *42*(2), 275–288. https://doi.org/10.1680/geot.1992.42.2.275

Li, Z., Luo, Z., Wang, Q., Du, J., Lu, W., & Ning, D. (2019). A three-dimensional fluid-solid model, coupling high-rise building load and groundwater abstraction, for prediction of regional

land subsidence. *Hydrogeology Journal*, *27*(4), 1515–1526. https://doi.org/10.1007/s10040-018-01920-x

Liang, R., Yin, Z. Y., Yin, J. H., & Wu, P. C. (2023). Numerical analysis of time-dependent negative skin friction on pile in soft soils. *Computers and Geotechnics*, *155*(October 2022), 105218. https://doi.org/10.1016/j.compgeo.2022.105218

Liu, J., Gao, H., & Liu, H. (2012). Finite element analyses of negative skin friction on a single pile. *Acta Geotechnica*, *7*(3), 239–252. https://doi.org/10.1007/s11440-012-0163-x

Lunne, T., Berre, T., Andersen, K. H., Strandvik, S., & Sjursen, M. (2006). Effects of sample disturbance and consolidation procedures on measured shear strength of soft marine Norwegian clays. *Canadian Geotechnical Journal*, *43*(7), 726–750. https://doi.org/10.1139/T06-040

Mahmoudpour, M., Khamehchiyan, M., Nikudel, M. R., & Ghassemi, M. R. (2016). Numerical simulation and prediction of regional land subsidence caused by groundwater exploitation in the southwest plain of Tehran, Iran. *Engineering Geology*, *201*(2016), 6–28. https://doi.org/10.1016/j.enggeo.2015.12.004

Mair, R. J., Taylor, R., & Burland, J. B. (1996). Prediction of ground movements and assessment of risk of building damage due to bored tunnelling. In R. J. Mair & R. Taylor (Eds.), *Geotechnical Aspects of Underground Construction in Soft Ground* (pp. 713–718). Balkema.

Matyas, E. L., & Santamarina, J. C. (1994). Negative skin friction and the neutral plane. *Canadian Geotechnical Journal*, *31*(4), 591–597. https://doi.org/10.1139/t94-069

McDonald, M. G., & Harbaugh, A. W. (1988). *A modular three-dimensional finite-difference ground-water flow model*. US Geological Survey.

Merisalu, J., Sundell, J., & Rosén, L. (2021). A Framework for Risk-Based Cost–Benefit Analysis for Decision Support on Hydrogeological Risks in Underground Construction. *Geosciences*, *11*(2), 82. https://doi.org/10.3390/geosciences11020082

Merisalu, J., Sundell, J., & Rosén, L. (2023). Probabilistic cost-benefit analysis for mitigating hydrogeological risks in underground construction. *Tunnelling and Underground Space Technology*, *131*(October 2022). https://doi.org/10.1016/j.tust.2022.104815

Meyerhof, G. G. (1982). Limit states design in geotechnical engineering. *Structural Safety*, *1*(1), 67–71. https://doi.org/10.1016/0167-4730(82)90015-7

Namazi, E., & Mohamad, H. (2013). Assessment of Building Damage Induced by Three-Dimensional Ground Movements. *Journal of Geotechnical and Geoenvironmental Engineering*, *139*(4), 608–618. https://doi.org/10.1061/(ASCE)GT.1943-5606.0000822

Netzel, H. (2009). *Building response due to ground movements* [Doctoral dissertation, TU Delft].

Ochoa-González, G. H., Teatini, P., Carreón-Freyre, D., & Gambolati, G. (2013). Modeling the deformation of faulted volcano-sedimentary sequences associated to groundwater withdrawal in the Querétaro Valley, Mexico. In J. Piantadosi, R. Anderssen, & J. Boland (Eds.), *MODSIM2013, 20th International Congress on Modelling and Simulation* (pp. 2737–2743). Modelling; Simulation Society of Australia; New Zealand (MSSANZ), Inc. https://doi.org/10.36334/modsim.2013.L10.ochoagonzalez

Ochoa-González, G., Carreón-Freyre, D., Franceschini, A., Cerca, M., & Teatini, P. (2018). Overexploitation of groundwater resources in the faulted basin of Querétaro, Mexico: A 3D deformation and stress analysis. *Engineering Geology*, *245*(August), 192–206. https://doi.org/10.1016/j.enggeo.2018.08.014

Olson, R. E., & Daniel, D. E. (1981). Permeability and Groundwater Contaminant Transport. In T. F. Zimmie & C. O. Riggs (Eds.), *Permeability and Groundwater Contaminant Transport, ASTM*

STP 746 (pp. 18–64). American Society for Testing; Materials. https://doi.org/10.1520/STP746-EB

Olsson, C., & Holm, G. (1993). *Pålgrundläggning*. Svensk Byggtjänst c/o Statens Geotekniska Institut (In Swedish).

Omer, J. R. (2012). Integrating finite element and load-transfer analyses in modelling the effects of dewatering on pile settlement behaviour. *Canadian Geotechnical Journal*, *49*(5), 512–521. https://doi.org/10.1139/T2012-013

Ortega-Guerrero, A., Rudolph, D. L., & Cherry, J. A. (1999). Analysis of long-term land subsidence near Mexico City: Field investigations and predictive modeling. *Water Resources Research*, *35*(11), 3327–3341. https://doi.org/10.1029/1999WR900148

Påsse, T., & Daniels, J. (2015). *Past shore-level and sea-level displacements*. Geological Survey of Sweden.

Peck, R. B. (1969). Deep excavation and tunnelling in soft ground. *Proceedings of the 7th international conference on soil mechanics and foundation engineering*, 225–290.

Peduto, D., Ferlisi, S., Nicodemo, G., Reale, D., Pisciotta, G., & Gullà, G. (2017). Empirical fragility and vulnerability curves for buildings exposed to slow-moving landslides at medium and large scales. *Landslides*, *14*(6), 1993–2007. https://doi.org/10.1007/s10346-017-0826-7

Peduto, D., Korff, M., Nicodemo, G., Marchese, A., & Ferlisi, S. (2019). Empirical fragility curves for settlement-affected buildings: Analysis of different intensity parameters for seven hundred masonry buildings in The Netherlands. *Soils and Foundations*, *59*(2), 380–397. https://doi.org/10.1016/j.sandf.2018.12.009

Peduto, D., Prosperi, A., Nicodemo, G., & Korff, M. (2021). District-scale numerical analysis of settlements related to groundwater lowering in variable soil conditions. *Canadian Geotechnical Journal*, *993*(September 2021), 1–16. https://doi.org/10.1139/cgj-2021-0041

Persson, J. (2007). *Hydrogeological methods in geotechnical engineering: Applied to settlements caused by underground construction* [Doctoral dissertation, Chalmers university of technology].

Phien-wej, N., Giao, P. H., & Nutalaya, P. (2006). Land subsidence in Bangkok, Thailand. *Engineering Geology*, *82*(4), 187–201. https://doi.org/10.1016/j.enggeo.2005.10.004

Phoon, K. K., & Kulhawy, F. H. (1999a). Characterization of geotechnical variability. *Canadian Geotechnical Journal*, *36*(4), 612–624. https://doi.org/10.1139/t99-038

Phoon, K. K., & Kulhawy, F. H. (1999b). Evaluation of geotechnical property variability. *Canadian Geotechnical Journal*, *36*(4), 625–639. https://doi.org/10.1139/t99-039

Piciullo, L., Ritter, S., Lysdahl, A. O. K., Langford, J., & Nadim, F. (2021). Assessment of building damage due to excavation-induced displacements: The GIBV method. *Tunnelling and Underground Space Technology*, *108*(1), 103673. https://doi.org/10.1016/j.tust.2020.103673

Polshin, D., & Tokar, R. (1957). Maximum Allowable Non-uniform Settlement of Structures. *Proceedings of the 4th international conference on soil mechanics and foundation engineering*, *Vol. 1*, 402–405.

Pool, R. (1995). *Assessment of damage in low-rise buildings*. Building Research Establishment (Digest 251).

Potts, D. M., & Addenbrooke, T. I. (1997). A structure's influence on tunnelling-induced ground movements. *Proceedings of the Institution of Civil Engineers - Geotechnical Engineering*, *125*(2), 109–125. https://doi.org/10.1680/igeng.1997.29233

Prosperi, A., Korswagen, P. A., Korff, M., Schipper, R., & Rots, J. G. (2023). Empirical fragility and ROC curves for masonry buildings subjected to settlements. *Journal of Building Engineering*, *68*(February), 106094. https://doi.org/10.1016/j.jobe.2023.106094

Prosperi, A., Korswagen, P. A., Longo, M., Korff, M., & Rots, J. G. (2025). Toward NLFEA-based fragility curves for unreinforced masonry buildings exposed to subsidence. *Journal of Building Engineering*, *112*(July), 113676. https://doi.org/10.1016/j.jobe.2025.113676

Prosperi, A. (2025). *Modelling of subsidence induced damage to masonry buildings: Influence of soil heterogeneity on settlement and development of fragility curves* [Doctoral dissertation, TU Delft University]. https://doi.org/10.4233/uuid:798679cf-f2a3-46fb-be53-93e07968e7a6

Rankin, W. J. (1988). Ground movements resulting from urban tunnelling: predictions and effects. In F. G. Bell, M. G. Culshaw, J. C. Cripps, & M. A. Lovell (Eds.), *Engineering Geology of Underground Movements, Geological Society Engineering Geology Special Publication* (pp. 79–92, Vol. 5). https://doi.org/10.1144/GSL.ENG.1988.005.01.06

Reul, O., & Randolph, M. F. (2003). Piled rafts in overconsolidated clay: comparison of in situ measurements and numerical analyses. *Géotechnique*, *53*(3), 301–315. https://doi.org/10.1680/geot.2003.53.3.301

Rodríguez-Rebolledo, J. F., Auvinet-Guichard, G. Y., & Martínez-Carvajal, H. E. (2015). Settlement analysis of friction piles in consolidating soft soils. *DYNA (Colombia)*, *82*(192), 211–220. https://doi.org/10.15446/dyna.v82n192.47752

Selemetas, D., & Standing, J. R. (2017). Response of full-scale piles to EPBM tunnelling in London Clay. *Geotechnique*, *67*(9), 823–836. https://doi.org/10.1680/jgeot.SIP17.P.126

Shen, S.-L., & Xu, Y.-S. (2011). Numerical evaluation of land subsidence induced by groundwater pumping in Shanghai. *Canadian Geotechnical Journal*, *48*(9), 1378–1392. https://doi.org/10.1139/t11-049

Sivasithamparam, N., Karstunen, M., & Bonnier, P. (2015). Modelling creep behaviour of anisotropic soft soils. *Computers and Geotechnics*, *69*, 46–57. https://doi.org/10.1016/j.compgeo.2015.04.015

Skempton, A. W., & MacDonald, D. H. (1956). The allowable settlements of buildings. *Proceedings of the Institution of Civil Engineers*, *5*(6), 727–768. https://doi.org/10.1680/ipeds.1956.12202

Son, M., & Cording, E. J. (2005). Estimation of Building Damage Due to Excavation-Induced Ground Movements. *Journal of Geotechnical and Geoenvironmental Engineering*, *131*(2), 162–177. https://doi.org/10.1061/(ASCE)1090-0241(2005)131:2(162)

Son, M., & Cording, E. J. (2007). Evaluation of Building Stiffness for Building Response Analysis to Excavation-Induced Ground Movements. *Journal of Geotechnical and Geoenvironmental Engineering*, *133*(8), 995–1002. https://doi.org/10.1061/(ASCE)1090-0241(2007)133:8(995)

Sundell, J., Rosén, L., Norberg, T., & Haaf, E. (2016). A probabilistic approach to soil layer and bedrock-level modeling for risk assessment of groundwater drawdown induced land subsidence. *Engineering Geology*, *203*, 126–139. https://doi.org/10.1016/j.enggeo.2015.11.006

Sundell, J., Haaf, E., Norberg, T., Alén, C., Karlsson, M., & Rosén, L. (2019a). Risk Mapping of Groundwater-Drawdown-Induced Land Subsidence in Heterogeneous Soils on Large Areas. *Risk Analysis*, *39*(1), 105–124. https://doi.org/10.1111/risa.12890

Sundell, J., Haaf, E., Tornborg, J., & Rosén, L. (2019b). Comprehensive risk assessment of groundwater drawdown induced subsidence. *Stochastic Environmental Research and Risk Assessment*, *33*(2), 427–449. https://doi.org/10.1007/s00477-018-01647-x

Sundell, J. (2018). *Risk Assessment of Groundwater Drawdown in Subsidence Sensitive Areas* [Doctoral dissertation, Chalmers University of Technology].

Tahershamsi, H., & Dijkstra, J. (2021). Towards rigorous boundary value level sensitivity analyses using FEM. *IOP Conference Series: Earth and Environmental Science*, *710*(1), 012072. https://doi.org/10.1088/1755-1315/710/1/012072

Tahershamsi, H., & Dijkstra, J. (2022). Using experimental design to assess rate-dependent numerical models. *Soils and Foundations*, *62*(6), 101244. https://doi.org/10.1016/j.sandf.2022.101244

Tahershamsi, H., Ahmadi Naghadeh, R., Zuada Coelho, B., & Dijkstra, J. (2023). Low amplitude strain accumulation model for natural soft clays below railways. *Transportation Geotechnics*, *42*(March), 101011. https://doi.org/10.1016/j.trgeo.2023.101011

Tavenas, F., Jean, P., Leblond, P., & Leroueil, S. (1983). The permeability of natural soft clays. Part II: Permeability characteristics. *Canadian Geotechnical Journal*, *20*(4), 645–660. https://doi.org/10.1139/t83-073

Teatini, P., Ferronato, M., Gambolati, G., & Gonella, M. (2006). Groundwater pumping and land subsidence in the Emilia-Romagna coastland, Italy: Modeling the past occurrence and the future trend. *Water Resources Research*, *42*(1), 1–19. https://doi.org/10.1029/2005WR004242

Thörn, J. (2015). *The Impact of Fracture Geometry on the Hydromechanical Behaviour of Crystalline Rock* [Doctoral dissertation, Chalmers University of Technology].

Timoshenko, S. P. (1957). *Strength of materials, part I, elementary theory and problems*. D van Nostrand Co, Inc.

Tomlinson, M. J. (1957). The adhesion of piles driven in clay soils. In *Proceedings of the 4th international conference on soil mechanics and foundation engineering* (Vol. 2, pp. 66–71). Butterworths Scientific Publications.

Tornborg, J., Karlsson, M., Kullingsjö, A., & Karstunen, M. (2021). Modelling the construction and long-term response of Göta Tunnel. *Computers and Geotechnics*, *134*(March), 104027. https://doi.org/10.1016/j.compgeo.2021.104027

Tornborg, J., Karlsson, M., & Karstunen, M. (2023). Permanent Sheet Pile Wall in Soft Sensitive Clay. *Journal of Geotechnical and Geoenvironmental Engineering*, *149*(6), 1–13. https://doi.org/10.1061/jggefk.gteng-10955

Trafikverket. (2014). *PM Inventering tidigare utförda hydrogeologiska undersökningar*.

TreMaps. (2021). *Follow up measurements with InSAR in Västlänken project in Gothenburg and Mölndal municipalities, Västra Götaland region (in Swedish)*.

TreMaps. (2024). Gothenburg TSX VERT MAY 2024.

Verruijt, A. (1984). The theory of consolidation. In J. Bear & M. Y. Corapcioglu (Eds.), *Fundamentals of transport phenomena in porous media* (pp. 349–368, Vol. 2). Springer. https://doi.org/10.1007/978-94-009-6175-3

Wahls, H. E. (1981). Tolerable Settlement of Buildings. *Journal of the Geotechnical Engineering Division*, *107*(11), 1489–1504. https://doi.org/10.1061/AJGEB6.0001204

Wang, R., & Brandenberg, S. J. (2013). Beam on Nonlinear Winkler Foundation and Modified Neutral Plane Solution for Calculating Downdrag Settlement. *Journal of Geotechnical and Geoenvironmental Engineering*, *139*(9), 1433–1442. https://doi.org/10.1061/(asce)gt.1943-5606.0000888

Wendel, E. H. (1900). Om profbelastning på pålar med tillämpning deraf på grundläggningsförhållandena i Göteborg. In *Tekni. samf. handlingar* (pp. 3–62). (In Swedish).

Wheeler, S. J., Näätänen, A., Karstunen, M., & Lojander, M. (2003). An anisotropic elastoplastic model for soft clays. *Canadian Geotechnical Journal*, *40*(2), 403–418. https://doi.org/10.1139/t02-119

Wikby, P., Abed, A., Karlsson, M., Sundell, J., & Karstunen, M. (2023). *The influence of parameter variability on subsidence* (L. Zdravkovic, S. Kontoe, D. Taborda, & A. Tsiampousi, Eds.). International Society for Soil Mechanics; Geotechnical Engineering. https://doi.org/10.53243/NUMGE2023-325

Wikby, P., Haaf, E., Abed, A., Rosén, L., Sundell, J., & Karstunen, M. (2024). A grid-based methodology for the assessment of time-dependent building damage at large scale. *Tunnelling and Underground Space Technology*, *149*, 105788. https://doi.org/10.1016/j.tust.2024.105788

Wikby, P., Abed, A., Karstunen, M., & Dijkstra, J. (2025a). Incorporating the impact of floating piles in prediction of large-scale subsidence. *Submitted manuscript*.

Wikby, P., Haaf, E., & Karstunen, M. (2025b). Modeling subsidence and building damage in central Gothenburg using machine learning. In Z. Liu, J. Dai, & K. Robinson (Eds.), *Proc. of the 9th International Symposium on Geotechnical Safety and Risk (ISGSR)* (pp. 375–378). Research Publishing. https://doi.org/10.3850/9789819440757

Williamson, M. G., Mair, R. J., Devriendt, M. D., & Elshafie, M. Z. E. B. (2017). Open-face tunnelling effects on non-displacement piles in clay – part 2: tunnelling beneath loaded piles and analytical modelling. *Géotechnique*, *67*(11), 1001–1019. https://doi.org/10.1680/jgeot.SIP17.P.120

Win, B. M., Arulrajah, A., & Choa, V. (1998). The hydraulic conductivity of Singapore Marine Clay at Changi. *Quarterly Journal of Engineering Geology and Hydrogeology*, *31*(4), 291–299. https://doi.org/10.1144/GSL.QJEG.1998.031.P4.02

Wu, J., Shi, X., Ye, S., Xue, Y., Zhang, Y., Wei, Z., & Fang, Z. (2010). Numerical Simulation of Viscoelastoplastic Land Subsidence due to Groundwater Overdrafting in Shanghai, China. *Journal of Hydrologic Engineering*, *15*(3), 223–236. https://doi.org/10.1061/(ASCE)HE.1943-5584.0000172

Ye, S., Xue, Y., Wu, J., Yan, X., & Yu, J. (2016). Progression and mitigation of land subsidence in China. *Hydrogeology Journal*, *24*(3), 685–693. https://doi.org/10.1007/s10040-015-1356-9

Yoo, C. (2005). Interaction between Tunneling and Groundwater—Numerical Investigation Using Three Dimensional Stress–Pore Pressure Coupled Analysis. *Journal of Geotechnical and Geoenvironmental Engineering*, *131*(2), 240–250. https://doi.org/10.1061/(ASCE)1090-0241(2005)131:2(240)

Zhang, L., & Ng, A. M. Y. (2005). Probabilistic limiting tolerable displacements for serviceability limit state design of foundations. *Géotechnique*, *55*(2), 151–161. https://doi.org/10.1680/geot.2005.55.2.151

Zhang, Y., Zhou, L.-P., Wang, M.-Y., Ding, X., & Wang, C. (2021). Experimental Study on the Negative Skin Friction of the Pile Group Induced by Rising and Lowering the Groundwater Level (Q. Tang, Ed.). *Advances in Civil Engineering*, *2021*(1). https://doi.org/10.1155/2021/2574727